TRANSIENT RECEPTOR POTENTIAL VANILLOID 3 (TRPV3) ION CHANNEL IN THE RAT BRAIN: DISTRIBUTION AND FUNCTIONAL SIGNIFICANCE

By
Uday Singh

LIFE11201004011

National Institute of Science Education and Research (NISER), Bhubaneswar

A thesis submitted to the

Board of Studies in Life Sciences
In partial fulfillment of requirements
for the Degree of

DOCTOR OF PHILOSOPHY
*of*
HOMI BHABHA NATIONAL INSTITUTE

December, 2016

Homi Bhabha National Institute[1]

Recommendations of the Viva Voce Committee

As members of the Viva Voce Committee, we certify that we have read the dissertation prepared by Mr. Uday Singh entitled, "Transient Receptor Potential Vanilloid 3 (TRPV3) Ion Channel in the Rat Brain: Distribution and Functional Significance" and recommend that it may be accepted as fulfilling the thesis requirement for the award of Degree of Doctor of Philosophy.

Chairman - Prof. B.S. Shankaranarayana Rao   Date: 15/05/2017
NIMHANS, Bengaluru
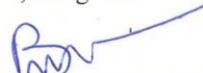
Guide / Convener - Dr. Praful Singru   Date: 15/05/2017
SBS, NISER

Co-guide - NA   Date:

External Examiner- Prof. B.S. Shankaranarayana Rao   Date: 15/05/2017
NIMHANS, Bengaluru
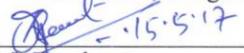
Member 1 - Prof. J. Dandapat   Date: 15/05/2017
Utkal, University

Member 2- Dr. Chandan Goswami   Date: 15/05/2017
SBS, NISER
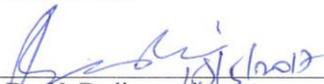
Member 3 - Dr. V. Badireenath   Date: 15/05/2017
SBS, NISER

Final approval and acceptance of this thesis is contingent upon the candidate's submission of the final copies of the thesis to HBNI.

I/We hereby certify that I/we have read this thesis prepared under my/our direction and recommend that it may be accepted as fulfilling the thesis requirement.

Date: 15/05/2017

Place: Bhubaneswar

Co-guide (if applicable)   Guide

---

[1] This page is to be included only for final submission after successful completion of viva voce.

Version approved during the meeting of Standing Committee of Deans held during 29-30 Nov 2013

STATEMENT BY AUTHOR

This dissertation has been submitted in partial fulfillment of requirements for an advanced degree at Homi Bhabha National Institute (HBNI) and is deposited in the Library to be made available to borrowers under rules of the HBNI.

Brief quotations from this dissertation are allowable without special permission, provided that accurate acknowledgement of source is made. Requests for permission for extended quotation from or reproduction of this manuscript in whole or in part may be granted by the Competent Authority of HBNI when in his or her judgment the proposed use of the material is in the interests of scholarship. In all other instances, however, permission must be obtained from the author.

Uday Singh

Date: 19.05.2017

DECLARATION

I, hereby declare that the investigation presented in the thesis has been carried out by me. The work is original and has not been submitted earlier as a whole or in part for a degree/diploma at this or any other Institution/University.

Uday Singh USingh

Date: 19.05.2017

LIST OF PUBLICATIONS ARISING FROM THE THESIS

JOURNALS

1. "Transient receptor potential vanilloid 3 (TRPV3) in the ventral tegmental area of rat: Role in modulation of the mesolimbic-dopamine reward pathway", **Singh U**, Kumar S, Shelkar GP, Yadav M, Kokare DM, Goswami C, Lechan RM, Singru PS. (2016). *Neuropharmacology***, 2016,** 110, 198-210.

2. "Interaction between dopamine- and isotocin-containing neurones in the preoptic area of the catfish, *Clarias batrachus*: role in the regulation of luteinising hormone cells", **Singh U**, Kumar S, Singru PS. *Journal of Neuroendocrinology*, **2012**, 24, 1398-1411.

3. "Synaptotagmin-1, a 'turbocharger' of synaptic vesicle exocytosis is recruited to the somatodendritic compartment of hypothalamic vasopressin neurons during hyperosmotic challenge", **Singh U,** Kumar S, Singh O, Singru PS., **2017,** (under review)

CHAPTERS IN BOOKS AND LECTURES NOTES

None

CONFERENCES

1. "TRPV3 as a novel regulator in the mesolimbic-dopamine food reward pathway", **Singh U,** Kumar S, Shelkar G, Kokare DM, Goswami C, Singru PS. *Second meeting of Indian sub-continental branch of the International Neuropeptide Society, NISER, Bhubaneswar, India,* **2015**.

2. "Transient receptor potential vanilloid 3 (TRPV3) in the cerebellum of rat: organization and significance", **Singh U,** Upadhya M, Kokare DM, Goswami CG, Singru PS. *International Symposium and Conference of Indian Academy of Neurosciences, NIMHANS, Bangalore, India*, **2014**.

3. "Organization of dopamine in the forebrain and pituitary of the catfish, *Clarias batrachus*: Relevance to reproduction", **Singh U,** Kumar S, Singru PS. *National Colloquium on Recent Advances in Molecular and Cellular Endocrinology, Department of Zoology, Baranas Hindu University, Varanasi, India*, **2011**.

OTHER PUBLICATIONS (AS CO-AUTHOR)

1. "Transient receptor potential vanilloid 5 (TRPV5), a highly Ca^{2+}-selective TRP channel in the rat brain: relevance to neuroendocrine regulation", Kumar S, **Singh U,** Goswami C, Singru PS, *Journal of Neuroendocrinology,* **2017,** 29, 4, DOI: 10.1111/jne.12466.

2. "Transient receptor potential vanilloid 6 (TRPV6) in the mouse brain: Distribution and estrous cycle-related changes in the hypothalamus", Kumar S, **Singh U,** Singh O, Goswami C, Singru PS., *Neuroscience,* **2017,** 344, 204-216.

3. "Cocaine- and amphetamine-regulated transcript peptide (CART) in the brain of zebra finch, *Taeniopygia guttata*: Organization, interaction with neuropeptide Y, and response to changes in energy status", Singh O, Kumar S, **Singh U**, Kumar V, Lechan RM, Singru PS, *Journal of Comparative Neurology,* **2016,** 524, 3014-3041.

4. "Role of isotocin in regulation of the hypophysiotropic dopamine neurons in the preoptic area of the catfish, *Clarias batrachus"*, Singh O, Kumar S, **Singh U**, Bhute Y, Singru PS. *Journal of Neuroendocrinol*ogy, **2016,** 28, 12, DOI: 10.1111/jne.12441.

5. "Alpha-melanocyte stimulating hormone modulates ethanol self-administration in posterior ventral tegmental area through melanocortin-4 receptors", Shelkar GP, Kale AD, **Singh U**, Singru PS, Subhedar NK, Kokare DM., *Addiction Biology,* **2015,** 20, 302-315.

6. "Interaction between dopamine and neuropeptide Y in the telencephalon of the Indian major carp, *Cirrhinus cirrhosis*", Saha S, Kumar S, **Singh U**, Singh O, Singru PS., *General and Comparative Endocrinology,* **2015,** 220, 78-87.

7. "Sexual dimorphism in the hypophysiotropic tyrosine hydroxylase-positive neurons in the preoptic area of the teleost, *Clarias batrachus*", Saha S, Patil S, **Singh U**, Singh O, Singru PS., *Biology of Sex Differences,* **2015,** 6, 23.

8. "Tyrosine hydroxylase in the olfactory system, forebrain and pituitary of the Indian major carp, *Cirrhinus cirrhosus*: organisation and interaction with neuropeptide Y in the preoptic area", Kumar S, **Singh U**, Saha S, Singru PS., *Journal of Neuroendocrinology*, **2014,** 26, 400-411.

9. "CART peptide in the nucleus accumbens shell acts downstream to dopamine and mediates the reward and reinforcement actions of morphine", Upadhya MA, Nakhate KT,

9. Upadhya MA, Nakhate KT, Kokare DM, **Singh U**, Singru PS, Subhedar NK. (2012). CART peptide in the nucleus accumbens shell acts downstream to dopamine and mediates the reward and reinforcement actions of morphine. *Neuropharmacology* 62, 1823-1833.

10. Ranganathan S, Singh PK, **Singh U**, Singru PS, Padinhateeri R, Maji SK. (2012). Molecular interpretation of ACTH-β-endorphin coaggregation: relevance to secretory granule biogenesis. *PLoS One* 7, e31924.

Uday Singh USingh

Date: 19.05.2017

DEDICATION

With great respect, I dedicate this thesis to my beloved parents who have been the source of inspiration and motivated me to pursue the Ph. D. program. Their guidance and endless support gave me the strength to achieve my goal.

ACKNOWLEDGEMENTS

my thesis writing. I am also thankful to my lab members Mr. Saptarsi, Soham, Sourabh, Aditi, Deepti, and Param for the interactive discussions on general neuroscience, which boosted my interest in neuroscience. Major part of my research work has been conducted in the SBS, transit lab at the Institute of Physics Campus, Bhubaneswar. There was a common lab and several Ph.D. students were working together and helping each other. Tapan and Sanjima were working on the adjacent bench and they took all the necessary steps to maintain a friendly atmosphere in the lab. Their research oriented queries, suggestions, and support helped me. Sanjima and Tapan's presence in the lab during the night and weekends was a great support to work even for longer time, which has helped me to increase my research productivity. I wish to record my special thank to my friends Anoop, Charles, and Sushmita for their support during the stressful time and for sharing the thoughts off the lab.

I am proud to say that I joined the laboratory of Dr. Praful Singru as his first Ph.D student. I was lucky enough that he himself taught me the basics of Neuroanatomy, and was available 24 X 7 for the lab work. His continous efforts and motivation has brought out the best in me.

CONTENTS

Chapter 1: TRPV3 mRNA expression and neuroanatomical organization of the channel

        protein-expressing elements in the brain

Chapter 2: Neurochemical characterization of TRPV3-expressing cells in the hypothalamic

        paraventricular (PVN) and supraoptic (SON) nuclei and its relevance to

        neuroendocrine regulation

Chapter 3: TRPV3 in the ventral tegmental area (VTA) of rat: role in modulation of the mesolimbic-dopamine reward pathway

Chapter 4: Expression of TRPV3 in the cerebellum of rat: significance in motor coordination

ABBREVIATIONS

10N	Dorsal motor nucleus of vagus
12N	Hypoglossal nucleus
A1	A1 noradrenaline cells
A11	A11 dopamine cells
A2	A2 noradrenaline cells
aca	Anterior commissure
Amg	Amygdaloid nucleus
ANS	Accessory neurosecretory nucleus
AH	Anterior hypothalamic area
AP	Area postrema
Aq	Aqueduct
ARC	Arcuate nucleus
AVPe	Anteroventral periventricular nucleus
C	Cerebral cortex
CB	Cerebellum
cc	Corpus callosum
CC	Central canal
CNS	Central nervous system
cp	Cerebral peduncle
csc	Commissure of the superior colliculus
DA	Dopamine
dcs	Dorsal corticospinal tract

DIII	Dorsal 3rd ventricle
fr	Fasciculus retroflexus
DMN	Hypothalamic dorsomedial nucleus
DMNd	DMN, dorsal subdivision
DR	Dorsal raphe nucleus
EW	Edinger-Westphal nucleus
f	Fornix
Hyp	hypothalamus
ic	Internal capsule
IP	Interpeduncular nucleus
IF	Interfascicular nucleus
III	3rd ventricle
IV	4th ventricle
LHA	Lateral hypothalamic area
LV	Lateral ventricle
LC	Locus coeruleus
LR	Lateral recess
ME	Median eminence
M	Medial mammillary nucleus
ml	Medial lemniscus
mlf	Medial longitudinal fasciculus
mp	Mammillary peduncle
MPA	Medial preoptic area

MPOM	Medial preoptic nucleus, medial part
MnPO	Median preoptic nucleus
MPT	Medial pretectal nucleus
MRe	Mammillary recess of the 3rd ventricle
MS	Medial Septum
mt	Mammillothalamic tract
NIc	Nucleus incertus, pars compacta
NId	Nucleus incertus, pars dissipata
NH	Neurohypophysis
NPO	Nucleus preopticus
NPOpv	Paraventricular subdivision of NPO
NPOso	Supraoptic sub-division of NPO
NPP	Nucleus preopticus periventricularis
NPPa	NPP anterior
NPPp	NPP posterior
och	Optic chiasm
opt	Optic tract
ON	Optic nerve
OC	Optic chiasm
PAG	Periaqueductal gray
pc	Posterior commissure
pe	Periventricular hypothalamic nucleus
PH	Posterior hypothalamic nucleus

PHA	Posterior hypothalamic area
PHT	Preoptico-hypophyseal tract
POR	Preoptic recess
PrC	Precommissural nucleus
PVN	Paraventricular nucleus
PVNap	PVN, anterior parvicellular subdivision
PVNdp	PVN, dorsal parvocellular subdivision
PVNlp	PVN, lateral parvocellular subdivision
PVNmp	PVN, medial parvicellular subdivision
PVNpm	PVN, posterior magnocellular subdivision
PVNvp	PVN, ventral parvocellular subdivision
RCh	Retrochiasmatic area
rs	Rubrospinal tract
SCO	Subcommissural organ
scp	Superior cerebellar peduncle
SHy	Septohypothalamic nucleus
SN	Substantia nigra
SNC	SN, compact part
SNCD	SN, compact part, dorsal tier
SNCM	SN, compact part, medial tier
SNL	SN, lateral part
SNR	SN, reticular part
Sol	Nucleus of the solitary tract

SON	Supraoptic nucleus
SOR	SON, retrochiasmatic part
ST	Bed nucleus of stria terminalis
STLV	ST, lateral division, ventral part
STMPL	ST, medial division, postero lateral part
SubB	Sub-brachial nucleus
SuM	Supramammillary nucleus
SuML	SuM, lateral part
SuMM	SuM, medial part
Tz	Nucleus of trapezoid body
TA	Tuberal area
TO	Optic tectum
V	Third ventricle
VDB	Nucleus of vertical limb of diagonal band
vLPAG	Ventrolateral PAG
VLPO	Ventrolateral preoptic nucleus
VMN	Ventromedial hypothalamic nucleus
VMPO	Ventromedial preoptic nucleus
VOLT	Vascular organ of lamina terminalis
VTA	Ventral tegmental area
VTAR	VTA, rostral
PBP	Parabrachial pigmented nucleus of VTA
PIF	Parainterfascicular nucleus of VTA

PN	Paranigral nucleus of VTA
VTM	Ventral tuberomammilary nucleus
aca	Anterior commissure
Acb	Nucleus accumbens
cc	Corpus callosum
Cli	Caudal linear nucleus of the raphe
CNS	Central nervous system
CtB	Cholera toxin b -subunit
DA	Dopamine
fr	Fasciculus retroflexus
GFP	Green fluorescent protein
IF	Interfascicular nucleus
IPR	Interpeduncular nucleus, rostral subnucleus
LV	Lateral ventricle
ml	Medial lemniscus
mp	Mammillary peduncle
PBP	Parabrachial pigmented nucleus of the VTA
PN	Paranigral nucleus of the VTA
Rli	Rostral linear nucleus of the raphe
RMC	Red nucleus, magnocellular part
SN	Substantia nigra
SNC	Substantia nigra, compact part
TH	Tyrosine hydroxylase

TRPV3	Transient receptor potential vanilloid 3
VTA	Ventral tegmental area
aVTA	Anterior VTA
pVTA	Posterior VTA
tVTA	Tail VTA
VTAC	VTA, caudal part
VTAR	VTA, rostral part

SYNOPSIS

The importance of cationic channels in generation and propagation of action potential along the axon, and neurotransmission across the synapse is well documented. Transient receptor potential vanilloid (TRPV) ion channels have emerged as novel component of neuronal signaling and their importance in the brain is being increasingly appreciated in recent years. TRPV subfamily includes six members *viz.* TRPV1-6 [1]. TRPV1-4 are thermosensitive, non-selective cationic channels and are also called as 'thermo TRPs'. On the contrary, TRPV5 and TRPV6 are temperature insensitive but highly Ca^{2+} selective [2]. Growing evidences suggest that the TRPV1-4 ion channels are expressed in the brain and play a role in regulating membrane potential, neurotransmitter release, synaptic plasticity, and Ca^{2+}-mediated cell signaling [2,3]. In spite of these studies, a major constraint in understanding the full functional spectrum of TRPV ion channels has been the lack of information on their neuroanatomical distribution.

Among the members of TRPV subfamily, TRPV3 draws attention since it is activated within range of physiological temperature and its gene is predominantly expressed in the nervous system [4,5]. There are reasons to believe that TRPV3 may play a role in neural regulation. While temperature of distinct brain regions is elevated when the animal is engaged in performing goal-directed behavior [6], the elevated temperature seems to be within the range of activation threshold of TRPV3. Unlike other members of the TRPV subfamily, TRPV3 and TRPV4 are gated by temperature within physiological range. While TRPV4 has wider range of activation threshold (25-43 °C) [7], TRPV3 is activated between 31-39 °C [8,9] and found to be uniquely sensitive around 37 °C [9]. Horvath et al. [10] suggested the existence of thermal synapses in the hypothalamic area and importance of heat in the modulation of neurotransmission. TRPV3 may therefore serve as novel candidate in the processing of information in neural circuits. As yet

only two reports demonstrate TRPV3 expression in the brain [5,9] but the neuroanatomical organization and functional significance of TRPV3 in the brain has remained unexplored.

The relevance of TRPV ion channels in neuroendocrine regulation has been suggested. The magnocellular vasopressin (VP) neurons in the hypothalamus express TRPV1, TRPV2 and TRPV4 and their significance has been tested [2,11–13]. Hypothalamic VP neurons are thermosensitive and showed increased neuronal firing when the temperature is elevated from 36 °C to 38 °C [14]. Interestingly, the supraoptic nucleus neurons which were insensitive to the treatment of TRPV1 agonist, capsaicin at 24 °C responded at the same concentration when the temperature was raised to 36 °C, the activation threshold temperature of TRPV3 [15]. Whether the vasopressin (VP) neurons in the hypothalamus are equipped with thermosensitive TRPV3 and the putative role of this ion channel in the regulation of VP secretion has remained unexplored.

Evidences suggest that TRPV3 may also play a role in the central regulation of behavior. Incensole acetate (IA), a plant derived product identified as TRPV3 agonist exerts anxiolytic effects [16]. TRPV channels are emerging as novel players in the modulation of mesolimbic dopamine (DA) neurons. Recently, capsaicin, has been implicated in the modulation of mesolimbic DA neurons, but the pathway seems to operate *via* presynaptic glutamate release [17]. The monoterpenoids, thymol and carvacrol, the active ingredients of oregano serve as TRPV3 agonists [18,19]. Role of carvacrol in DAergic neurotransmission and reward has recently been suggested [20,21]. While these observations hint at the role of TRPV3 in the modulation of DAergic system, the underlying mechanism and nature of TRPV3-elements driving the mesolimbic-DA reward pathway are not known.

In this background, we explored the organization of TRPV3-equipped cells/fibers in the brain and determined their role in the regulation of hypothalamic neurons, mesolimbic-DA reward pathway, and motor coordination. Experiments were conducted on the adult, male, Sprague-Dawley/Wistar rats and C57/B6 mice. The results are presented in four chapters. In chapter 1, we have described the neuroanatomical organization of TRPV3-expressing elements in the brain of rat. The neurochemical phenotype of TRPV3-expressing cells in the hypothalamus; their response to hyperosmotic challenge and involvement in the somatodendritic release of VP is described in chapter 2. In chapter 3, we present our data on the presence of TRPV3 in DA neurons in the ventral tegmental area (VTA) of rat brain and demonstrate the significance of this channel in the modulation of the mesolimbic-DA food reward pathway. The expression of TRPV3 in the cerebellar Purkinje neurons and importance of TRPV3 in the modulation of motor coordination is presented in chapter 4. A brief outline of the results presented in each chapter is given below.

Chapter 1: TRPV3 mRNA expression and neuroanatomical organization of the channel protein-expressing elements in the brain

TRPV3 mRNA expression was observed in the olfactory bulb, cerebral cortex, hippocampus, hypothalamus, midbrain, brainstem, and cerebellum of rat. TRPV3-immunoreactive neurons and fibers were observed in the medial septum, preoptic area, hypothalamic supraoptic (SON), paraventricular (PVN) nuclei, arcuate, and dorsomedial nuclei. In midbrain, conspicuous TRPV3-immunoreactive neurons were seen in the substantia nigra, ventral tegmental area (VTA), and Edinger-Westphal nucleus. In the brainstem, TRPV3-immunoreactivity was observed in the neurons of nucleus tractus solitarius and cerebellar

Purkinje cells. Application of antisera directed against N- as well as C-terminus TRPV3 revealed similar immunostaining patterns in the rat brain hypothalamus. Analysis of the mouse brain also showed comparable results. Widely distributed TRPV3-elements in the brain suggests a role of these ion channels in the range of CNS functions including, neuroendocrine regulation, energy balance, motor coordination and modulation of mesolimbic reward pathway.

Chapter 2: Neurochemical characterization of TRPV3-expressing cells in the hypothalamic paraventricular (PVN) and supraoptic (SON) nuclei and its relevance to neuroendocrine regulation

The intravenous injection of the retrograde neuronal tracer, fluoro-gold (FG) resulted in labelling of neurons in the PVN and SON. Using double immunofluorescence, majority of the FG-positive neurons in PVN and SON showed TRPV3-immunoreactivity. Majority of TRPV3 equipped VP neurons were observed in the PVN and SON. Rats were given hyperosmotic saline (HS) i.e. drinking water containing 2 % NaCl in place of drinking water and response of TRPV3-expressing VP neurons was studied. HS-treatment stimulated c-Fos expression in TRPV3-expressing VP neurons. Following HS, an unusual expression of synaptic vesicle protein-2 (SV2) and synaptogagmin-1 (SYT-1, v-SNARE complex protein) was observed in the PVN and SON. The SYT-1 and SV2 immunoreactivity was observed in the cell bodies of these neurons. Microtubule associated protein-2 (MAP2)/or glutamic acid decarboxylase (GAD) and Syt-1 double immunofluorescence revealed the presence of SYT-1 in the somatodendritic compartments of PVN and SON neurons. Using retrograde neuronal tracing, the SYT-1-expressing neurons in the hypothalamus seem hypophysiotropic, suggesting engagement of a neuron in axonal as well as somatodendritic neurohormone secretion. Double

immunofluorescence study showed co-expression of SYT-1 and TRPV3 in neurons of the PVN and SON after HS. The expression of SNARE proteins in the cell bodies of TRPV3-expressing VP neurons suggests potential significance of TRPV3 ion channel in the differential regulation of somatodendritic secretions, apart from axonal VP release for osmotic balance.

Chapter 3: TRPV3 in the ventral tegmental area (VTA) of rat: role in modulation of the mesolimbic-dopamine reward pathway

The VTA DA neurons projecting to the nucleus accumbens (Acb) serve an important purpose in the mesolimbic-reward circuitry [22,23] and considered the best characterized, reward pathway in the brain [24,25]. We observed TRPV3 mRNA as well as TRPV3-immunoreactive neurons in the VTA of Wistar rats. We therefore explored whether these ion channels participate in modulating mesolimbic-DA reward pathway. Application of TRPV3 antiserum showed a vast majority of the TRPV3 neurons co-expressing tyrosine hydroxylase (a marker for DA neurons) in the posterior VTA (pVTA) region. Using retrograde neuronal tracing study, a majority of DA neurons projecting to the Acb Shell co-expressed TRPV3. While *ex vivo* treatment of midbrain slices with thymol increased $[Ca^{2+}]_i$-activity in pVTA neurons, intra-pVTA injections of thymol in freely-moving, satiated rats enhanced positive reinforcement for active lever pressings in an operant chamber to self-administer sweet pellets. This behavior was attenuated by prior treatment with DA D_1- and D_2-like receptor-antagonists. These results demonstrate a role for TRPV3 in modulating mesolimbic-DA food-reward pathway, and underscore the importance of TRPV channels in the VTA as key components in reward processing.

Chapter 4: Expression of TRPV3 in the cerebellum of rat: significance in motor coordination

Using double immunofluorescence, calbindin D28k-positive Purkinje neurons in the cerebellum of rat showed co-expression of TRPV3. All the calbindin D28k-positive Purkinje neurons were TRPV3 immunoreactive. Infusion of TRPV3 inhibitor directly into the cerebellum resulted in a significant alteration in behaviors including walking pattern, decreased locomotor count, and number of crossover.

Major findings of the thesis:

1. TRPV3-equipped elements are widely distributed in the brain.

2. TRPV3 may serve as a potential Ca^{2+} entry channel for axon terminal/somatodendritc secretion of VP from hypothalamic neuroendocrine neurons during osmotic challenge.

3. DA neurons in VTA are equipped with TRPV3 and activation of this channel in VTA drives the mesolimbic-DA food reward pathway.

4. TRPV3 may regulate cerebellar Purkinje neurons and control motor coordination.

LIST OF FIGURES

Chapter 3

Chapter 4

LIST OF TABLES

GENERAL INTRODUCTION

Neurons integrate complex synaptic inputs; translate these into action potentials which finally culminates in neurotransmission [26,27]. Dendrites along with cell body serve as primary sites for integration of the synaptic inputs [26,27]. The pioneering work carried out during 1950-1960s has provided a basic understanding about the mechanism of generation and propagation of action potential [28–33]. In 1952, Alan Hodgkin and Andrew Huxley measured the ionic conductance and current in squid axon, and proposed the ionic basis of initiation and propagation of action potential [34–36]. Evidence suggests the existence of an electrical filtering process at dendritic arborization, formation of miniature electrical currents, their conversion into electrical excitation [31,32]. The sub-threshold miniature excitatory postsynaptic potentials generated at dendritic sites has been shown to activate the cationic channels [37–41]. This was further substantiated by a series of experiments suggesting the involvement of voltage-sensitive ion channels (Na^+ and K^+ channels) in the generation and propagation of action potential [26,27,39,42–44].

Ca^{2+} ions play a crucial role in intracellular signaling cascade [45–47]. It acts as secondary messenger and connects complex extracellular signals essential for the regulation of cellular functions [46,47]. Although the intracellular concentration of Ca^{2+} ions (0.1 µM) is lower than extracellular Ca^{2+} ions (1-2 mM), higher Ca^{2+} levels are observed in the endoplasmic reticulum, lysosomes and mitochondria [47,48]. The Ca^{2+} ATPase and the internal stores of Ca^{2+} ions are responsible to maintain the concentration gradient of these ions at the cellular level [49]. In neurons, Ca^{2+} ions plays an important role in action potential, neurotransmission at synapse, somato-dendritic release of neurotransmitters, and intracellular signaling [46,47]. In addition to

the voltage-gated Ca^{2+} channels (VOCC), three other proteins allow Ca^{2+} ions entry inside the cell [50]. The neuronal acteylcholine receptors, ionotropic glutamate receptors (NMDA and AMPA), and the cyclic nucleotide gated channels show significant permeability for Ca^{2+} ions [50]. The extracellular ATP acts on P2X receptors (purinergic receptor); these receptors serve as cationic channels and regulate intracellular Ca^{2+} ions [50]. The store-operated Ca^{2+} entry (SOCE) is also known as capacitive Ca^{2+} entry which opens a Ca^{2+} influx after intracellular Ca^{2+} stores are depleted [50]. Among a range of ion channels recruited on neurons, the importance of yet another set of interesting cationic channels known as transient receptor potential (TRP) ion channels in neuronal function is emerging [51–53]. These ion channels have been suggested as important component in cellular excitability in neurons whereas in non-excitable cells these ion channels are known to regulate diverse functions ranging from Ca^{2+} homeostasis to chemical release [53]. In neuronal cells these ions channels play a role in neurotransmission, cellular signaling, and their presence and role in the CNS and neuronal function is increasingly being appreciated [2].

TRP is a family of ion channels, initially cloned from *Drosophila melanogaster* [54]. It was referred as TRP since the mutation at *trp* locus resulted in transient potential response to light illuminated insect photoreceptor cells [54]. TRP channels are Ca^{2+} permeable ion channels since mutation at *trp* locus decreases Ca^{2+} permeability in the photoreceptor cells [55]. Presence of TRP channels have been described in different organisms including algae, insect, yeast, frog, chicken, zebrafish, mice, rat, and humans [45,56–62]. These channels are interesting due to their thermosensitive nature and modulation by a range of stimuli including mechanical, chemical, and changes in pH, and these properties seems evolutionary conserved [60–63]. The mammalian

TRP ion channels superfamily comprises of six sub-families *viz.* TRP ankyrin (TRPA), TRP canonical (TRPC), TRP melastin (TRPM), TRP mucolipin (TRPML), TRP polycystin (TRPP), and TRP vanilloid (TRPV) [1,64,65].

Mammalian TRP ion channels are ubiquitously expressed and possess different splice variants [66–68]. Most of the cell types seem to express specific TRP ion channels which correlate with the cellular function [69]. While it is generally believed that the activation of TRP channels leads to Ca^{2+} permeation, several members of this family contribute to only a small fraction of Ca^{2+} currents. For example TRPV1 and TRPM8 have been shown to contribute approximately 5 and 3 % fraction of Ca^{2+} currents, respectively [70]. The channels like TRPV5 and TRPV6 along with TRPA1 and TRPM3 possess higher selectivity for Ca^{2+} ions [71]. In excitable cells including neurons, the TRP ion channels belonging to the TRPC and TRPV subfamily have been suggested to play a role in the electrical firing [2,72,73].

TRPV subfamily

Based upon the structural and biophysical properties, six members of the mammalian TRPV subfamily *viz.* TRPV1, TRPV2, TRPV3, TRPV4, TRPV5, and TRPV6 have been identified [60,74,75]. TRPV1-4 are non-selective cation channels and known as 'thermo TRPs' due their gating by temperature and are also activated by other endogenous and exogenous stimuli [74,76–78]. In contrast, TPRV5 and TRPV6 are temperature insensitive but are highly Ca^{2+} selective [2,73,79]. Compared to the permeability ratio (P_{Ca}/P_{Na}~1-10) of TRPV1-4, TRPV5-6 possesses high permeability ratio (P_{Ca}/P_{Na} >100) [73].

Distribution of TRPV ion channels in the brain

Evidence suggests that the TRPV1-4 ion channels are expressed in the brain [2,80]. Although the relevance of these ion channels in neural regulation has been suggested, advancement in the field is limited due to the non-availability of in-depth information of the regions of the brain expressing TRPV. Expression of TRPV1-4 ion channels in the brain has been demonstrated using a range of techniques including immunohistochemistry, *in situ* hybridization, radio ligand binding, and RT-PCR [81–85]. The distribution of TRPV-immunoreactive elements in the brain is shown in Figure 1.

TRPV1-expressing elements were observed in the cortex, limbic system, striatum, preoptic area, hypothalamus, thalamus, midbrain, reticular formation, locus coeruleus, cerebellum, and inferior olive of rat (Fig. 1A) [85]. TRPV2-expressing cells were seen in the forebrain, preoptic area, hypothalamus and brainstem of rat (Fig. 1B) [12] and in the hypothalamus of macaque, *Macaca fascicularis* [13]. In rat brain, TRPV3-immunoreactivity was observed in the nucleus of solitary tract (NTS) (Fig. 1C) [86]. TRPV4 immunoreactive elements were observed in the cerebral cortex, organum vasculosum of laminae terminalis (OVLT), thalamus, hippocampus, and cerebellum of rat (Fig. 1D) [7,87]. Information about the neuroanatomical distribution of the highly selective Ca^{2+} ion channels *viz.* TRPV5 and TRPV6 in the brain is not available (Fig. 1E and F).

Importance of TRPV ion channels in osmoregulation

Ca^{2+} ions trigger the release of peptides from the hypothalamic magnocellular neurosecretory cells (MNC) into the neurohypophysial portal system during parturition, diuresis, and lactation [88,89]. A schematic representation of the neurophypophysial system is given in
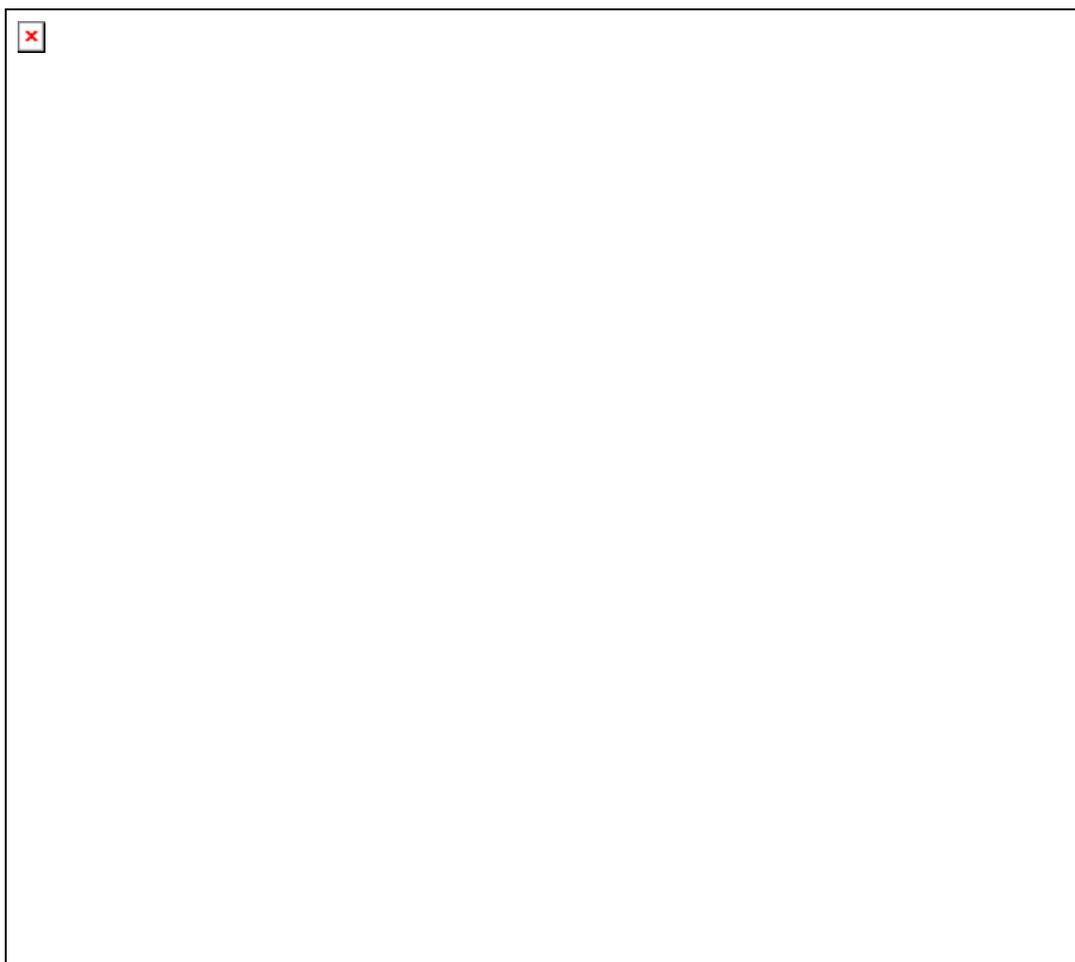
Figure 1: Distribution of TRPV1-6 ion channels in the rat brain.
Schematics depicting the distribution of (A) TRPV1, (B) TRPV2, (C) TRPV3, (D) TRPV4, (E) TRPV5, and (F) TRPV6 ion channels in the rat brain. The schematic of the brain were redrawn from the rat brain atlas [150]. The available information on distribution of each ion channel in the brain is depicted in A-D (TRPV1 [83]; TRPV2: [12]; TRPV3: [86]; TRPV4: [7,87]. TRPV1-4 ion channels are thermosensitive, non-selective cation channels. The temperature (*T*) threshold and permeability (*P*) ratio of each TRPV ion channel [2] is given below the respective schematic. TRPV5 and TRPV6 are insensitive to temperature but are highly permeable to Ca^{2+} ions. The neuroanatomical distribution of TRPV1, TRPV2 and TRPV4 ion channels in the brain is well established, but the relevant aspect about TRPV3 and TRPV5/6 has remained unexplored.

Figure 2. The influx of Ca^{2+} ions across MNC membrane is mediated by a range of cation permeable ion channels [89,90]. Recently the members of TRPV subfamily have emerged as novel candidates for Ca^{2+} entry in a range of cells [91]. Both *in vitro* and *in vivo* studies supports the functional significance of TRPV channels in the regulation of osmotic homeostasis, and the role of TRPV ion channels as osmoceptors has been suggested [11–14]. The presence of N-terminal splice variant of the TRPV1 in the hypothalamic supraoptic nucleus (SON) neurons has been shown to play a role in osmosensory transduction during hyperosmotic stimulation [92]. In another study, Sharif-Naeini et al [14] observed that the thermal stimuli equivalent of core body temperature activates TRPV1 ion channels in the VP neurons. The study has defined the thermosensitive nature of VP neurons and elucidated the mechanism of VP release during thermal challenge. In addition, VP neurons in the hypothalamus of rat also express TRPV2 [11,12] and TRPV4 [11]. It has been suggested that the TRPV1 and/or TRPV4 are not the only channels by which brain responds to systemic osmotic changes [93]. In view of this, exploring the relevance of other members of the TRPV subfamily in the regulation of VP neurons seems important to understand their role in the hypophysiotropic regulation.

TRPV ion channels at synapse

Recent evidences have demonstrated the co-expression of TRPV1 and synaptophysin, a presynaptic protein, in the cultured sensory neurons; and activation of glutamatergic nerve terminals with capsaicin enhanced neurotransmitter secretion [2,94]. Similar results showing expression of TRPV channels in presynaptic terminal are reported in the brain regions including
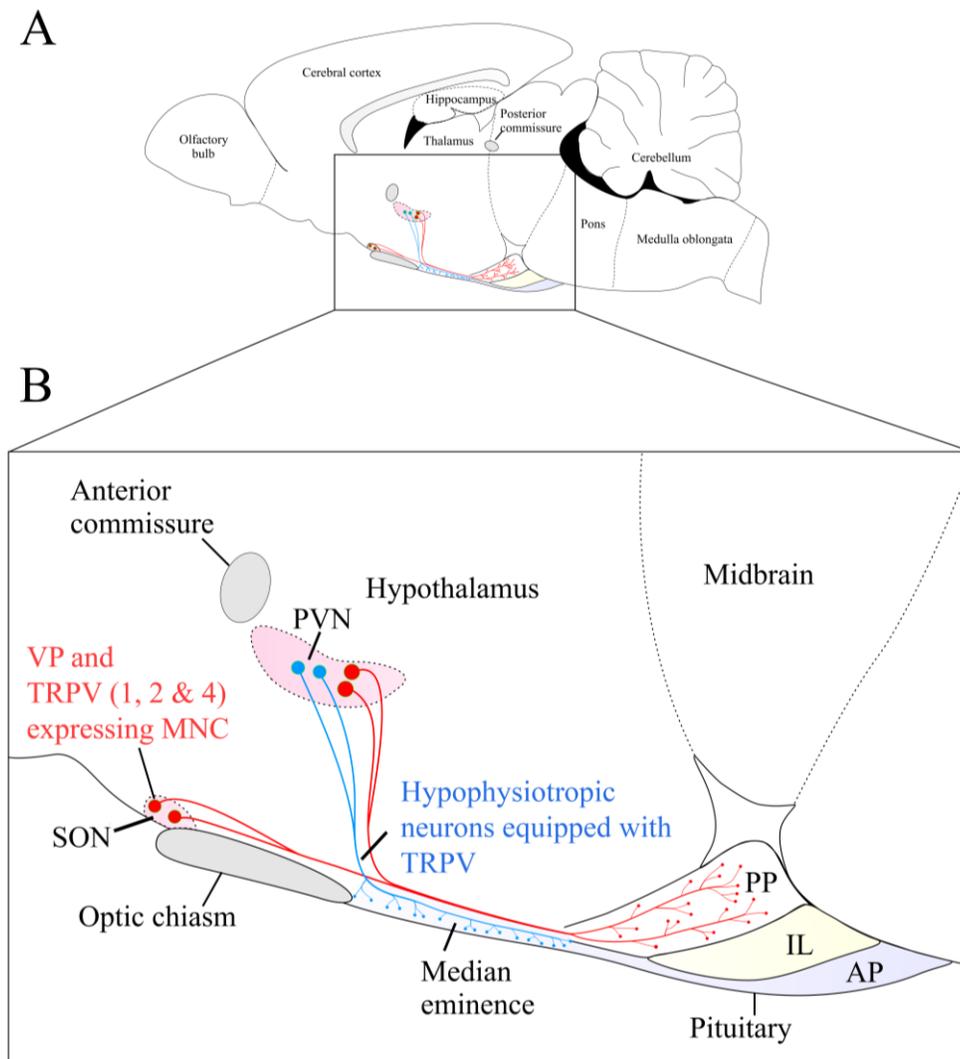
Figure 2: The hypophysiotropic neurosecretory system in the hypothalamus.
(A) Schematic showing the projections of hypophysiotropic neurosecretory neurons from the hypothalamic paraventricular (PVN) and supraoptic nuclei (SON). The schematic showing sagittal view of the rat brain was redrawn from the rat brain atlas [150]. (B) Magnified view of the region shown in rectangle in the upper panel is shown below. PVN harbors two populations of neurons *viz*. magnocellular neurosecretory cells (MNC; red) and parvocellular cells (blue). SON also contains MNC. Both MNC and parvocellular neurons are hypophysiotropic. Neurons in the parcocellular subdivision of the PVN projects to the external zone of the median eminence (ME) and release their content into the portal capillaries. The secreted neurohormone/releasing factors are then carried to the anterior pituitary. Oxytocin and vasopressin (VP) expressing MNC population directly release their secretion in the posterior pituitary. MNC in PVN and SON express TRPV1, TRPV2, and TRPV4 ion channels [11–14]. TRPV1/V2 is positive and TRPV4 is negative regulator of vasopressin secretion. AP, anterior pituitary; IL, intermediate lobe; PP, posterior pituitary.

the hippocampus, preoptic area, and midbrain [2,17]. The expression of TRPV ion channels at synapse and their role in neurotransmission is described in Figure 3.

TRPV ion channels at synapse

Recent evidences have demonstrated the co-expression of TRPV1 and synaptophysin, a presynaptic protein, in the cultured sensory neurons; and activation of glutamatergic nerve terminals with capsaicin enhanced neurotransmitter secretion [2,94]. Similar results showing expression of TRPV channels in presynaptic terminal are reported in the brain regions including the hippocampus, preoptic area, and midbrain [2,17]. The expression of TRPV ion channels at synapse and their role in neurotransmission is described in Figure 3.

Temperature and 'Thermo' TRP ion channels in neurotransmission

In vivo thermal stimulations and brain lesion studies revealed that the brain possesses regulatory centres in the hypothalamus, brainstem and spinal cord to maintain thermal homeostasis [95]. Recently, the VP neurons of SON have been suggested as thermosensitive [14]. While, temperature seems essential to regulate water loss in sweating during elevated body temperature and to maintain osmotic balance [14], an increase in the firing frequency of VP neurons at 39 °C [14]. Horvath et al. [10] has demonstrated the existence of thermal synapses in the hypothalamus and underscored the importance of heat in the modulation of neurotransmission. Among the members of TRPV subfamily, TRPV3 is interesting. It is activated within physiological temperature range and uniquely sensitive around 37 °C [5,9]. 'Thermo' TRPV ion channels may serve as potential candidates in the neural circuits to regulate temperature-induced CNS functions. This phenomenon has been demonstrated for substantia

nigra (SN) neurons in the midbrain [4]. Guatteo et al. [4] observed that the elevation of temperature in physiological range is responsible for increased neuronal firing and Ca^{2+} influx in dopamine neurons in SN. The authors further suggested that the temperature sensitive TRPV3/V4 ion channels are involved in mediating this response [4].

Structural and physical properties of TRPV3 ion channel

TRPV3 shares 43 % sequence homology with TRPV1 [5,9]. Similar to other members in the TRPV subfamily, TRPV3 subunits seem to interact and form a functional tetrameric ion channel with other TRPV channels [5]. The tetrameric arrangement might be arise due to the interaction between isoforms or subunits from different members of the TRPV subfamily [96]. Based upon sequence similarity among TRPV subfamily members, each TRPV3 subunit seems to consists of six transmembrane (TM1-6) spanning segments and a cytosol facing segment from N- and C- terminals respectively [97]. While TM1-4 adhere the channel to the membrane, TM5-6 form the functional cation conducting channel [97]. The N-terminal region possesses an ankyrin repeat domain (ARD). Each domain is known to contain 3-6 ARD repeats [62] and conserved binding sites for ATP and calmodulin [97]. The mutagenesis study of the ARD domain revealed that the finger 3 of TRPV3-ARD is necessary of physiological activity [98].

TRPV3 interacting partners including calmodulin (CaM), epithelial growth factor receptor (EGFR), and TRPV1 have been identified [5,57,97,99]. The functional properties of heteromeric channel are different from the channel which has homomeric arrangement [96]. Due to heteromeric structure, there seems to be a shift in the conductance and voltage dependence [96]. In addition, the heteromeric channels are sensitive to both temperature, and capsaicin [96,100].
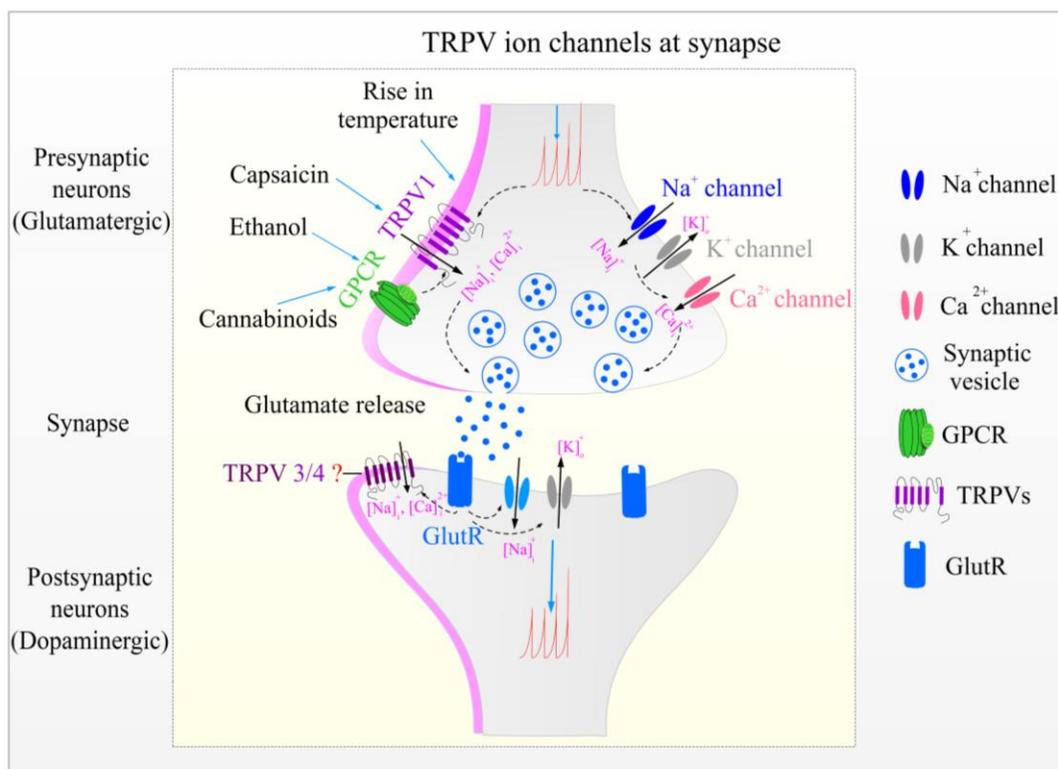
Figure 3: Significance of TRPV ion channels in synaptic transmission.
Diagrammatic representation of a synapse in the midbrain. The presynaptic neuron contributing to this synapse is glutamatergic in nature, whereas the postsynaptic neuron is dopaminergic (DAergic). In addition to the classical cation channels *viz.* Na^+, K^+, and Ca^{2+}, the presynaptic terminal is also equipped with TRPV1 [17] and its activation by capsaicin modulates glutamate release. Activated channels through calcium signaling may drive the fusion of synaptic vesicle, release of glutamate, and regulate DAergic neurons. Glutamate may regulate activity of the DA neurons *via* glutamate receptors. At presynaptic terminal ethanol and endocannabinoids may modulate the TRPV1 ion channel function by GPCR coupling. The increase in TRPV3/4 activity in the postsynaptic neuron by elevated temperature [4] may serve as an additional regulatory mechanism for the regulation for the DAergic neurons.

Apart from the chemical agonist-induced activation, temperature and voltage sensation are two unique features of TRPV3 [9,98]. Generally, TRP-related voltage-gated ion channels sense the membrane potential through positively charged residues in the fourth transmembrane domain; undergo the conformational change in the nearby pore forming domain which can directly gate the channel [101,102]. Similar mechanism might be applicable for TRPV3. Through random mutagenesis, TM6 and the adjacent extracellular loop have been shown necessary for temperature sensation [100]. It is speculated that due to proximity with the pore region the temperature-induced conformational change in TM6 and extracellular loop may gate the channel [100].

The permeability of TRPV3 to Ca^{2+} ions is in moderate range (P_{Ca}/P_{Na} ratio is ∼ 10) [73]. Since the channel is permeable to Na^+ and Ca^{2+}, negatively charged amino acids plays an important role in cation permeability through the channel pore [103]. Like other members in the TRPV subfamily, TRPV3 display an unusually high conductance at specific temperature range. Chung et al. [104] observed that at 39 °C the TRPV3 conductance increases dramatically. While the other members of TRPV subfamily show desensitization upon repeated stimulation, it potentiates the activity of TRPV3 [9,104–106]. Additionally, TRPV3 also showed cross sensitization by different modulators *viz.* ATP, protein kinase C, and proinflammatory agents [9,97,106,107]. Both ATP and calmodulin bind to ARD of TRPV1 and TRPV3 but their activation properties are different [98]. The repetitive stimulations with these modulators desensitizes TRPV1 but has sensitizing effects on TRPV3 [107]. Based upon the available evidences, an overview of TRPV3 ion channel signaling cascade in excitable and non-excitable cells is shown in Figure 4.
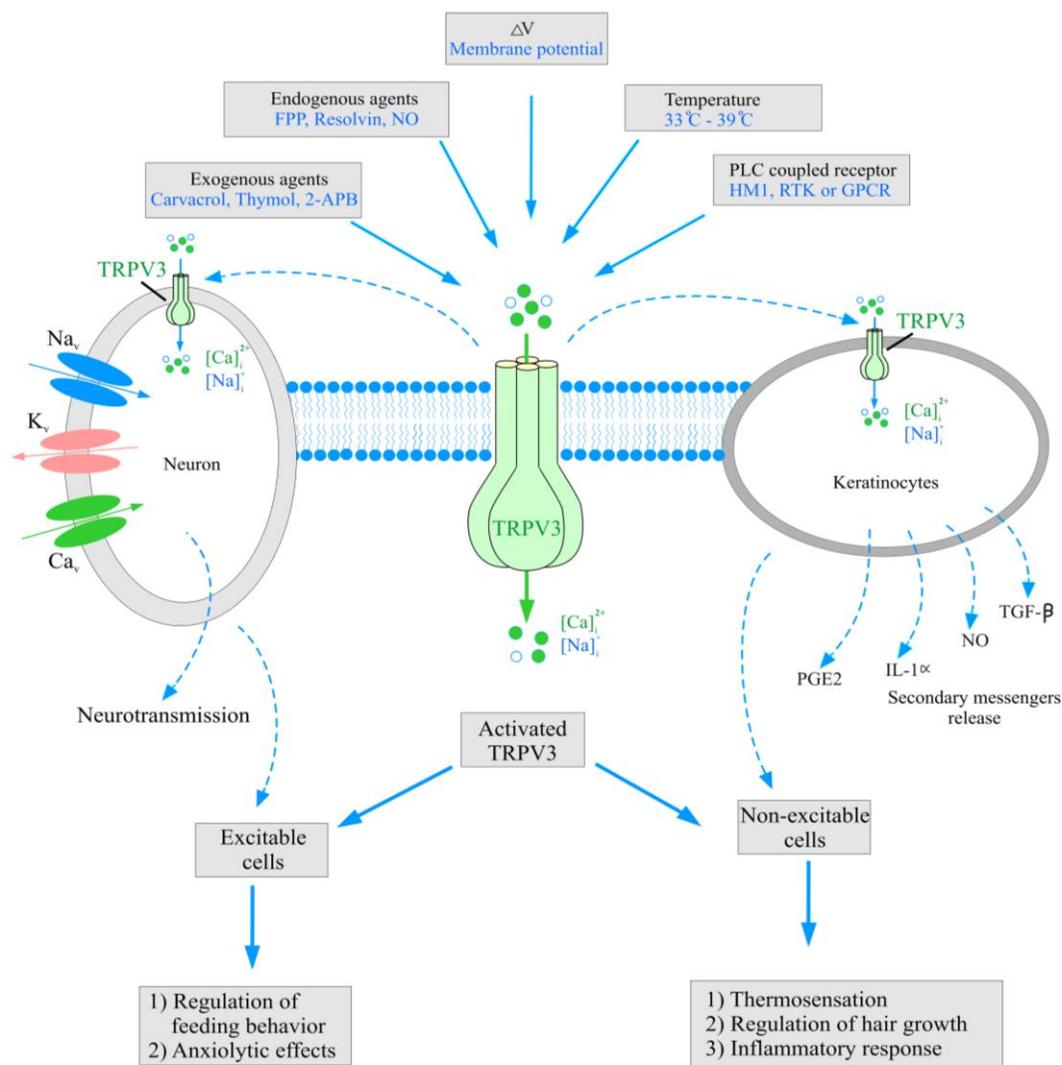
Figure 4: TRPV3 ion channel mediated signaling.
Schematic representation of TRPV3-mediated cellular signaling cascade based on Nilius and Bíró [108]. TRPV3 is expressed in the neurons [86] and peripheral cells (keratinocytes, oral, and nasal epithelium [5]. Activity of TRPV3 can be regulated or potentiated by a range of exogenous or endogenous intracellular modulators. Exogenous agents include monoterpenoids (carvacrol, thymol, eugenol) and synthetic 2-Aminoethyl diphenylborinate (2-APB). Endogenous agents are metabolic byproducts *viz.* farnesyl pyrophosphate (FPP), isopentenyl pyrophosphate (IPP), resolvin, and nitric oxide (NO). TRPV3 currents can also be activated or potentiated by intracellular signaling driven by G-protein-coupled receptors (GPCRs), receptor tyrosine kinases (RTK), and human muscarinic subtype-1 receptor (HM1). TRPV3 is also responsive to thermal changes and membrane potential difference (ΔV). In keratinocytes, the activated TRPV3 brings Ca^{2+} ions in the cell which modulates the release of effectors molecules *viz.* interleukin 1 alpha (IL-1α), adenosine triphosphate (ATP), transforming growth factor beta (TGF-β) and prostaglandin E2 (PGE2). These molecules regulate peripheral thermosensation and skin functions. TRPV3 may play a role in the oral and nasal epithelium as sensor of flavoring compounds and regulation of behavior.

TRPV3 in health and diseases

Abnormalities in the critical domains of TRPV3 lead to multiple human diseases [97,108]. Our understanding about the functional significance of TRPV3 is limited to the peripheral sense organs [97]. Form cell division to cell death, TRPV3 regulates keratinocytes functions [103,109–111]. In rodents and humans, TRPV3 has been shown to play a role in hair morphogenesis and hair follicle cycling [112–115]. Increased TRPV3 activity due to 'gain-of-function' mutations leads to Olmsted syndrome in humans [116,117]. In this major form of cutaneous channelopathy, three mutations (Gly573Ser, Gly573Cys and Trp692Gly) in the C-terminal region of the TRPV3 channel seem important [116,117]. Physiologically upon activation in the keratinocytes, TRPV3 promotes the release of algogenic and pruritogenic substances *viz.* interleukins, ATP and PGE2. These substances act locally to stimulate nearby sensory processes in the skin to induce pain and itch [19,99,118,119]. The itch-related behavior was suppressed in TRPV3 knockout animals [120].

Evolutionary aspect of TRPV3

To study the impact of evolutionary drive on 'thermo' TRPs the comparative analysis of mammalian 'thermo' TRP homolog was performed from the genome sequence database of various vertebrates species [121]. While the N- and C- terminal regions of mammalian TRPV3 are incomplete in the western clawed, TRPV3 homolog in frog neither gets activated with known TRPV3 agonist nor with temperature [121]. Further, the fusion of N- and C- terminal regions of mouse TRPV3 with central portion of western clawed frog TRPV3 protein has resulted in restoration of the chemical and temperature sensitivity [100]. Similar phenomenon of temperature sensitivity has also been reported among other TRP channels. While TRPA1 is

thermosensitive in certain snake and insect species, TRPA1 in mouse is sensitive to cold temperature [122,123]. Similarly, TRPM8 is a cold sensitive channel but the activation threshold of this channel in western and African clawed frog is lower than that of TRPM8 of rat and chicken [124]. Similar to higher vertebrates TRPV3 is highly expressed in frog skin and the physiological function is likely to sense noxious cold temperature [121]. Therefore it is suggested that the shift in temperature sensitivity might be due to the environmental and physiological requirements for survival during evolution [121].

Regulation of TRPV3 ion channel

In vitro studies on keratinocytes and *in vivo* studies in mice have demonstrated that certain phenolic compounds like monoterpenoids *viz.* carvacrol, thymol, and thymol serve as potent activators of TRPV3 [19,20]. Incensole and incensole acetate (IA) from *Boswellia papyrifera* are diterpenic cembrenoids represent a class of natural TRPV3 activators [16]. While IA showed anxiolytic- and antidepressive-like behaviors, these behaviors were absent in TRPV3 knockout mice [16,125,126]. Additionally, certain bioactive cannabinoids such as cannabidiol and tetrahydrocannabivarin (THCV) also serve as TRPV3 activators [127].

Importance of endogenous intermediate molecules produced in the cholesterol synthesis pathway have been suggested as novel TRPV3 regulators [128]. Farnesyl pyrophosphate (FPP) serve as TRPV3-agonist and endogenous pain producing molecule [129]. Inositol pyrophosphate (IPP) is an endogenous TRPA1 and TRPV3 inhibitor [130]. In *in vivo* model system FPP-induced pain was ameliorated by pretreatment with ruthenium red or knockdown of TRPV3 [129]. Local application of IPP attenuated TRPV3 agonist-induced acute pain and rescued mechanical and thermal hypersensitivity in inflamed animals [130]. Hu et al [131] demonstrated

another class of endogenous biomolecules known as arachidonic acid (AA), which potentiates TRPV3-induced current. AA also elevates cross sensitization due to different stimuli *viz.* 2-APB [131]. Recently, the occurrence of other endogenously derived TRPV3 lipid inhibitor resolvin *viz.* 17R-RvD1, a product of omega-3 lipid metabolism has been described which display antinociceptic properties [132–134]. Locally administered 17R-RvD1 showed analgesic effects in both the heat and FPP-induced nociception [135].

Recent studies have demonstrated the importance of ATP, Ca^{2+} ions, Mg^{2+} ions, calmodulin (CaM), phosphoinositieds, and free fatty acids as endogenous modulators of TRPV channels [136–139]. ATP has high affinity for TRPV-ARD and is sensitive to divalent Ca^{2+} ions concentration. Ca^{2+} ions regulate TRPV3 from either side of the plasma membrane. From the extracellular side, Ca^{2+} inhibits TRPV3 by binding to Asp-641 at the pore loop and this residue gates the channel by high affinity binding to Ca^{2+} ions that enter the pore [106]. Intracellularly, Ca^{2+}-CaM binds to the CaM binding site at N-terminus in the ARD of TRPV3 [106]. The mutations that disrupts the CaM binding site has been shown to abolish the sensitization effect in TRPV3 expressing cells [106]. In experimental model of atopic dermatitis, Mg^{2+} ions deficiency leads to scratching behavior [140–142]. Additionally, the naturally occurring gain-of-function point mutations are associated with spontaneous dermatitis due to constitutive activation of TRPV3 [106,112,143,144]. It has been suggested that the Mg^{2+} ions negatively regulate TRPV3 ion channel and gating mechanism is voltage depended [145]. In mouse epidermal keratinocytes, single aspartic acid residue (D641) toward the extracellular pore loop and two amino acid residues (E679, E682) in the intracellular pore region rescued the inhibitory effect of Mg^{2+} ions [145]. This mechanism is in contrast to that of TRPV1 where extracellular Mg^{2+} sensitized the channel [146].

The activation threshold of TRPV3 lies in between 33-39 °C, therefore it was proposed to be a warm sensory receptor in the skin [5,9]. The temperature sensing property was assigned to the TM6 and pore region of functional ion channel [100]. The mechanism underlying the thermosensation involve structural changes and accessibility of critical amino acids Ile652 and Leu655 in the pore region of the channel at ~30 °C or above [147]. Upon activation, TRPV3 equipped keratinocytes releases secondary messengers like ATP, which then activates thermosensory nerve fibers of the dorsal root ganglion (DRG) neurons [119]. Contrary to this, the TRPV3 deficient mice showed no thermal preference upon conditioning behavior [148]. Altogether, TRPV3 may serve as polymodal receptor where multiple environmental stimuli converge to transduce extracellular information into intracellular signals. Topological structure and the modulatory agents of TRPV3, and their importance in the regulation of crucial biological functions are summarized in Figure 5.

TRPV3 therefore is an important ion channel recruited in the peripheral systems and has emerged as novel player in their regulation. Although accruing data underscores the importance of other TRPV ion channels in neural regulation, in-depth analysis of the organization of TRPV3- expressing neurons in the brain and their functional significance remained unexplored. In this background, I explored the organization of TRPV3-equipped cells/fibers in the brain, and determined the role of these ion channels in the regulation of hypothalamic neurons, mesolimbic-dopamine reward pathway, and motor coordination.
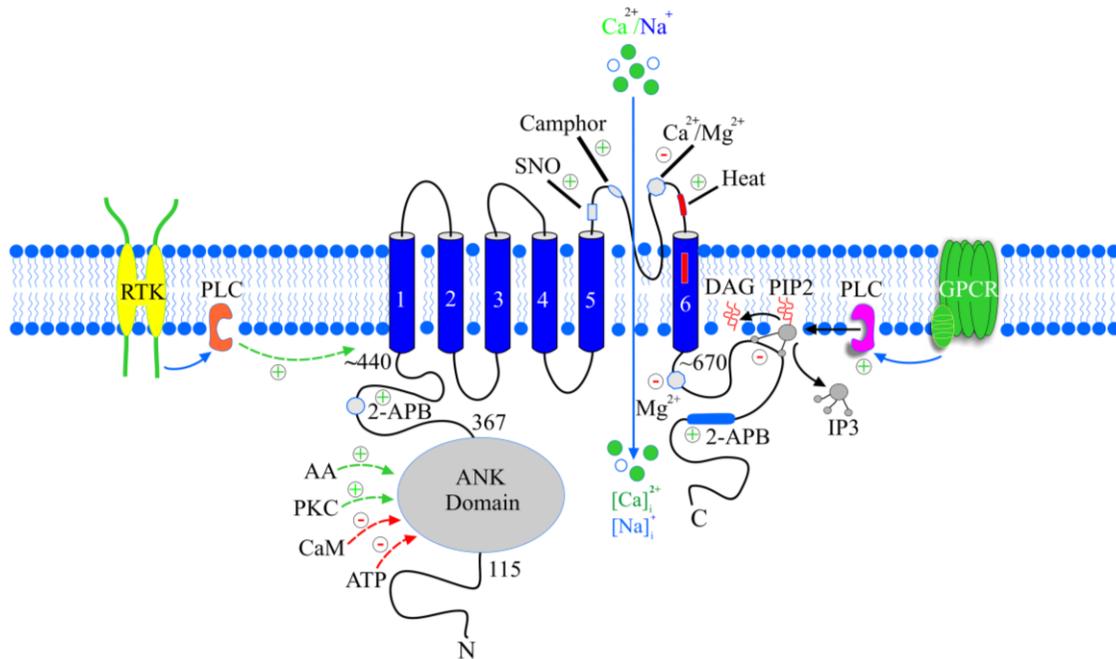
Figure 5: Topological structure of TRPV3 and its regulatory sites.
TRPV3 is a tetrameric channel whose monomeric subunits comprises of 1-6 transmembrane (TM1-TM6) spanning segments and N- and C-terminal domains. The channel pore is located between the TM5 and TM6 and their connecting loop acts as selective filter. The connecting pore loop is direct sensor for exogenous plant derived agent *viz.* camphor, thermal stimulus and endogenous S-nitrosylation (SNO) post-translation modification. The N-terminal domain plays an important role in protein-protein interactions. TRPV3 is positively regulated by 2-aminoethoxydiphenyl borate (2-APB), arachidonic acid (AA), and protein kinase C (PKC) acting at N-terminus. Calmodulin (CaM) and adenosine triphosphate (ATP) interacts at ankyrin repeat domain (ARD), and Ca^{2+}/Mg^{2+} ions binding on the both sides of pore loop negatively regulate the channel. In addition, the G-protein-coupled receptors (GPCRs) and receptor tyrosine kinases (RTK) via intracellular phospholipase C (PLC) positively regulate the channel activity. Upon activation, TRPV3 brings Ca^{2+} ions in the cell and transduce the signal for downstream actions [99]. PIP2, Phosphatidylinositol 4,5-bisphosphate; DAG, diacylglycerol; IP3, Inositol triphosphate (Adapted with modification form [99]).

PLAN OF WORK

Experiments were conducted on the adult, male, Sprague Dwaley/Wistar rats, C57/B6 mice, and adult catfish, *Clarias batrachus*. The results are presented in following four chapters.

(1) TRPV3 mRNA expression and neuroanatomical organization of the channel protein-expressing elements in the brain.

(2) Neurochemical characterization of TRPV3-expressing cells in the hypothalamic paraventricular (PVN) and supraoptic (SON) nuclei, its relevance to neuroendocrine regulation, and evolutionary significance.

(3) TRPV3 in the ventral tegmental area (VTA) of rat: role in modulation of the mesolimbic-dopamine reward pathway.

(4) Expression of TRPV3 in the cerebellum of rat: significance in motor coordination.

The chapter 1 deals with neuroanatomical mapping of TRPV3-expressing elements in the brain of rat and mouse. In chapter 2, the neurochemical phenotype of TRPV3-expressing cells in the hypothalamus, their response to hyperosmotic challenge, and involvement in somatodendritic release of vasopressin is described. We have also explored the relevance of TRPV3 in neuroendocrine regulation of a teleost fish. In chapter 3, we present our data on the involvement of TRPV3 in the modulation of mesolimbic-DA food reward pathway and demonstrate the significance of this ion channel in the modulation of the reward circuitry. The presence of TRPV3 ion channel in cerebellar Purkinje neurons and role in motor coordination is described in chapter 4.

CHAPTER 1

TRPV3 mRNA expression and neuroanatomical organization of the channel protein-expressing elements in the brain

INTRODUCTION

Growing evidence suggest that the TRPV1-4 ion channels are expressed in the brain and play a role in neural regulation including membrane potential, neurotransmitter release, synaptic plasticity, and Ca^{2+}-mediated cell signalling [2,80]. The neurons expressing TRPV1, TRPV2 and TRPV4 have been described in the brain of rodents [11,12,81,83], human [83], and hypothalamus of macaque [13].

Among the members of TRPV subfamily, TRPV3 draws attention since it is activated within range of physiological temperature and its gene is predominantly expressed in the nervous system [4,5]. As yet only two reports demonstrate TRPV3 expression in the brain [5,9]. *In situ* hybridization revealed the TRPV3 expression in the cortex, thalamus, dorsal spinal cord, trigeminal ganglion, superior cervical ganglion and dorsal root ganglion of monkey [5]. Caterina [3] highlighted the lack of information of the organization of TRPV3 elements in the hypothalamus. Horvath et al. [10] suggested the existence of thermal synapses in the hypothalamic area and importance of heat in the modulation of neurotransmission. Studies exploring the functional significance of TRPV3 in the brain are limited. Intraperitoneal administration of incensole acetate, a TRPV3 agonist, resulted in c-Fos activation in different regions of the brain and the agent seem to be anxiolytic [16]. TRPV3 may therefore serve as novel candidate in the processing of information in neural circuits. In spite of these early clues, the neuroanatomical organization and functional significance of TRPV3 in the brain has remained unexplored.

In this background, we explored the presence and functional significance of TRPV3 in the CNS of adult, male, Sprague-Dawley/Wistar rats and C57/B6 mice. While the rat is used as model in a range of pharmacological and behavioural studies, mice is useful for studying the effect of knocking out a gene on physiology and behaviour. Exploring the neuroanatomical

organization of TRPV3 in the brain of rat and mice might be useful to study the functional significance of these ions channel in the brain. We employed RT-PCR analysis, to study the TRPV3 mRNA expression in different regions of rat brain. Immunofluorescence using TRPV3 specific antiserum raised against N- terminal TRPV3 was employed to study the neuroanatomical organization of TRPV3-equipped cells/fibers in the brain of rat and mice. To determine the specificity of the TRPV3 antiserum stringent control procedures including transfection of the F11 cells with mouse TRPV3 and other TRPV ion channel expressing plasmids followed by TRPV3 immunofluorescence, Western blot analysis of the homogenate of the brain, application of the preadsorbed TRPV3 antiserum with control peptide on rat brain sections, and comparison of the immunostaining pattern with two different TRPV3 antisera, were employed.

1.2 MATERIALS AND METHODS

1.2.1 Animals

Adult, male, Wistar rats [250-280 g body weight (BW)] and C57/B6 mice [25-30 g BW] were used. In addition adult, male, Sprague-Dawley [250-280 g BW] rats were also used for comparing the TRPV3-immunoreactivity in the brains of these strains of rats. The animals were acclimatized to the standard conditions of the animal house for at least one week (light between 0600-1800 h, temperature 22 ± 1 °C), and given food and water *ad libitum*. All the experimental protocols were reviewed and approved by the Institutional Animal Ethics Committee (IAEC) at NISER, Bhubaneswar under the supervision of CPCSEA, New Delhi, India.

1.2.2 Total RNA isolation and RT-PCR analysis

To determine TRPV3 mRNA expression in different brain regions, rats (n = 3) were anaesthetized with an intraperitoneal (i.p.) injection of mixture of ketamine [Neon Laboratories Ltd., Mumbai, India; 90 mg/kg body weight (BW)] and xylazine (Stanex Drugs and Chemicals Pvt. Ltd., Hyderabad, India; 10 mg/kg BW). The brains were dissected out, frozen on dry-ice, mounted on a cryostat, and the olfactory bulb, cerebral cortex, hippocampus, midbrain, brainstem, and cerebellum, were isolated in sterile condition. The tissues were processed for RNA isolation and RT-PCR analysis as previously described [149]. The total RNA was isolated using TRIZOL reagent (Invitrogen), first stand cDNA was synthesized with high-capacity cDNA reverse transcription kit (Invitrogen), and cDNA was amplified using Phusion® High-Fidelity DNA Polymerase (NEB) at 57 °C. The N-terminus TRPV3 was amplified using primers specific to exon/exon junction 7/8 of rat TRPV3 (forward: ACCCCATCCAATCCCAACAGTCC; reverse: CAGGGGCGTCTCACCAAAATAG) [149]. Specific primers for glyceraldehyde 3-

phosphate dehydrogenase (GAPDH) (forward: AACTTTGGCATTGTGGAAGG and reverse: ACACATTGGGGGTAGGAACA) from rat origin were used as control. The PCR product was analysed on 1 % agarose gel and the N-terminal (~514bp) band in each tissue sample indicated the expression of TRPV3 mRNA. Image of the gel was acquired using Gel-Doc (Bio-Rad) and edited in Adobe Photoshop. A reaction without a template served as control. The PCR product was extracted and sequenced.

1.2.3 Tissue processing and immunofluorescence

Animals were deeply anaesthetized with an i.p. injection of mixture of ketamine (90 mg/kg BW) and xylazine (10 mg/kg BW), and perfused transcardially with phosphate buffered saline (PBS, pH 7.4) followed by 4 % paraformaldehyde in phosphate buffer (PB, pH 7.4). Brains were dissected out, post-fixed, and cryoprotected in 25 % sucrose solution in PBS overnight at 4 °C. Sections (25 µm thick) through the rostro-caudal extent of the brain and spinal cord were cut on a cryostat (Leica CM3050 S, Leica Microsystems, Nussloch GmbH, Germany), and collected in PBS to obtain four sets of floating sections.

Sections were processed for immunofluorescence as previously described [149]. One set of sections from each animal (n = 3) was rinsed in PBS, treated with 0.5 % triton X-100 in PBS for 15 min, and immersed in blocking solution (3 % normal horse serum, 0.01 % triton X-100 in PBS) for 30 min. Sections were incubated in rabbit polyclonal TRPV3 antiserum (N-term. 1:5000) overnight at 4 °C followed by incubation in biotinylated anti-rabbit IgG (Vector Laboratories, Burlingame, 1:400) for 4 h at room temperature, and avidin-biotin-peroxidase complex (ABC, Vector; 1:1000) for 4 h. As per the instructions of the manufacturer, the biotin-tyramide amplification protocol (NEN Life Sciences products, Boston, MA) was employed to

enhance the immunofluorescence signal. After rinsing in PBS and incubation in DTAF-avidin (Jackson Immunoresearch, 1:300), the sections were mounted on glass slides, coverslipped with VECTASHIELD^{TM} mounting medium containing DAPI (Vector), and observed under an AxioImager M2 fluorescence microscope (Carl Zeiss).

Photomicrographs of the TRPV3 labeled sections of the brain at different levels from bregma were captured such that the entire section is covered. The images were organized in Adobe Photoshop CS4 software and a photomontage of the entire brain section was prepared. The image was imported in CorelDraw 12 (Corel Corporation, Ottawa, Canada) and the line drawings were prepared. The cyctoarchitectonic areas and nuclei with TRPV3-immunoreactivity were identified and delineated using the rat brain atlas [150]. The terminology for nucleus incertus was adopted from Ryan et al. [151].

1.2.4 Specificity of the TRPV3 antiserum

We have recently established the specificity of TRPV3 antiserum in rat brain [149]. Briefly, the specificity of the TRPV3 antiserum in rat brain was validated using (i) Western blotting and (ii) immunofluorescence in TRPV3 overexpressing F11 cells. In addition, section were also incubated in C-terminal TRPV3 antiserum and processed for immunofluorescence as described above.

1.2.5 Western blot analysis

Rats (n = 3) were anaesthetized, decapitated, and brains were removed. A tissue block containing brain was isolated and homogenised in lysis buffer containing 0.15 mM NaCl, 5 mM EDTA (pH 8), 1 % Triton X-100, and 10 mM Tris-Cl (pH 7.4) with 1 % protease inhibitor

cocktail (Sigma) and the homogenate was centrifuged at 13,000 rpm for 20 min. The protein sample was added to an equal volume of 2X sample buffer [130 mM Tris-Cl (pH 8), 20 % Glycerol, 4.6 % SDS, 0.02 % Bromophenol blue, 2 % DTT] and denatured at 95 °C for 5 min. The protein sample along with prestained protein marker was electrophoresed using minigel apparatus (BioRad). Proteins were transferred to Immobilon®-P Polyvinylidene difluoride membrane (PVDF, Millipore) using a minigel electrotransfer system (BioRad). The membrane was blocked in 5 % skim milk (HIMEDIA, India) and incubated in rabbit anti-TRPV3 antiserum (1:1500) for 2 h at room temperature. After washing in 1X Tris-buffered saline and tween 20 (TBST), membrane was incubated in goat anti-rabbit horseradish peroxidase-conjugated antibody (Cell Signaling Technology, USA) and the immunoreactive protein was visualised using SuperSignal™ West Femto maximum sensitivity substrate (Thermo Scientific).

1.2.6 Cell culture, *in vitro* transfection and immunofluorescence

The cell culture, transfection, and immunofluorescence labeling procedures have already been described [149]. Briefly, F11 cells were transfected with a plasmid encoding mouse TRPV3 cloned in pIRES2-EGFP vector (kind gift of Dr. Michael X. Zhu) [106]. While F12 Ham's medium (HIMEDIA) supplemented with 10 % FBS (HIMEDIA) containing penicillin (100 U/ml) and streptomycin (100 µg/ml) was used for cell culture, the serum-free F12 Ham's media was used for transfection. The cells were fixed with 4 % paraformaldehyde and processed for immunofluorescence. Following immersing in the blocking solution, the cells were incubated in diluted N- and C- terminal TRPV3 antisera (1:500); followed by Cy3 conjugated secondary antibodies (Jackson Immunoresearch; 1;500). The coverslips were washed in PBS and mounted on glass slides with Fluoromount-G (Southern Biotech) and observed under

confocal laser scanning microscope (LSM-780, Carl Zeiss). The images were captured and analyzed using Zeiss LSM image analysis software and adjusted for brightness and contrast in Adobe Photoshop CS4.

1.3   RESULTS

1.3.1 TRPV3 expression in the brain

Using RT-PCR, TRPV3 mRNA expression was observed in the olfactory bulb, cerebral cortex, hippocampus, hypothalamus, midbrain, brainstem and cerebellum (Fig. 1A). Sequencing of the N-terminal fragment matched with that of the rat TRPV3 cDNA. By Western blot analysis, TRPV3 antiserum recognized a protein of ~90 kDa, equivalent to the molecular weight of TRPV3 (Fig. 1B). Application of TRPV3 antiserum resulted in immunofluorescence labelling of cells and fibers in the hypothalamus and other brain regions. Two different antisera raised against the N- and C- terminus TRPV3 sequences of mouse TRPV3 and human TRPV3 respectively. Applications of these antisera on sections of the rat brain resulted in comparable labelling of cell bodies and fibers in the hypothalamic PVN (Fig. 1C, D) as well as other brain regions. The immunoreactivity was abolished following application of the preadsorbed TRPV3 antiserm with control peptide (Fig. 1E). Further, the application of N- as well as C-terminus TRPV3 antisera on the F11 cells transfected with pIRES2-EGFP-mouse TRPV3 resulted in intense immunofluorescence labeling of the cells (Figs. 1F-I, 1J-M; 2I-L). Application of normal serum without the primary antiserum on the F11 cells transfected with pIRES2-EGFP-mTRPV3 (Fig. 2E-H) or application of the N-terminal TRPV3 antiserum on F11 cells expressing rat TRPV2-EGFP (Fig. 2M-P) and human TRPV4-EGFP (Fig. 2Q-T) did not show any immunolabeling.

1.3.2 Organization of TRPV3-immunoreactivity in the brain of rat

The relative intensity of immunofluorescence and number of TRPV3 neurons in different regions of the rat brain is given in Table 1. Schematic showing the distribution of TRPV3-
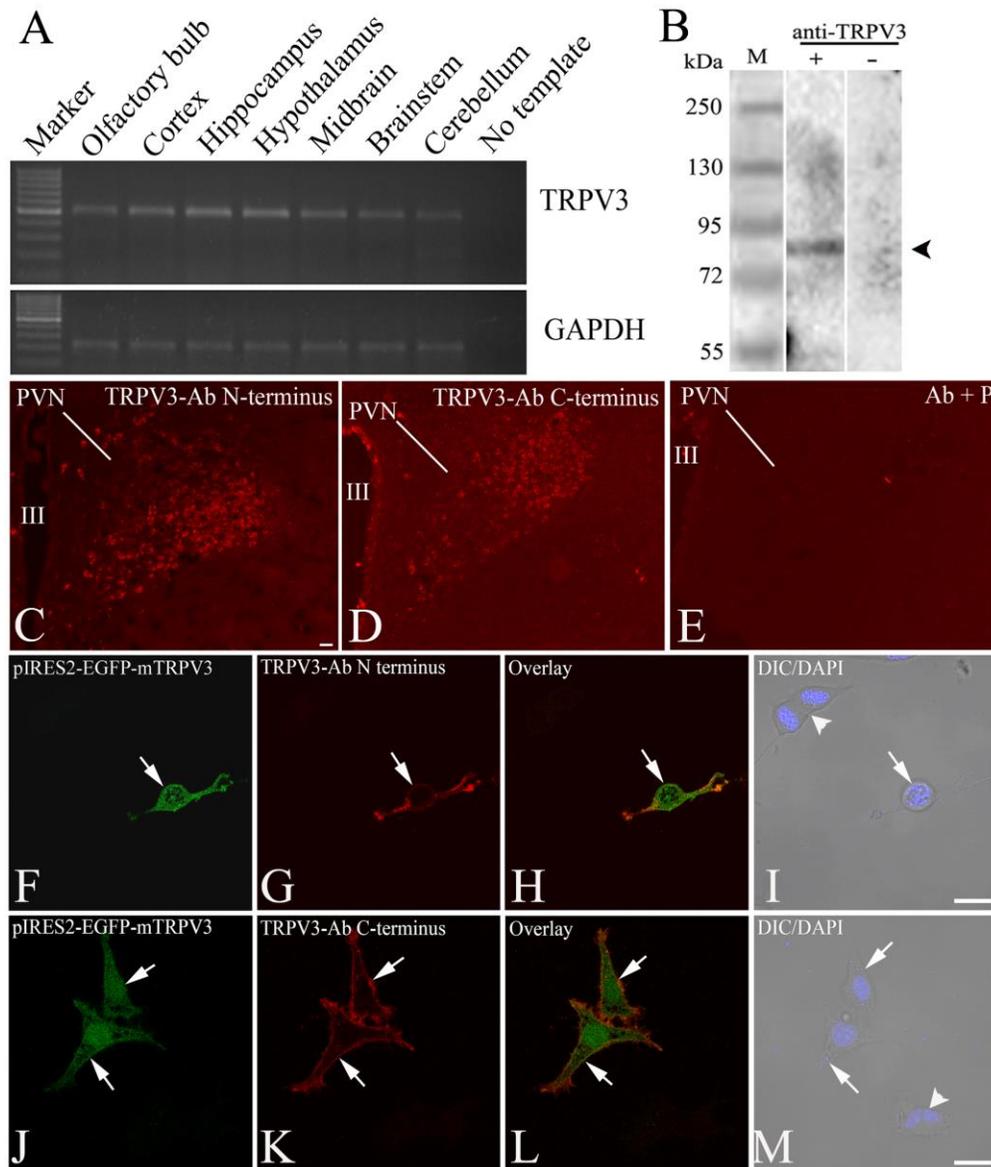
Figure 1: Expression of TRPV3 in the rat brain.
(A) RT-PCR analysis of TRPV3 mRNA expression in different regions of the brain. GAPDH served as internal control. (B) Immunoblot showing core TRPV3-immunoreactive band (arrowhead) while omission of antiserum does not show any immunoreaction. Fluorescence photomicrographs showing TRPV3-immunoreactive cells in the hypothalamic paraventricular nucleus (PVN) following application of the (C) N- and (D) C-terminal TRPV3 antisera. (E) No immunoreactivity is seen in the PVN following incubation of the sections with TRPV3 antiserum (Ab) preadsorbed with the control peptide (P). The (F-I) N- and (J-M) C-terminal TRPV3 antisera labelled F11 cells transfected with pIRES2-EGFP-mouse TRPV3 (arrows). Note the absence of TRPV3 labelling in a non-transfected cell (arrowhead in I and M). III, third ventricle. Scale bar = 50µm in C-E and 20 µm = F-M.
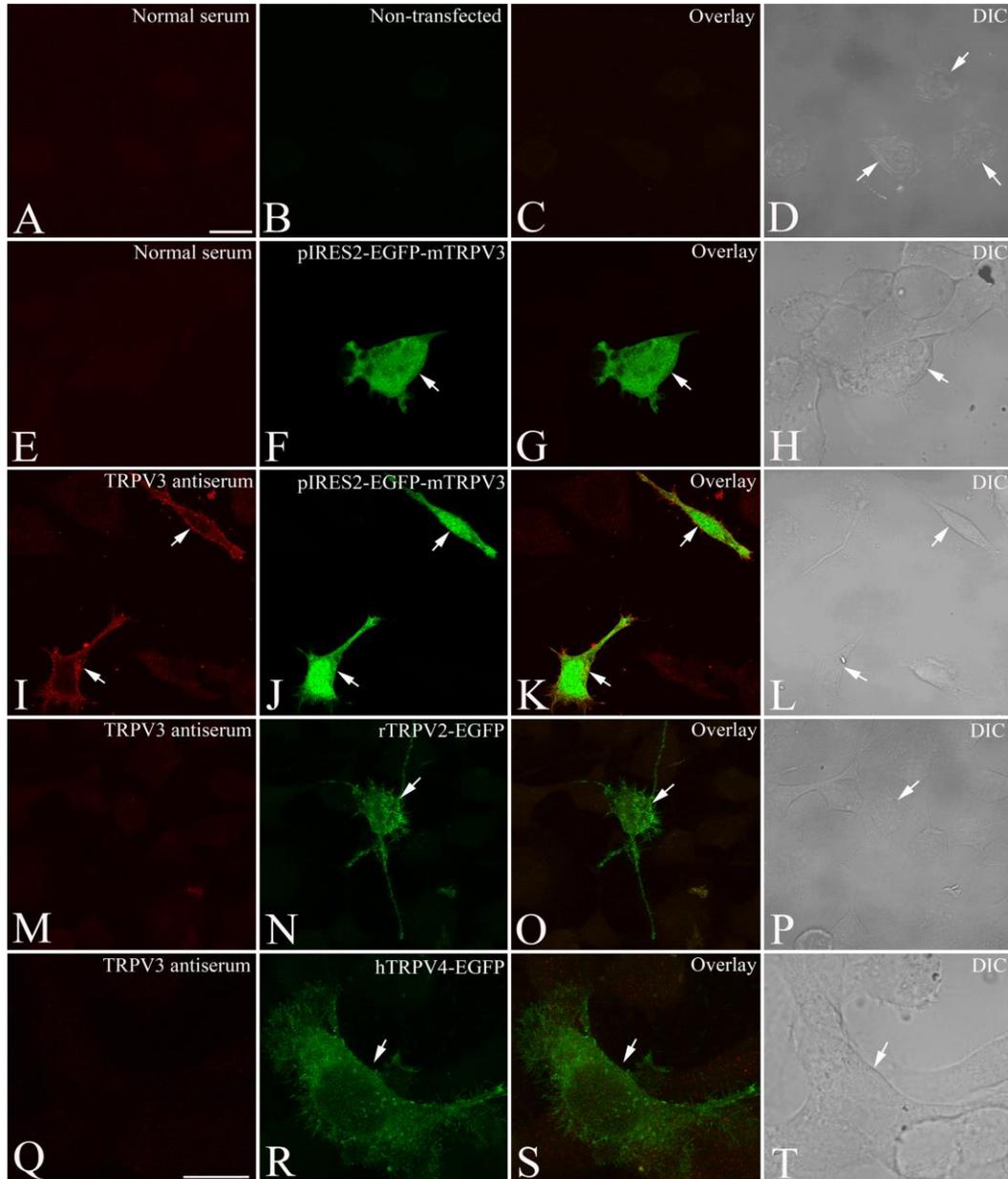
Figure 2: Specificity of the TRPV3 antiserum in F11 cells.
Fluorescence photomicrographs showing specificity of the N- terminal TRPV3 antiserum on (A-C) non-transfected or (E-G) transfected F11 cells. (E-G) When the TRPV3 antiserum was replaced with normal serum, no TRPV3 immunofluorescence is visible in cells expressing pIRES2-EGFP-mTRPV3 (arrow). (I-K) pIRES2-EGFP-mTRPV3-expressing cells show intense TRPV3 immunofluorescence (arrows). No immunolabeling is seen following application of TRPV3 antiserum on F11 cells transfected with (M-O) rat TRPV2-EGFP (rTRPV2-EGFP, arrow) or (Q-S) human TRPV4-EGFP (hTRPV4-EGFP, arrow). The antiserum shows no cross-reactivity with TRPV2 and TRPV4. (D, H, L, P, T) DIC photomicrographs of the cells shown in A-C, E-G, I-K, M-O, and Q-S. Scale bar = 20 µm.

immunoreactive elements in rat brain is shown in Figure 3. No difference in the organization of TRPV3-immunoreactivity was observed in the brain the of Sprague-Dawley and Wistar rats.

Forebrain

While moderate immunoreactive neurons were observed in the medial septum (MS) (Figs. 3A, 4A) and nucleus of the vertical limb of diagonal band (VDB) (Fig. 3A), few intensely labelled neurons were seen in the bed nucleus of stria terminalis (ST) [lateral division, ventral part (STLV) (Fig. 3B) and medial division postero-lateral part (STMPL)]. Scattered, weakly immunoreactive neurons were seen in the medial amygdaloid nucleus (Fig. 3E, F).

TRPV3-immunoreactive neurons were observed in several discrete nuclei in the preoptic area (POA) including vascular organ of lamina terminalis (VOLT) (Fig. 4B), medial preoptic nucleus, medial part (MPOM) (Figs. 3B, 4C), median preoptic nucleus (MnPO) (Figs. 3B, 4D), and anteroventral periventricular nucleus (AVPe) (Fig. 3B). A discrete organization of TRPV3-immunoreactivity was observed in the hypothalamus (Figs. 3, 5). Neurons in the septohypothalamic nucleus (SHy) (Figs. 3B, 5A), supraoptic nucleus (SON) (Figs. 3B-D, 5B), and the retrochiasmatic part of SON (SOR) were intensely immunoreactive (Fig. 3E-F). In the periventricular nucleus (pe), TRPV3-immunoreactive cell bodies and fibers were present along the wall of third ventricle (Figs. 3C-E, 5C, D). TRPV3-immunoreactive cell bodies and fibers were observed in the parvo- and magnocellular subdivisions of the hypothalamic paraventricular nucleus (PVN) (Figs. 3C-E, 5E-G, I). In the parvocellular subdivisions of the PVN, several intensely labelled cell bodies and fibers were observed in the anterior (PVNap), medial (PVNmp), ventral (PVNvp), and dorsal (PVNdp) regions (Figs. 3C-E, 5E-G). TRPV3-immunoreactive neurons in the posterior magnocellular (PVNpm) (Fig. 5F), and ventral (Fig. 5F)

and lateral (PVNlp) (Fig. 5I) parvocellular subdivisions of the PVN were compactly arranged. Several fibers from the PVNpm travels laterally and swing ventrally in the hypothalamus (Figs. 3C-F, 5F, G, I). In the PVNmp, few TRPV3-immunoreactive neurons were closely associated with the blood vessels (Fig. 5H). Accessory groups of neurosecretory cells (ANS) and fibers were strongly immunoreactive (Figs. 3C-E, 5J). In the hypothalamic dorsomedial nucleus (DMN), scattered cells were seen in the dorsal subdivision (DMNd) (Figs. 3F, 5K) but no immunoreactivity was observed in other subdivisions of DMN. TRPV3-immunoreactive cells were observed in the lateral hypothalamic (LHA) (Figs. 3F, 5L) and retrochiasmatic (Rch) (Figs. 3D, E, 5M) areas; and hypothalamic arcuate nucleus (ARC) (Figs. 3F, G, 5N). In the median eminence, intensely labelled TRPV3-immunoreactive fibers were present in the internal zone (Fig. 5O); the external zone was devoid of TRPV3-immunoreactivity (Figs. 3F, 5O). Moderately immunoreactive cell bodies were observed in the ventral tuberomammillary nucleus of the hypothalamus (VTM) (Figs. 3G, 5P) and posterior hypothalamic nucleus (PH) and posterior hypothalamic area (PHA) (Figs. 3G, H, 6A).

Midbrain

TRPV3-immunoreactive neurons were seen in the precommissural nucleus (PrC) (Figs. 3G, 6B) and medial pretectal nucleus (MPT) (Figs. 3H, 6C). In the A11 dopamine cell area, scattered and moderately labelled neurons were observed (Figs. 3G, 6D). Ependymocytes in the subcommissural organ (SCO) showed TRPV3-immunoreactivity localized towards the ventricular space (Figs. 3H, 6E). Few scattered, moderately immunoreactive neurons were present in the periaquaductal grey (PAG) (Figs. 3I-K, 6F) whereas several intensely TRPV3 immunoreactive neurons were observed in the Edinger-Westphal nucleus (EW) centrally
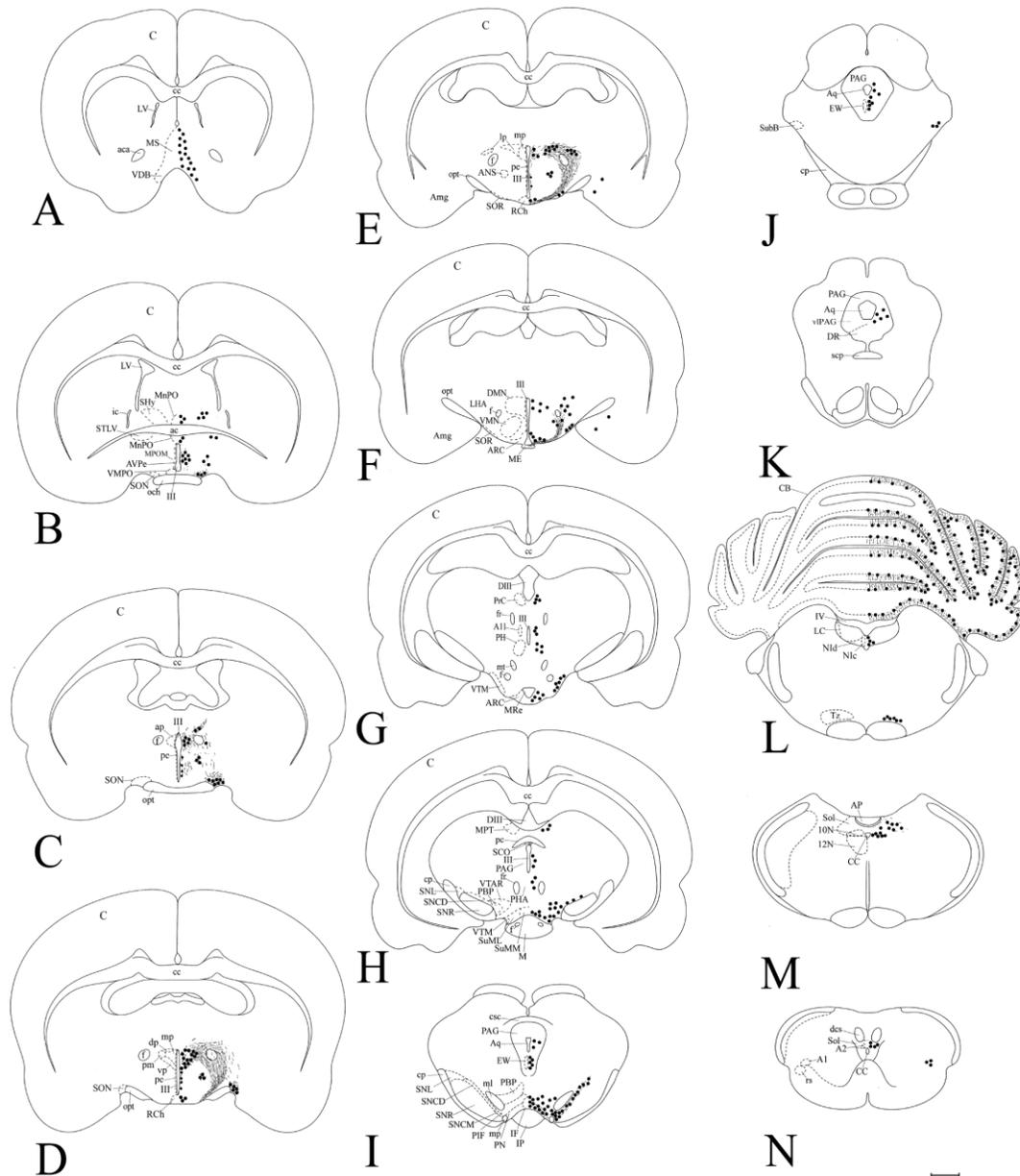
Figure 3: Neuroanatomical organization of TRPV3-immunoreactive elements in rat brain.
Schematic drawings of the rostro-caudal series of transverse sections (A-N) of rat brain showing cytoarchitectonic areas on left and TRPV3-immunoreactive cells (circles) and fibers (dots and dashed lines) on the right. For details of the brain regions and nuclei, please see abbreviations. Scale bar = 1 mm.
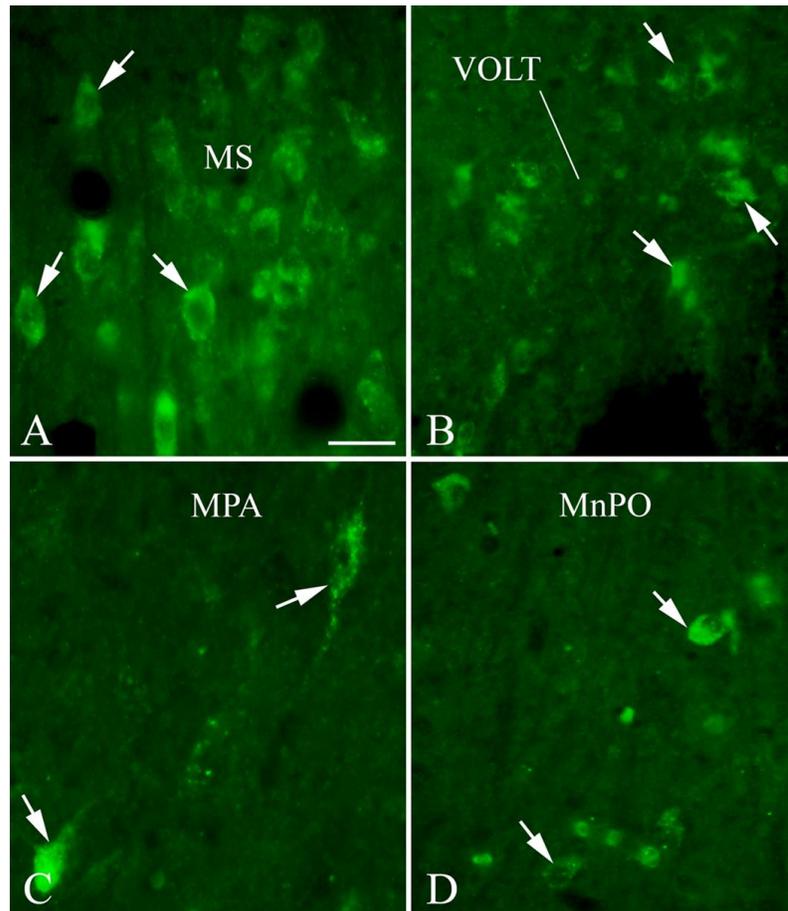
Figure 4: Organization of TRPV3-immunoreactive elements in the forebrain of rat.
Photomicrographs showing TRPV3-immunoreactive cells (arrows) in the (A) medial septum (MS), (B) vascular organ of lamina terminalis (VOLT), (C) medial preoptic area (MPA), and (D) median preoptic nucleus (MnPO). Scale bar = 25 µm.
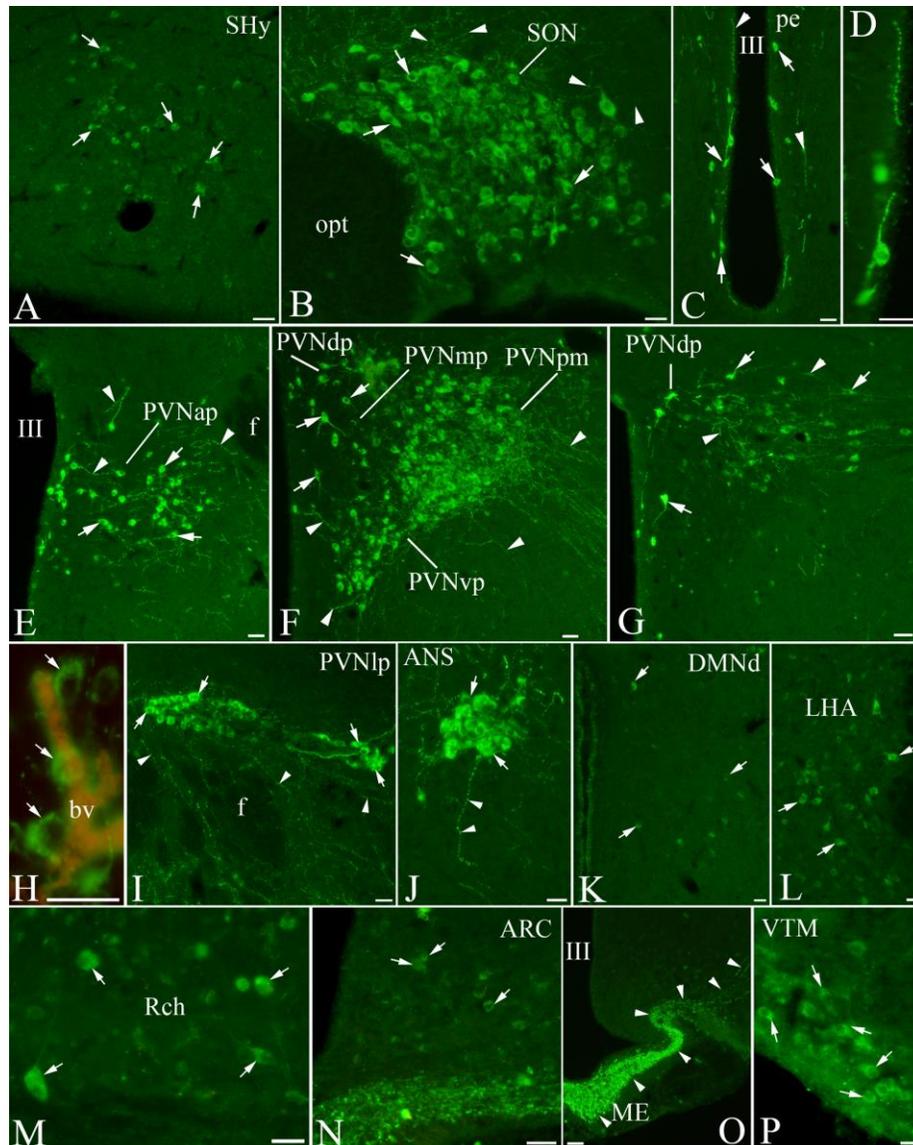
Figure 5: Organization of TRPV3-immunoreactive elements in the hypothalamus of rat. Photomicrographs showing TRPV3-immunoreactive cells (arrows) and fibers (arrowheads) in the (A) septo-hypothalamic nucleus (SHy), (B) supraoptic nucleus (SON), (C) periventricular hypothalamic nucleus (pe). (D) Magnified view of a region in C. In the hypothalamic paraventricular nucleus (PVN), TRPV3-immunoreactive cells and fibers are seen in the (E) anterior (PVNap), (F) medial (PVNmp), (F) ventral (PVNvp), and (F and G) dorsal (PVNdp) parvocellular subdivisions. Several cells are observed in the (F) posterior magnocellular subdivision of PVN (PVNpm). Few TRPV3-immunoreactive neurons in (H) PVNmp are closely associated with blood vessel (bv). Several TRPV3-immunoreactive neurons are seen in the (I) lateral parvocellular subdivision of the PVN (PVNlp) and (J) accessory neurosecretory nucleus (ANS). Few TRPV3-immunoreactive cell bodies are visible in the (K) dorsal subdivision of dorsomedial nucleus (DMNd), (L) lateral hypothalamic area (LHA), (M) retrochiasmatic area (Rch), and (N) arcuate nucleus (ARC). Intensely labelled fibers are seen entering into the (O) median eminence (ME). TRPV3-immunoreactive cells are seen in the (P) ventral tuberomammillary nucleus (VTM). opt, optic tract; f, fornix; III, third ventricle. Scale bar = 25 µm.

projecting neuronal population (Figs. 3I, J, 6G). The supramammillary nucleus (SuM), ventral tegmental area (VTA), and substantia nigra (SN) contained several moderately immunoreactive neurons (Figs. 3H, I, 6H-J). TRPV3 cell bodies were observed in the sub-brachial nucleus (SubB) (Fig. 3J).

Hindbrain

TRPV3-immunoreactive cell bodies were seen in the nucleus incertus, pars compacta (NIc) (Figs. 3L, 6K) and nucleus of trapezoid body (Tz) (Figs. 3L, 6L). In the cerebellum, several Purkinje cells (Figs. 3L, 6M) and their dendrites in the molecular layer (Fig. 3L) were TRPV3-immunoreactive. Several intensely labelled neurons were seen throughout the rostro-caudal extent of nucleus of the solitary tract (Sol) and seem more concentrated in the dorsomedial subdivision of Sol (Figs. 3M, N, 6N). TRPV3-immunoreactive neurons were seen in the 10N (Figs. 3M, 6O) as well as A1 region (Fig. 3N).

1.3.3   Organization of TRPV3-immunoreactivity in the brain of mouse

The comparison between TRPV3-immunoreactive elements in the rat and mouse brain is given in the Table 2. The organization of TRPV3-immunoreactive elements in the mouse brain seems similar to that in the rat brain. TRPV3 immunoreactive cells/fibers were observed in the forebrain, midbrain, and hindbrain. In the forebrain, TRPV3-immunoreactive cells were observed in the septum and POA. TRPV3-immunoreactive cells and fibers were seen in SON (Fig. 7A) and PVN (Fig. 7B-E). Moderately TRPV3-immunoreactive cells were observed
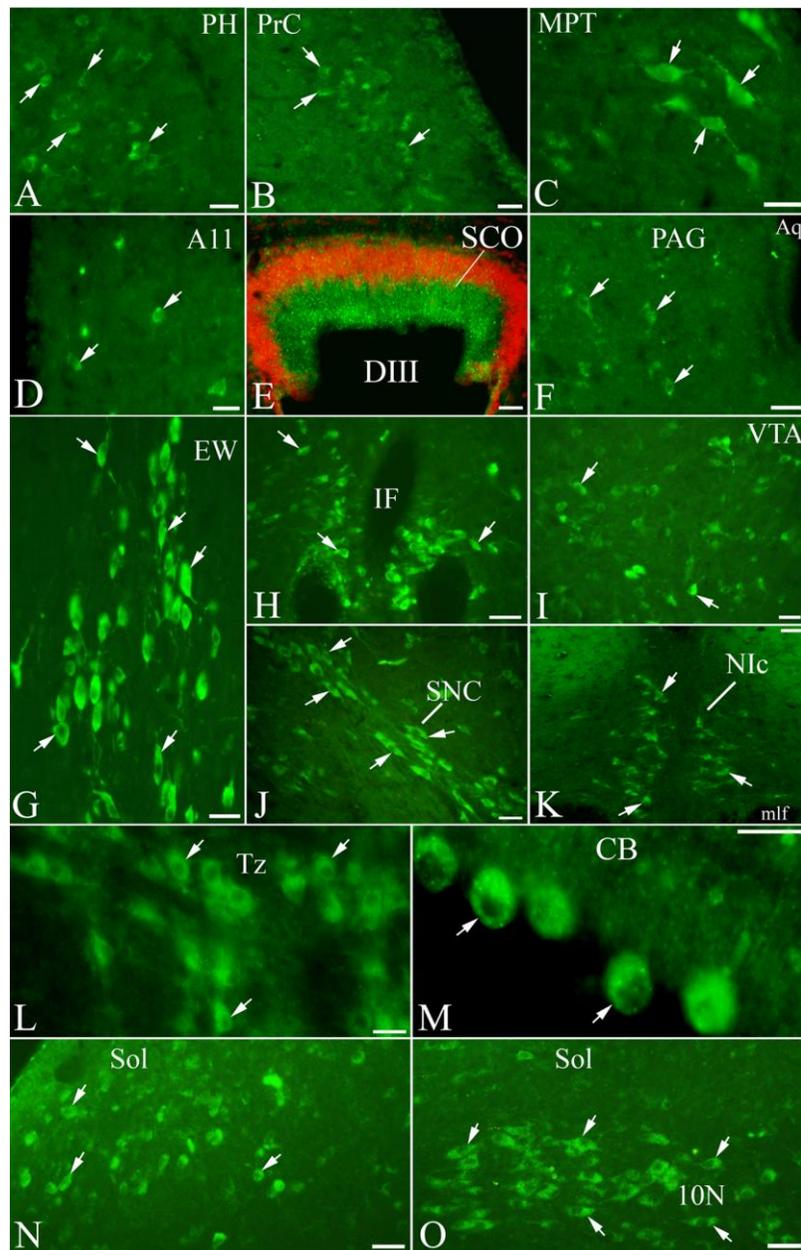
Figure 6: Organization of TRPV3-immunoreactive elements in the posterior hypothalamus, midbrain and hindbrain of rat.
Photomicrographs showing TRPV3-immunoreactive cells (arrows) and fibers (arrowheads) in the (A) posterior hypothalamic nucleus (PH), (B) precommissural nucleus (PrC), (C) medial pretectal nucleus (MPT), (D) A11 dopamine cells, (E) subcommissural organ (SCO), (F) periaquaductal gray (PAG), and (G) Edinger-Westphal nucleus (EW). The DAPI staining is pseudocolored red in E. TRPV3-immunoreactive cells are seen in the (H) interfascicular nucleus (IF) and (I) ventral tegmental area (VTA). TRPV3-immunoreactive cells are also seen in the (J) substantia nigra, compact part (SNC), (K) nucleus incertus, pars compacta (NIc), (L) trapezoid body (Tz), (M) Purkinje neurons in the cerebellum (CB), (N) nucleus of the solitary tract (Sol), and (O) the dorsal motor nucleus of vagus (10N). DIII, dorsal third ventricle; Aq, aqueduct; mlf, medial longitudinal fasciculus. Scale bar = 25 µm.

in the ANS, ZI, DMN, SOR and VTM (Fig 7F, G, I, L, N). TRPV3 immunoractive cells in Rch, LHA, ARC and SuM were compactely arranged (Fig. 7H, J, K, M). Several intensely labelled TRPV3-immunoreactive fibers were seen entering in the internal zone of the median eminence (Fig. 7K, O; Table 2).

In the midbrain, moderately labelled TRPV3-immunoreactive cells were observed in the A11 dopamine cell area. The ependymocytes in the SCO and cells in SuM were TRPV3-immunoreactive. The centrally projecting neuronal population of EW cells showed intense TRPV3-immunoreactivity. In the VTA and SN, several neurons were moderately TRPV3-immunoreactive (Table 2).

In the hindbrain, isolated TRPV3-immunoreactive cells were seen in the PAG and raphe pallidus nucleus (RPa). Several intensely labelled neurons were seen throughout the rostro-caudal extent of Sol, area postrema (AP), and 10N. In the cerebellum, the Purkinje neurons were TRPV3-immunoreactive (Table 2).
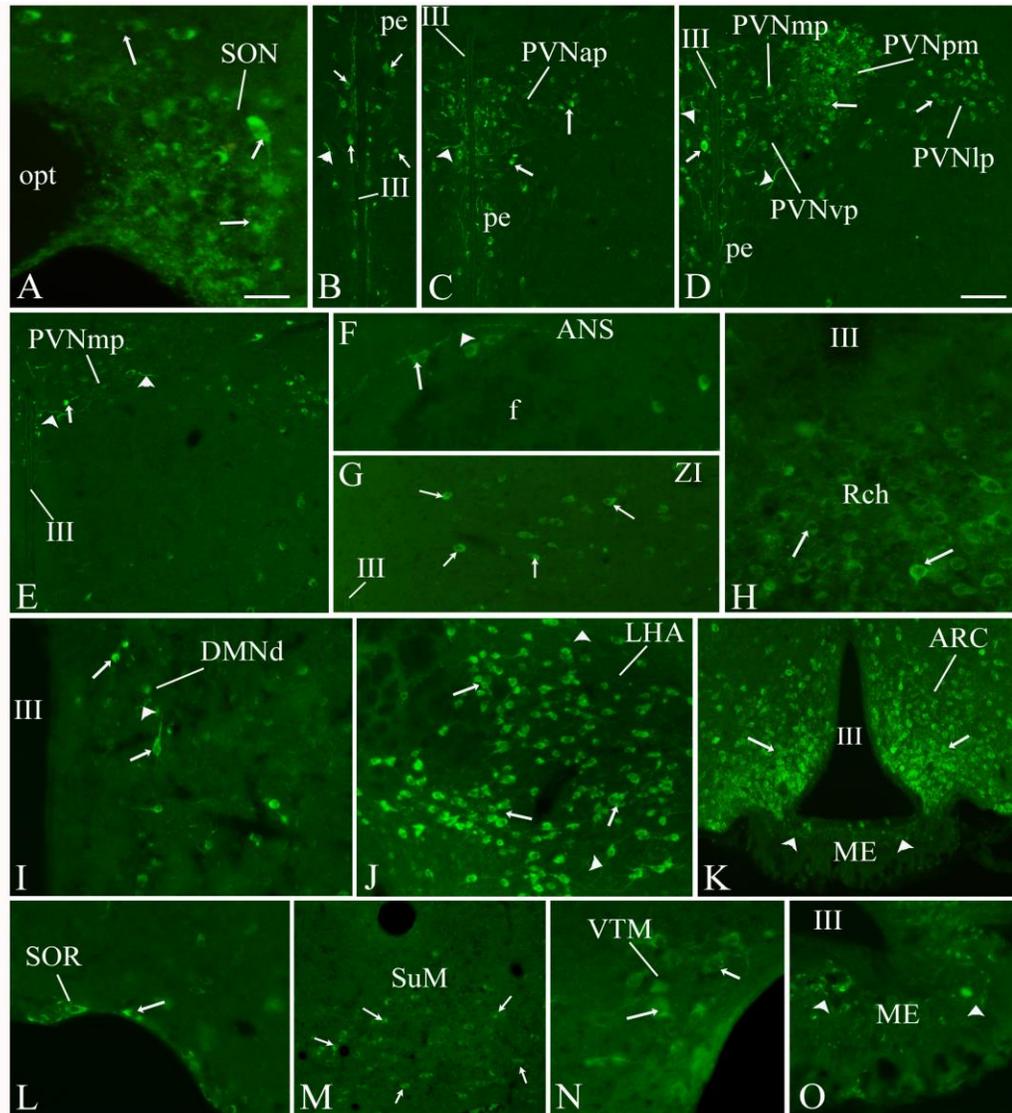
Figure 7: Organization of TRPV3-immunoreactive elements in the hypothalamus of mouse.
Photomicrographs showing TRPV3-immunoreactive cells (arrows) and fibers (arrowheads) in the hypothalamic; (A) supraoptic nucleus (SON), (B) periventricular nucleus (pe), and (C, D) hypothalamic paraventricular nucleus (PVN). TRPV3-immunoreactive cells and fibers are seen in the (C) anterior (PVNap), (D, E) medial (PVNmp) and (D) ventral (PVNvp) parvocellular subdivisions of PVN. TRPV3-immunoreactive neurons are also seen in the (D) lateral parvocellular subdivision of the PVN (PVNlp) and (F) accessory neurosecretory cells (ANS). Few TRPV3-immunoreactive cell bodies are seen in the (G) zona incerta (ZI), (H) retrochiasmatic area (Rch), and (I) dorsal subdivision of the hypothalamic dorsomedial nucleus (DMNd). TRPV3 neurons are observed in the (J) lateral hypothalamic area (LHA) and (K) arcuate nucleus (ARC). Few TRPV3-immunoreactive cells are seen in the (L) retrochiasmatic part of the SON (SOR), (M) mamillary nucleus (SuM), (N) ventral tuberomammillary nucleus (VTM). Intensely labelled TRPV3-immunoreactive fiber terminals are seen in the (O) median eminence (ME). opt, optic tract; f, fornix; III, third ventricle. Scale bar = 50 µm A, F, H, L, N, O; and 100 µm in B, C, D, E, G, I, J, K, M.

Table 1: TRPV3-immunoreactivity in the rat brain.

Brain structure	TRPV3-immunoreactivity	
	cell number	intensity
Forebrain		
Septum		
medial septum (MS)	++	M
nucleus of vertical limb of diagonal band (VDB)	++	M
septohypothalamic nucleus (SHy)	++	W
bed nucleus of stria terminalis (ST)		
lateral division, ventral part (STLV)	+	W
medial division, postero lateral part (STMPL)	++	I
Cortex and amygdala	+	W
Epithalamus		
medial pretectal nucleus (MPT)	+	W
Hypothalamus		
Preoptic area		
medial preoptic nucleus, medial part (MPOM)	+++	W
anteroventral periventricular nucleus (AVPe)	+++	W
ventrolateral preoptic nucleus (VLPO)	++	M
vascular organ of lamina terminalis (VOLT)	+	M
Periventricular nucleus (pe)	++	M
Paraventricular nucleus (PVN)		
anterior parvicellular subdivision (PVNap)	++	I
medial parvicellular subdivision (PVNmp)	++	I
posterior magnocellular subdivision (PVNpm)	+++	I
lateral parvocellular subdivision (PVNlp)	++	I
ventral parvocellular subdivision (PVNvp)	+++	I
dorsal parvocellular subdivision (PVNdp)	++	I
Accessory neurosecretory nucleus (ANS)	+++	I
Retrochiasmitic area (RCh)	++	M
Supraoptic nucleus (SON)	+++	I
Arcuate nucleus (ARC)	+	W

Hypothalamic dorsomedial nucleus (DMN)		
dorsal subdivision of DMN (DMNd)	+	W
Lateral hypothalamic area (LHA)	++	M
A11 dopamine cells	+	M
Posterior hypothalamic nucleus (PH)	+	M
Ventral tuberomammilary nucleus (VTM)	++	M
Subcommissural organ (SCO)	++	I
Midbrain		
Precommisural nucleus (PrC)	+	M
Periaqueductal gray (PAG)		
ventrolateral periaqueductal gray (vLPAG)	+	M
Supramammillary nucleus (SuM)	++	M
Edinger Westphal nucleus (EW)	+++	I
Sub-brachial nucleus (SubB)	+	M
Interfascicular nucleus (IF)	+++	I
Ventral tegmental area (VTA)	++	M
Substantia nigra, compact part (SNC)	++	M
Hindbrain		
Nucleus incertus, compacta (NIc)	++	M
Nucleus of trapezoid body (Tz)	+++	I
Cerebellum (Purkinje cells)	+++	I
Nucleus of the solitary tract (Sol)	++	I
Dorsal motor nucleus of vagus (10N)	+++	M
A1 noradrenaline cells (A1)	++	I
Cell number: +++, high; ++, moderate; +, scattered		
Intensity of immunoreactivity: W, weak; M, moderate; I, intense		

Table 2: Comparison of TRPV3-immunoreactivity in the brain of rat and mouse.

Brain structure	TRPV3 positive neurons	
	Rat	**Mouse**
Forebrain		
Septum		
medial septum (MS)	++	+
nucleus of vertical limb of diagonal band (VDB)	++	+
septohypothalamic nucleus (SHy)	++	++
bed nucleus of stria terminalis (ST)	++	++
Cortex and amygdala	+	+
Hypothalamus		
Preoptic area		
medial preoptic nucleus, medial part (MPOM)	+++	++
anteroventral periventricular nucleus (AVPe)	+++	++
ventrolateral preoptic nucleus (VLPO)	++	+++
vascular organ of lamina terminalis (VOLT)	+	++
Periventricular nucleus (pe)	++	++
Paraventricular nucleus (PVN)		
anterior parvicellular subdivision (PVNap)	++	++
medial parvicellular subdivision (PVNmp)	++	+
posterior magnocellular subdivision (PVNpm)	+++	+++
lateral parvocellular subdivision (PVNlp)	++	+++
ventral parvocellular subdivision (PVNvp)	+++	++
dorsal parvocellular subdivision (PVNdp)	++	++
Accessory neurosecretory nucleus (ANS)	+++	++
Retrochiasmitic area (RCh)	++	+++
Supraoptic nucleus (SON)	+++	+++
Arcuate nucleus (ARC)	+	+++
Hypothalamic dorsomedial nucleus (DMN)		
dorsal subdivision of DMN (DMNd)	+	+
Lateral hypothalamic area (LHA)	++	+++
A11 dopamine cells	+	++
Posterior hypothalamic nucleus (PH)	+	++
Ventral tuberomammilary nucleus (VTM)	++	++
Subcommissural organ (SCO)	++	++

Midbrain		
Periaqueductal gray (PAG)	+	+
Supramammillary nucleus (SuM)	++	+++
Edinger Westphal nucleus (EW)	+++	+++
Interfascicular nucleus (IF)	+++	++
Ventral tegmental area (VTA)	++	++
Substantia nigra, compact part (SNC)	++	++
Hindbrain		
Nucleus incertus, compacta (NIc)	++	++
Nucleus of trapezoid body (Tz)	+++	++
Cerebellum (Purkinje cells)	+++	+++
Nucleus of the solitary tract (Sol)	++	+++
Dorsal motor nucleus of vagus (10N)	+++	+++
A1 noradrenaline cells (A1)	++	++
Cell number: +++, high; ++, moderate; +, scattered		

1.4 DISCUSSION

TRPV3 is the most wide and discretely organized TRP channel in the CNS of rat and mouse. RT-PCR analysis further validated the presence of TRPV3 in the different areas of the rat brain. Our observation is supported by previous studies demonstrating the presence of TRPV3 mRNA in the brain [4,5,9,149]. Although widely distributed in the brain, the channel protein-expressing neurons were discretely organized in the preoptic area, hypothalamus, midbrain, and hindbrain of both the species. While Smith et al. [5] suggested TRPV3 as predominantly a gene of the nervous system, Caterina [3] highlighted the lack of information about TRPV3 expression in the hypothalamus. To our knowledge, this is the first study demonstrating a detailed neuroanatomical organization of TRPV3-expressing elements in the brain of rat and mouse. Along with other TRPV channels, TRPV3 may serve as crucial regulatory element of the hypothalamic neuroendocrine system.

Comparison of TRPV3-immunoreactivity pattern in the brain of rat and mouse showed a similar neuroanatomical organization. Distinct TRPV3-immunoreactive cell bodies were observed in the hypothalamic nuclei. In addition to the cell bodies, several intensely TRPV3 labelled fibers were also seen in the hypothalamus. Occurrence of TRPV3-immunoreactive fibers in the hypothalamus is not surprising since application of the TRPV2 antiserum resulted in similar labelling of fibers in the hypothalamus of macaque [13]. In the POA, TRPV3-immunoreactive neurons were seen in the VOLT, this region contains osmosensory neurons, and role of TRPV channels has been suggested in osmosensation [2]. In the hypothalamus, TRPV3-immunoreactive cells were also observed in DMNd, ARC, and LHA. The presence TRPV2 has been demonstrated in the ARC but not in DMN and LHA of rat and importance of these ion channels in the regulation of food intake and energy balance has been suggested [12]. The ARC

contains two feeding-related neuronal populations *viz*. orixigenic (NPY/AGRP) and anorexigenic (CART/α-MSH) [152,153]. Since the importance of Ca^{2+} signalling in ARC neurons has been demonstrated [154], we suggest that the feeding-related neurons in the ARC might co-express TRPV3 channels and play a role in Ca^{2+} signalling in these neurons. In the midbrain, brainstem and cerebellum, while several subpopulations of neurons showed TRPV3 immunofluorescence, prominent immunoreactive neurons were observed in the SN, VTA, EW, and Sol. The subcommissural organ and Purkinje cells in the cerebellum were also TRPV3-immunoreactive. The presence of TRPV1 [81], TRPV2 [12] and TRPV3 [86] was observed in the Sol. Our observation of the presence of TRPV3 neurons in SN is supported by a recent report showing TRPV3 mRNA expression in this nucleus [4]. Studies exploring the functional significance of TRPV3 in the brain are limited. Intraperitoneal administration of incensole acetate, a TRPV3 agonist, resulted in c-Fos activation in different regions of the brain and the agent seem to be anxiolytic [16]. We observed that TRPV3 is present in DA neurons of VTA and may serve as a novel regulator of mesolimbic dopamine neurons [149]. This is described in detail in chapter 3.

Cerebellar Purkinje cells are essential for the motor coordination and are known to express TRP ion channels [68]. The TRPC knockout mice revealed the significance of this ion channels in the development of Purkinje cells and motor function [155]. Recently the mRNA expression of TRPV ion channels including TRPV3 has been demonstrated in the cerebellum of mouse [68]. Interestingly, the Purkinje cells are spontaneously active and their activity seem to be temperature dependent [156]. The molecular determinant underlying this complex spontaneous activity at physiological temperature and dominant expression of functional thermosensitive TRPV ion channel species in Purkinje neurons is not known. Presence of TRPV3 in Purkinje neurons may play a role in the regulation its activity and motor coordination.

The expression of TRPV3 in Purkinje cells and relevance to motor coordination has been described in chapter 4.

We have provided the neuroanatomical organization of TRPV3 expressing elements in the brain of rat as well as mice. While rats serve as a useful model system for pharmacological and behavioural studies; mice has become an important model for genetic manipulation. The study of TRPV3 distribution in the brain may help in future to target TRPV3 ion channel in a particular brain region to study its effect on physiology and behaviour. Using this information, we have explored the functional significance of TRPV3 ion channel in the brain (please see chapters 3 and 4). Güler et al. [157] has developed a conditional transgenic mouse model known as DAT-TRPV1 for transient activation of VTA dopaminergic neurons. The non-invasive model is advantageous since it can reversibly activate specific neuronal population without elevating stress. Our study on mice may help to understand the complexity of TRPV3 ion channel organization in the mice model and may help to design TRPV3 chimaeras model to drive specific neuronal pathway.

We conclude that the TRPV3-equipped neurons are discretly organized in the brain of rat and mice, and seem to be the most widely distributed TRP channel in the brain. The wide distribution of these ion channels in the brain supports the notion that TRPV3 might be a predominant gene of the nervous system and may play role in the regulation of a range of CNS functions ranging from neuroendocrine, reward, and motor coordination. Further studies are essential to establish the functional significance of TRPV3 in neuronal function.

<div style="border:1px solid #000; background:#cce0f5;">

CHAPTER 2

</div>

Neurochemical characterization of TRPV3-expressing cells in the hypothalamic paraventricular (PVN) and supraoptic (SON) nuclei and its relevance to neuroendocrine regulation

2.1 INTRODUCTION

The magnocellular neurons in the hypothalamus express TRPV1, TRPV2, and TRPV4, and their relevance in the regulation of these neurons has been demonstrated [2,11–13]. While the thermosensitivity of magnocellular vasopressin (VP) neurons was lower in the *trpv1*^{-/-} mice [14], TRPV1 in the hypothalamic suraoptic nucleus (SON) neurons seem essential for the somatodendritic VP secretion [158]. In mice, TRPV4 has been suggested to play an inhibitory role in VP secretion [159]. The VP neurons in SON and hypothalamic paraventricular nucleus (PVN) of rat co-express TRPV2 [11,12] and their number increases following bile duct ligation (BDL), a condition known to be associated with elevated plasma VP levels [11]. In these animals, approximately two fold increase in the TRPV2 and TRPV4 mRNA expression was associated with a 4-fold increase in VP expression in SON [11]. Whether VP neurons in the hypothalamus are equipped with TRPV3 and these ion channel play a role in the regulation of these neurons has remained unexplored.

VP neurons in the SON and PVN nuclei project to the posterior pituitary and upon stimulation release the neurohormone from the axon terminals into the circulation [160]. Additionally, these neurons release the nonapeptides through somatodendritic release [161,162]. The increased somatodendritic release of VP was observed in hypothalamic neurons following hyperosmotic stimulation [163,164]. The magnocellular neurons in the hypothalamus contain large dense-core vesicles (LDCVs), which undergo exocytosis from the axon terminals and cell body or dendrites [161]. The LDCVs and synaptic vesicles seem to share similar mechanism of fusion of vesicular and plasma membranes, and release of neurotransmitters. Although N-ethylmaleimide sensitive fusion protein attachment protein receptor (SNARE) complex play crucial role in stimulated release of LDCVs [161], some of the core proteins in SNARE complex were not detected in the somata/dendrites of the magnocellular neurons [165]. Synaptic vesicle

protein 2 (SV2), an integral membrane glycoprotein found in the secretory vesicles in the neurons and endocrine cells [166,167], play a role in priming of vesicles and neurotransmission [166,168]. SV2 expression was observed in the hypothalamus of rat [169] and was localized on both small clear synaptic vesicles and LDCVs in neurons and neuroendocrine cells [167,170]. The regulatory component of the SNARE complex, synaptotagmin-1 (SYT-1) is present in the presynaptic terminal of the magnocellular neurons [165]. In the brain, SV2- and SYT-1-immunoreactivity was observed primarily in the presynaptic terminals of the neurons [165,171]. While SYT-1 serve as Ca^{2+} sensor, turbocharges synaptic vesicles [172], and modulate fast calcium triggered neurotransmitter release from the axon terminals, SV2 serve as unique modulator of Ca^{2+}-mediated neurotransmitter release in neurons and endocrine cells in vertebrates [173]. SV2 and SYT-1 interacts to modulate Ca^{2+}-mediated exocytosis of the synaptic vesicles [174–176]. SV2 regulates the amount of synaptotagmin recruitment in synaptic vesicles, and the lack of SV2 show reduced synaptotagmin and less vesicles capable of Ca^{2+}-mediated fusion [177]. While the mechanism of exocytosis of the synaptic vesicles at axon terminal and role of SYT-1 and SV2 is well established, the relevant aspect in somatodendritic release of neurotransmitters is poorly understood.

In the normal as well as in lactating and post-natal day 8 rats, when there is high somato/dendritic secretion [178,179], the vesicular membrane associated protein-2 (VAMP2)-immunoreactivity was not detected in the somatodendritic component of oxytocin or VP neurons [165]. While the axon terminals of oxytocin and VP neurons express VAMP-2, SNAP-25, and syntaxin-1, the somatodendritic component of these neurons contained syntaxin-1-, munc-18-, and CAPS-1-immunoreactivity [161,165]. In such animals, VAMP-2 and SYT-1 immunoreactivity were observed in the presynaptic contacts and does not seem to colocalize

with oxytocin or VP in the cell bodies or dendrites [165,180]. Using *in situ* hybridization, increased VAMP2 and SNAP-25, mRNA expression was observed in the PVN and SON after salt loading [181]. Whether these proteins are recruited on somata/dendrites of these neurons is still not known. Hyperosmotic challenge is known to trigger the axonal as well as somatodendritic VP secretion [161]. Present study was conducted to explore if the somatodendritic compartment of all or a sub-population of the VP neurons express SYT-1/SV2 during osmotic challenge. Since several neurons in the PVN and SON showed TRPV3-immunoreactivity, we hypothesized that the TRPV3 may serve as potential Ca^{2+} channel for secretion of VP from the somatodendritic compartment of PVN and SON neurons.

As described in chapter 1, TRPV3-immunoreactivity was observed in the hypothalamic PVN and SON neurons and their fibers. We have characterized the neurochemical phenotype of these neurons and explored the relevance of TRPV3 ion channel in neuroendocrine regulation. Double immunofluorescence was employed to find out if VP neurons in the PVN and SON are equipped with TRPV3. Retrograde neuronal tracing using fluoro-gold (FG) was used to determine the hypophysiotropic nature of TRPV3-equipped neurons in the PVN and SON. As demonstrated earlier [161], in a pilot study, we confirm the presence of SV2- and SYT-1-immunoreactivity in the presynaptic terminals in the hypothalamus of normal untreated rats. Using immunofluorescence we determined whether hypertonic sodium chloride (NaCl) treatment recruit SYT-1 and SV2 proteins in the somata/dendrites of VP neurons in the PVN and SON. Double immunofluorescence was employed to determine if the PVN and SON neurons engaged in somatodendritic secretion are equipped with TRPV3. To find out if VP neurons in the PVN and SON, engaged in the somatodendritic release also participate in systemic secretion of

peptide, FG was administered intravenously and using double immunofluorescence identified the SYT-1-expressing FG neurons.

In addition, an attempt was also made to determine the evolutionary significance of TRPV3-expressing system in the brain. We used teleost fish, *Clarias batrachus* as model to find out if TRPV3 is expressed in the brain, and dopamine- (DA) or isotocin (IST)-producing neurons in the preoptic area and hypothalamus are equipped with TRPV3. Since there was no information available on DAergic or ISTergic systems in the brain of *C. batrachus*, we studied the organization of DA- and IST-containing systems in the brain of this fish. Using tyrosine hydroxylase (a marker for DA neurons) immunohistochemistry/immunofluorescence, we mapped the DA-containing neurons in the preoptic area/hypothalamus. Retrograde neuronal tracer, DiI was used to identify the hypophysiotropic nature of DA and NPO neurons. Using oxytocin antiserum, we studied the organization of IST-containing neurons in the preoptic area/hypothalamus and pituitary of *C. batrachus*. The sections of the brain containing the preoptic area and hypothalamus of *C. batrachus* were processed for TRPV3 immunofluorescence. Double immunofluorescence was employed to study the association between TRPV3/DA, TRPV3/IST, and DA/IST neurons in the preoptic area/hypothalamus of *C. batrachus*.

2.2 MATERIALS AND METHODS

2.2.1 Animals

Adult, male, Sprague-Dawley rats [250-300 g body weight (BW)] were used. The rats were acclimatized to the standard environmental conditions of the animal house for a week prior to the experimentation (light between 0600-1800 h, temperature 22 ± 1 °C). Food and water were provided *ad libitum*. To study the evolutionary significance of TRPV3, we used adult, female, catfish, *C. batrachus* (100–120 g BW). The fish were collected during December and January, which coincides with the resting phase of the reproductive cycle of the fish. The fish were maintained for a week in the normal photoperiodic conditions. The fish were fed with small pieces of goat liver two times during the day. All the experimental protocols were reviewed and approved by the Institutional Animal Ethics Committee (IAEC) at NISER, Bhubaneswar, under the supervision of CPCSEA, New Delhi, India.

2.2.2 Hyperosmotic saline treatment and tissue processing

Rats were challenged with a hyperosmotic stimulus as described previously with minor modifications [182,183]. While the animals in control group were provided normal drinking water, other group of animals received hyperosmotic saline (HS) i.e. drinking water containing 2 % NaCl. After 24, 48, 72 and 84 h, the rats were deeply anaesthetized with a mixture of ketamine [Neon Laboratories Ltd., Mumbai, India; 90 mg/kg BW] and xylazine [Stanex Drugs and Chemicals Pvt. Ltd., Hyderabad, India; 10 mg/kg BW], and perfused transcardially with phosphate buffered saline (PBS, pH 7.4) followed by 150 ml 4 % paraformaldehyde in phosphate buffer (PB, pH 7.4). Brains were dissected out, post-fixed in the same fixative and cryoprotected in 25 % sucrose solution in PBS overnight at 4°C. Serial 25 µm thick coronal sections through

the rostro-caudal extent of the brain were cut on a cryostat (Leica CM3050 S, Leica Microsystems, Nussloch GmbH, Germany) to obtain four sets of free floating sections in PBS.

2.2.3 Retrograde neuronal tracing

To determine whether the hypophysiotropic neurons in PVN and SON are equipped with TRPV3, retrograde neuronal tracing was employed, as previously described [184]. Rats (n = 3) were administered intravenous injection of Fluoro Gold (FG, 15 µg/g BW in 100 µl 0.9 % saline, Fluorochrome LLC., CO, USA). After 48 h, animals were deeply anesthetized with an i.p. injection of mixture of ketamine (90 mg/kg BW) and xylazine (10 mg/kg BW), perfused transcardially as described above, and the brains were dissected out. Coronal sections (25 µm thick) through the rostro-caudal extent of the hypothalamus containing PVN and SON were cut on a cryostat and processed for TRPV3 immunofluorescence using biotin-tyramide amplification as described in chapter 1 and visualized using DTAF-avidin. The FG labelled neurons were directly visualized under AxioImager M2 fluorescence microscope using a DAPI/350 filter. The FG photomicrographs were pseudocolored red in Adobe Photoshop.

In the second set of experiment, to determine whether the hypophysiotropic neurons in PVN and SON are expressing SYT-1, after HS stimulus; retrograde neuronal tracing coupled HS stimulus was employed. First, the animals (n = 3) were challenged with HS and after 48 h animal were administered intravenous injection of FG (15 µg/g BW in 100 µl 0.9 % saline). After 84 h, animals were deeply anesthetized as described above, perfused transcardially as described above, and the brains were dissected out. Coronal sections (25 µm thick) through the rostro-caudal extent of the hypothalamus containing PVN and SON were cut on a cryostat and processed for SYT-1 and FG immunofluorescence. Sections were incubated in a mixture of

rabbit polyclonal FG (1:1000) and mouse monoclonal SYT-1 antibody (1:1000). FG and SYT-1 immunoreactivities were localized using Alexa Fluor 594-conjugated anti-rabbit IgG (1:500) and Alexa Fluor 488-conjugated anti-mouse IgG (1:500), respectively. Sections were rinsed in PBS, mounted on glass slides, coverslipped with mounting medium (Vector), and observed under the fluorescence microscope.

2.2.4 Immunofluorescence

Double immunofluorescence was employed to determine whether VP neurons in the PVN and SON co-express TRPV3. One set of coronal sections through the rostro-caudal extent of the hypothalamus containing PVN and SON of each animal (n = 3) was rinsed in PBS, treated with 0.5 % triton X-100 in PBS for 15 min, and immersed in blocking solution (3 % normal horse serum, 0.01 % triton X-100 in PBS) for 30 min. Sections were incubated overnight at 4 °C in a mixture of rabbit polyclonal TRPV3 antiserum (1:5000) and mouse monoclonal VP antibody (1:500). For TRPV3 immunofluorescence, biotin-tyramide amplification protocol was employed as described in chapter 1. For visualization of VP, sections were incubated in Alexa Fluor-549-conjugated anti-mouse IgG (Invitrogen, 1:500) for 2 h at room temperature. After rinsing in PBS, sections were mounted on glass slides, coverslipped with mounting medium containing DAPI, and observed under fluorescence microscope.

One set of sections from each animal was processed for c-Fos, SYT-1 or SV2 immunofluorescence as described above. Sections were incubated in a mixture of goat polyclonal c-Fos antiserum (1:500) and mouse monoclonal SYT-1 (1:500). One set of sections was also processed for SV2 immunofluorescence using mouse monoclonal SV2 antibody (1:500). The sections were rinsed in PBS and incubated in a mixture of Alexa Fluor-594

conjugated anti-goat IgG (1:300; Life Technologies) and Alexa Fluor-488 conjugated anti-mouse IgG (1:300; Life Technologies) for 2 h at room temperature. After further rinses, sections were mounted on glass slides, cover slipped with mounting medium (Vector) and observed under the fluorescence microscope. SV2 antiserum has been used as endogenous synaptic vesicle marker [185] and is known to label the LDCVs [167,170]. The SV2 antiserum used in the present study has been used in previous reports [167,186]. The specificity of the monoclonal SYT-1 antibody in mouse brain is well established and is known to recognize SYT-1, but does not cross react with SYT-2 [187].

To find out whether VP neurons in the PVN and SON express SYT-1/SV2 after hypertonic saline treatment, one set of sections from each animal in the control and 84 h HS-treated group was processed for double immunofluorescence. Sections were prepared for immunofluorescence as described above and incubated in a mixture of mouse monoclonal SV2 antibody (1:500) and rabbit VP antiserum (1:1000) or SYT-1 antibody (1:500) and rabbit VP antiserum (1:1000), overnight at 4 °C. The sections were rinsed in PBS and incubated in a mixture of Alexa Fluor-488-conjugated anti-mouse IgG (Life Technologies, 1:500) and Alexa Fluor-594-conjugated anti-rabbit IgG (Life Technologies, 1:500).

To find out whether TRPV3 neurons in PVN and SON express SYT-1 after HS-treatment, one set of sections from each animal in the control and 84 h HS-treated group was processed for double immunofluorescence. Sections were incubated in a mixture of rabbit polyclonal TRPV3 antiserum (1:5000) and mouse monoclonal SYT-1 antibody (1:500). For TRPV3 immunofluorescence, biotin-tyramide amplification protocol was employed. For the visualization of SYT-1, sections were incubated in Alexa Fluor-488-conjugated anti-mouse IgG (Invitrogen, 1:500).

Double immunofluorescence using MAP2/GAD65 antiserum and SYT-1 antibody was employed to determine the somatodendritic localization of SYT-1 after HS treatment. Sections containing the PVN and SON of control and 84 h HS-treated rats were incubated in a mixture of rabbit polyclonal MAP2 antiserum (1:1000) and monoclonal mouse SYT-1 antibody (1:500), overnight at 4 °C. The sections were rinsed in PBS and incubated in a mixture of Alexa Fluor-488-conjugated anti-mouse IgG (Life Technologies, 1:500) and Alexa Fluor-594-conjugated anti-rabbit IgG (Life Technologies, 1:500) for 1 h at room temperature.

The sections containing SON and PVN of HS-treated rats were incubated in a mixture of rabbit polyclonal glutamic acid decarboxylase (GAD65) antiserum (1:1000) and mouse monoclonal SYT-1 antibody (1:500) overnight at 4 °C. The sections were rinsed in PBS and incubated in a mixture of secondary antibodies [Alexa Fluor-594-conjugated anti-rabbit IgG (Life Technologies, 1:500) and Alexa Fluor-488-conjugated anti-mouse IgG (1:500)] for 1 h at room temperature. After rinsing in PBS, sections were mounted on glass slides, coverslipped with mounting medium containing DAPI, and observed under a fluorescence microscope.

The sections were observed under an AxioImager M2 fluorescence microscope (Carl Zeiss, Germany). Images were captured using AxioCam digital camera (Carl Zeiss) attached to the microscope. The images were superimposed, and adjusted for the brightness and contrast in Adobe Photoshop software. In addition, the SYT-1, TRPV3/SYT-1 and SYT-1/GAD double labelled sections were analyzed under a laser-scanning confocal microscope (LSM780, Carl Zeiss, Germany). The immunofluorescence signal was detected at excitation/emission wavelengths of the fluorophores [495/517 nm (DTAF, green) and 590/619 nm (Alexa Fluor 594, red)].

Fish were anaesthetised with 2-phenoxyethanol (1:2000; Sigma) and perfused

transcardially with PBS followed by an equal volume of 4% paraformaldehyde in 0.1M PB. Brains along with the pituitary were dissected out, postfixed in the same fixative overnight at 4 °C, cryoprotected in 25% sucrose overnight, embedded in tissue mounting media and serially cut on a cryostat in transverse or sagittal plane. Sections were mounted on poly-L-lysine (Sigma) coated slides for immunohistochemistry or directly collected in 1X PBS for immunofluorescence labelling using free-floating processing.

To study the organization of DA-containing neurons in the POA of *C. batrachus*, 25 µm thick transverse sections through the rostro-caudal extent of the preoptic area were processed for immunohistochemistry as described [188]. Sections were washed in PBS and prepared for immunohistochemical labeling as described above. Sections were incubated in rabbit polyclonal anti-TH antiserum (1:2000; Cat. # AB152; Millipore, USA) overnight at 4 °C. After washing in PBS, sections were incubated in biotinylated donkey anti-rabbit immunoglobulin IgG (1:100; Jackson Immunoresearch) for 2 h at room temperature. Sections were washed in PBS and incubated in streptavidin-peroxidase (1:100; Vector) for 2 h at room temperature. Sections were rinsed in PBS and incubated in 0.025% diaminobenzedine containing 0.0036% H_2O_2 in 0.05 M Tris buffer (pH 7.6) for 5 min to visualize the immunoreaction. Sections were coverslipped with glycerol-gelatin mounting medium and observed under the microscope. For identification of the hypophysiotropic nature of DA neurons in NPP, neuronal tracer DiI crystal was implanted into the pituitary [188]. The site of implant was sealed using agar and the brains were kept in 4% paraformaldehyde in dark. The brains were cryoprotected in sucrose and cut on cryostat. Sections were incubated in rabbit anti-TH antiserum and processed for immunofluorescence labeling as described above. The sections were mounted on glass slides and observed under a fluorescence microscope using dual fliter sets. The images were capured and panels were

prepared in Adobe Photoshop.

A set of sections of the preoptic area/hypothalamus was processed for TH or IST immunofluorescence labelling. The sections were prepared for immunofluorescence labeling as describe above. Sections were incubated in either rabbit polyclonal anti-TH antiserum (1:500) or mouse monoclonal anti-oxytocin antibody (1:500; gift from Dr. Harold Gainer, NIH) overnight at 4 °C, followed by incubation in Cy3-conjugated donkey anti-rabbit or anti-mouse IgG (1:250), respectively. One set of sections containing preoptic area and hypothalamus were processed for TRPV3 immunofluorescence as described in chapter 1. Sections were incubated in rabbit anti-TRPV3 antiserum (1:500) followed by incubation in Cy3 conjugated donkey anti-rabbit IgG. After rinsing in in PBS, sections were rinsed in Tris (pH 7.6), mounted with Vectashield mounting medium containing DAPI, observed under an Olympus fluorescence microscope, and images were captured. To safe guard against the possibility of any cross reactivity, sections of the preoptic and hypothalamic regions were incubated in the anti-TRPV3 antiserum preadsorbed with the control peptide.

To study the (i) spatial organization of TH-containing neurons in the NPP in relation to the NPO, (ii) the DAergic innervation of the IST neurons of the NPO, and (iii) association of DA or IST with TRPV3, sections through the rostro-caudal extent of the preoptic and tuberal areas of *C. batrachus* were processed for double labelling immunofluorescence using mixture of either TH/oxytocin, TH/TRPV3, or oxytocin/TRPV3 antibodies. Sections were incubated in a mixture of either (i) mouse monoclonal anti-oxytocin antibody (1:500) and rabbit polyclonal anti-TH antiserum (1:1000), (ii) rabbit anti-TRPV3 antiserum (1:500) and sheep polyclonal anti-TH antiserum (1:1000), or (iii) rabbit anti-TRPV3 antiserum (1:500) and mouse monoclonal anti-oxytocin antibody (1:500), for 24 h at 4 °C. The immunofluorescence signal was visualized

using respective fluorescence conjugated secondary antibodies. For TRPV3, signal amplification protocol was used as described in chapter 1. Sections were rinsed in PBS, mounted on glass slides, and covers-lipped with Vectashield mounting medium containing DAPI. Sections were observed under the fluorescence microscope and images were captured. The images were adjusted for brightness and contrast in Adobe Photoshop CS4 software. Sections of the hypothalamus of rat containing PVN and SON were processed for oxytocin/TRPV3 double immunofluorescence as described above.

2.2.5 Image and statistical analyses

Relative quantitative image analysis was employed to determine the time dependent (24-84 h) changes in number of SYT-1 immunoreactive neurons in PVN and SON after HS-treatment. Six sections through the rostro-caudal extent of the hypothalamus containing PVN and SON of each animal in the control and HS-treated groups (24-84 h) were analyzed under the AxioImager M2 fluorescence microscope. For each rat, the total number of SYT-1 immunoreactive cells throughout the rostro-caudal extent of the PVN and SON were counted on either side of the brain. The data from each animal in a group was pooled and mean ± SEM was calculated. The data analysis was performed using Prism 4 software (GraphPad Software, Inc., CA), with One way ANOVA followed by Bonferroni's multiple comparison test. $P < 0.05$ was considered statistically significant.

Semi-quantitative image analysis was performed to determine the percentage of VP neurons in PVN and SON expressing (i) TRPV3 (ii) c-Fos and TRPV3 (iii) SYT-1 (iv) SV2 was calculated. Five double labelled sections through the rostro-caudal extent of PVN and SON from each animal were analyzed under 200X magnification. By switching the filter sets, (i) green for

TRPV3/SYT-1/SV2 and red for VP, (ii) green for TRPV3, red for cFos and magenta for VP, the number of VP neurons co-expressing TRPV3, SYT-1/SV2, or c-Fos on either side of PVN and SON were counted for each animal, percentages determined and ± SEM calculated. Similarly, TRPV3 or SYT-1-immunoreactive neurons in the PVN and SON containing the retrograde accumulated FG were counted for each rat, and percentages were determined. The percentage of IST/TRPV3 neurons in the NPO of *C. batrachus* and oxytocin/TRPV3 neurons in the PVN and SON of rat were determined.

2.3 RESULTS

2.3.1 Hypophysiotropic neurons in the SON and PVN are equipped with TRPV3

As previously described [184], the intravenous injection of the retrograde neuronal tracer, FG resulted in labeling of neurons in PVN (Fig. 1A, D) and SON (Fig. 1G). Using double immunofluorescence, majority of the FG-positive neurons showed TRPV3-immunoreactivity in PVN (Fig. 1A-F) and SON (Fig. 1G-I). Approximately 86 % TRPV3-immunoreactive neurons in the PVN and ~96 % neurons in SON contained retrograde accumulation of FG.

2.3.2 VP neurons in the hypothalamus are equipped with TRPV3

VP-immunoreactive neurons were observed in the magnocellular subdivisions of the PVN and SON (Fig. 2). Double immunofluorescence showed co-localization of VP and TRPV3 in neurons of both these nuclei (Fig. 2C, F). Semi-quantitative image analysis revealed approximately 96.7 ± 1.55 % VP neurons in the SON and 88 ± 4 % VP neurons in the PVN co-expressed TRPV3.

2.3.3 Effect of HS treatment on neuronal activation in TRPV3-equipped VP neurons

While isolated c-Fos cells were seen in the hypothalamic SON (Fig. 3A) and PVN (Fig. 3I) of the control rats, HS treatment resulted in a robust expression of c-Fos in the SON (Fig. 3E) as well as PVN (Fig. 3M). By relative-quantitative image analysis, approximately 3.22 ± 2.78 % VP-immunoreactive neurons in SON and 1.25 ± 1.03 % VP-ir neurons in the PVN showed c-Fos in the control animals. Compared to controls, approximately 66.82 ± 5.3 % VP neurons in the SON ($P < 0.001$) and 54.86 ± 5.1 % VP-immunoreactive neurons in the PVN ($P < 0.001$)
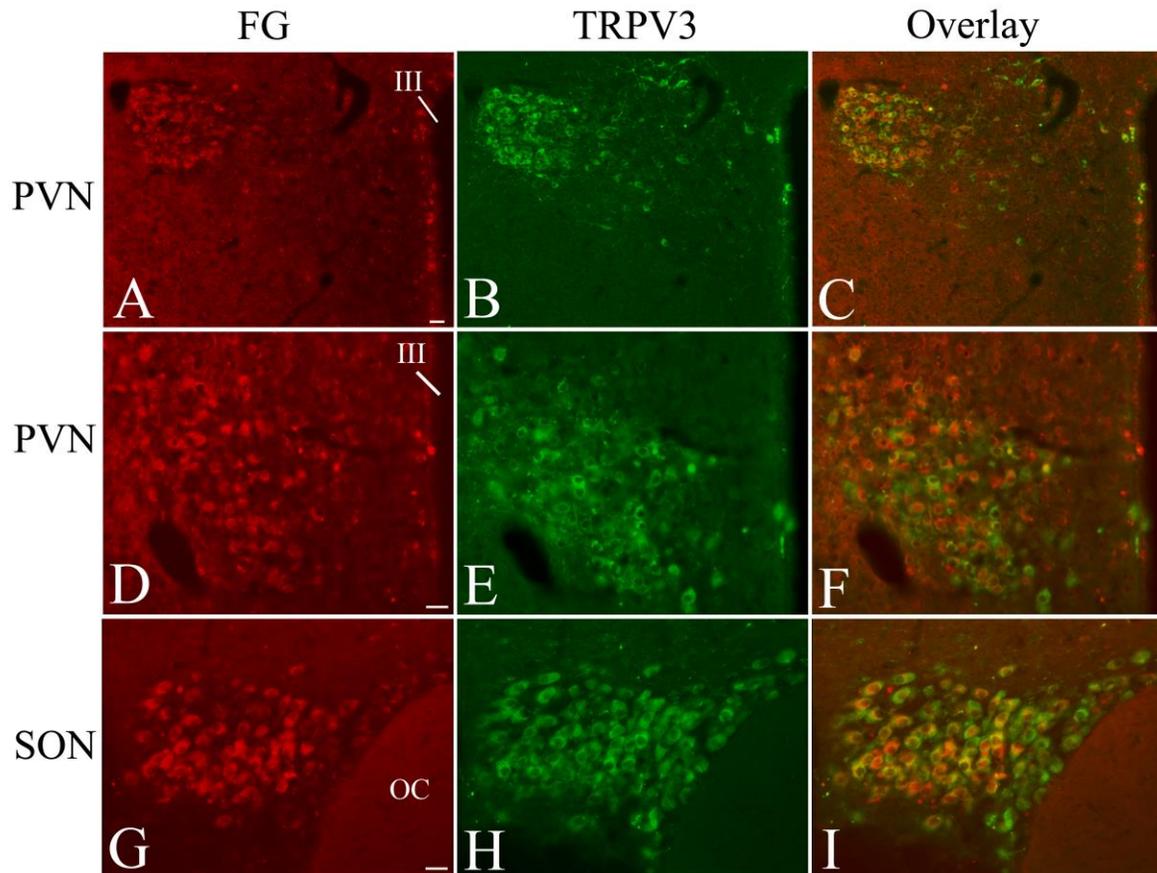
Figure 1: Neurons in the hypothalamic paraventricular (PVN) and supraoptic (SON) nuclei are equipped with TRPV3 and are hypophysiotropic.
Fluorescence photomicrographs showing (A, D, G) fluoro-gold (FG, blue) and (B, E, H) TRPV3-immunoreactive neurons (green) in the hypothalamic (A-F) PVN and (G-I) SON of rat. Note the co-localization of FG and TRPV3 (arrows) in the (C, F) PVN and (I) SON neurons. opt, optic tract; III, third ventricle. The FG photomicrographs were pseudocolored red in Adobe Photoshop. Scale bar = 25 µm.
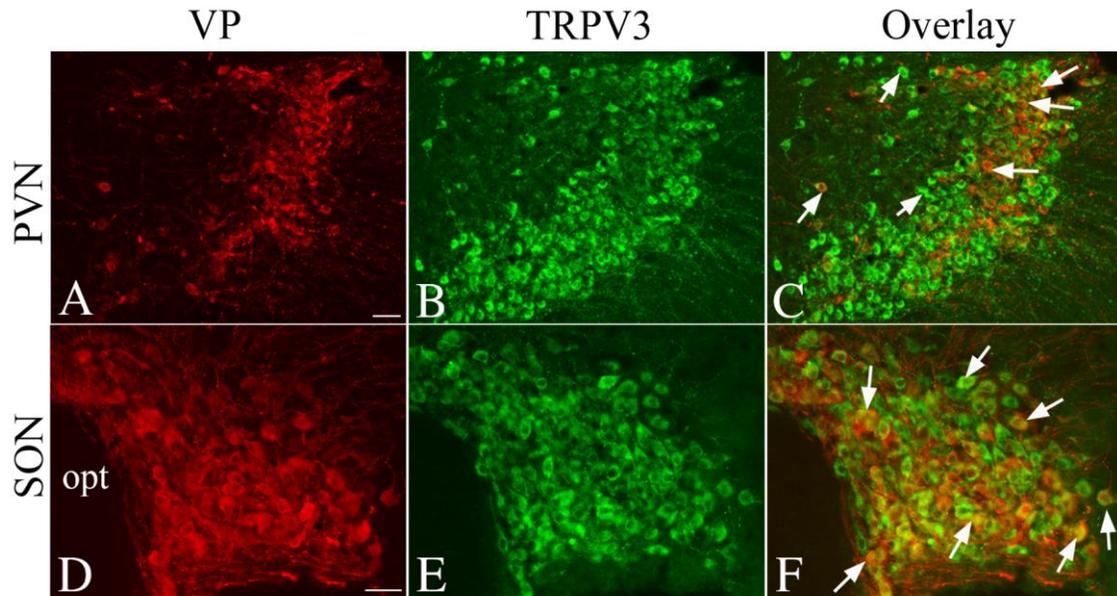
Figure 2: Vasopressin (VP) neurons in the hypothalamic paraventricular (PVN) and supraoptic (SON) nuclei co-express TRPV3.
Fluorescence photomicrographs showing the association between (A, D) VP (red) and (B, E) TRPV3 (green) in the (A-C) posterior magnocellular subdivision of PVN and (D-F) SON of rat. Note a majority of VP neurons co-expressing TRPV3 (arrows) in the (C) PVN and (F) SON. Co-localized cells appear yellow due to color mixing. Scale bar = 25 µm.
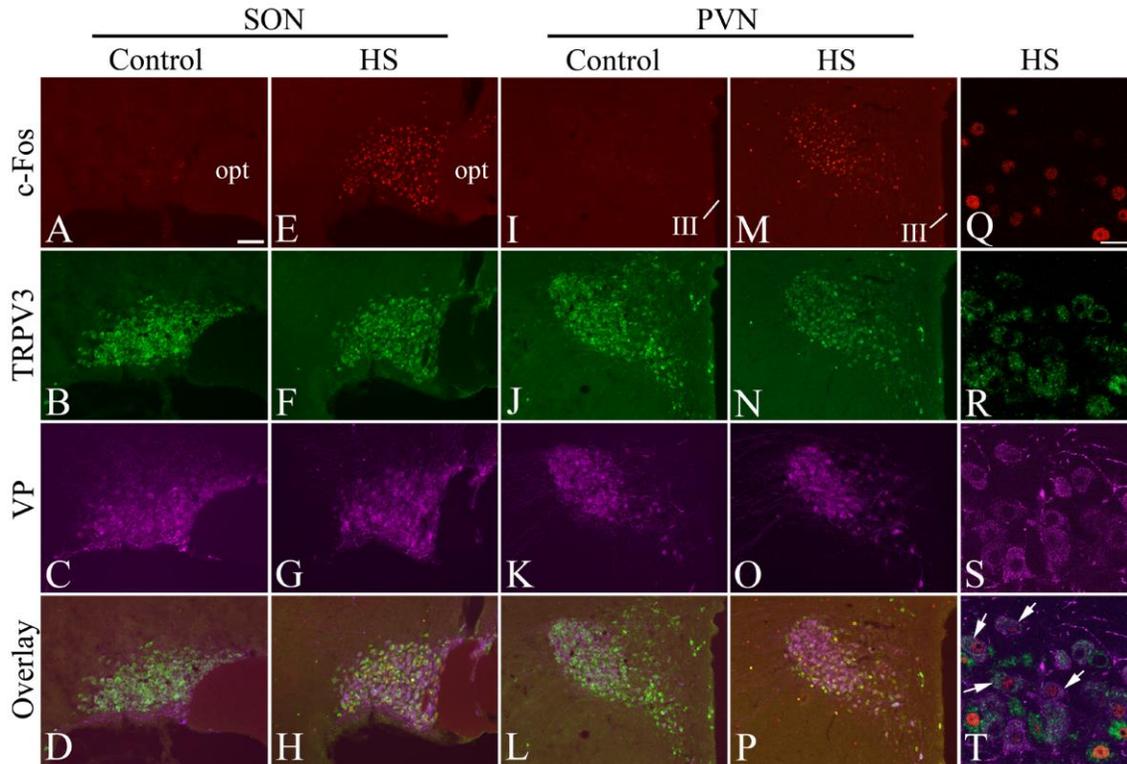
Figure 3: TRPV3-equipped vasopressin (VP) neurons in the hypothalamic supraoptic (SON) and paraventricular (PVN) nuclei respond to hyperosmotic challenge.

Fluorescence photomicrographs showing (A, E, I, M, Q) c-Fos (red), (B, F, J, N, R) TRPV3 (green), (C, G, K, O, S) VP (magenta) in the hypothalamic (A-H) SON and (I-P) PVN of (A-D and I-L) control and (E-H and M-P) hyperosmotic saline (HS)-treated rats. (D, H, L, P, T) Overlaid images of respective columns. High magnification photomicrographs showing (Q-T) c-Fos expression in TRPV3-equipped VP neurons (arrows in T). opt, optic tract; III, third ventricle. Scale bar = 50 µm in A-P and 20 µm in Q-T.

contained c-Fos after HS treatment. Triple immunofluorescence revealed that all the HS-activated VP neurons in the SON (Fig. 3E-H) and PVN (Fig. 3M-P) were TRPV3-immunoreactive. As reported previously, HS-treatment also resulted in c-Fos activation in OVLT neurons. Although TRPV3-ir neurons were observed in OVLT, no c-Fos was detected in TRPV3-ir neurons of OVLT.

2.3.4 Effect of HS treatment on SYT-1 and SV2-immunoreactivity in the hypothalamus

In the control rats, the SYT-1 was observed around the cell bodies of the PVN (Fig. 4A) and SON (Fig. 4C, E) neurons. Similarly, the SV2-immunoreactivity was also observed in the presynaptic terminals around the cell bodies of PVN and SON. The SYT-1 or SV2-immunoreactivity was not observed in the cell bodies of the hypothalamic neurons. A similar pattern of SYT-1 and SV2-immunoreactivity was also seen in other hypothalamic regions. The pattern of SYT-1 and SV2-immunoreactivity seen in the hypothalamus of control animals seem comparable to earlier reports [165,186]. After HS treatment, however, a dramatic induction in SYT-1-immunoreactivity was observed in the cell bodies of the PVN (Fig. 4B) and SON (Fig. 4D, F) neurons. The HS treatment also resulted in appearance of SV2-immunoreactivity in the cell bodies of PVN and SON neurons.

The salt loading resulted in appearance of c-Fos and SYT-1 immunoreactivity in the neurons of PVN and SON in a time dependent manner. Compared to controls (Figs. 5A, 6A), the 24, 48, 72, and 84 h of salt loading resulted in robust activation of c-Fos in the PVN (Fig. 5D, G, J, M) and SON (Fig. 6D, G, J, M) neurons. As described above, no SYT-1-immunoreactive neurons were seen in the PVN (Fig. 5B, C) and SON (Fig. 6B, C) of control rats. HS treatment
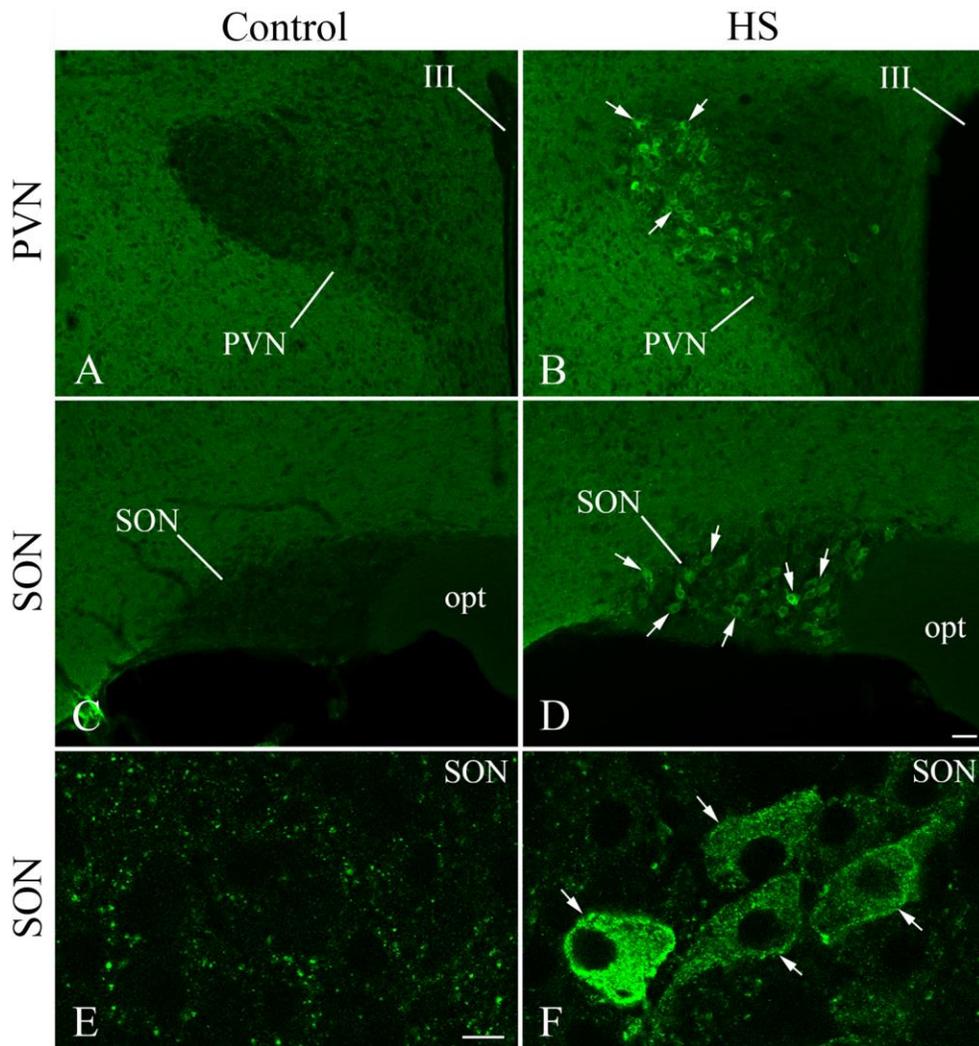
Figure 4: Synaptotagmin-1 (SYT-1) is expressed in cell bodies of the neurons of the hypothalamic paraventricular (PVN) and supraoptic (SON) nuclei after salt loading.
Fluorescence photomicrographs showing SYT-1 immunofluorescence (green) in the (A, B) PVN and (C, D) SON of (A, C) control and (B, D) hypertonic saline (HS)-treated animals. (E, F) Confocal photomicrographs show SYT-1-immunofluorescence in the SON of (E) control and (F) HS-treated rats. In control animals, SYT-1 immunoreactivity is seen in the presynaptic terminals around the cell bodies of PVN and SON neurons. Note the appearance of SYT-1 immunoreactivity (arrows) in the cell bodies of (B, D, F) PVN and SON neurons after HS treatment. opt, optic tract; III, third ventricle. Scale bar = 50 µm in A-D and 10 µm in E, F.
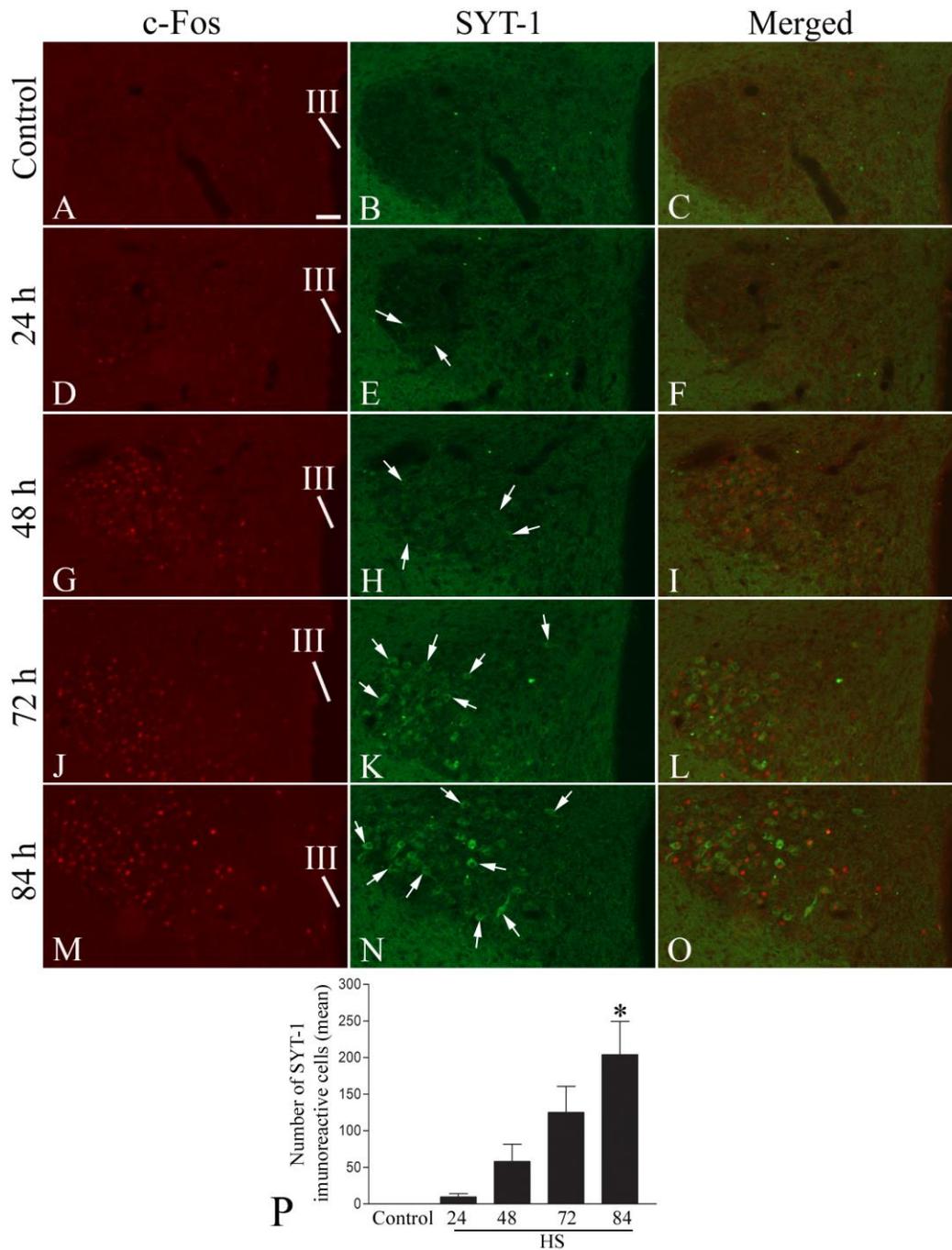
Figure 5: Activation of c-Fos and expression of synaptotagmin-1 (SYT-1) in the hypothalamic paraventricular nucleus (PVN) neurons after salt loading.
Fluorescence photomicrographs showing (A, D, G, J, M) c-Fos (red) and (B, E, H, K, N) SYT-1 (green) immunoreactivity in the PVN of (A-C) control and hypertonic saline (HS) treatment for (D-F) 24, (G-I) 48, (J-L) 72, and (M-O) 84 h. (C, F, I, L, O) Merged photomicrographs show c-Fos expression in SYT-1 immunoreactive neurons in the PVN. Note the SYT-1-immunoreactivity in the cell bodies of PVN (arrows in E, H, K, N) after salt loading. (P) Semi-quantitative analysis of number of SYT-1-immunoreactive cells in the PVN of control and salt loaded animals. III, third ventricle. Values represent mean ± SEM; *$P < 0.001$ *vs* control group (n = 3). Scale bar = 100 µm in A-O.
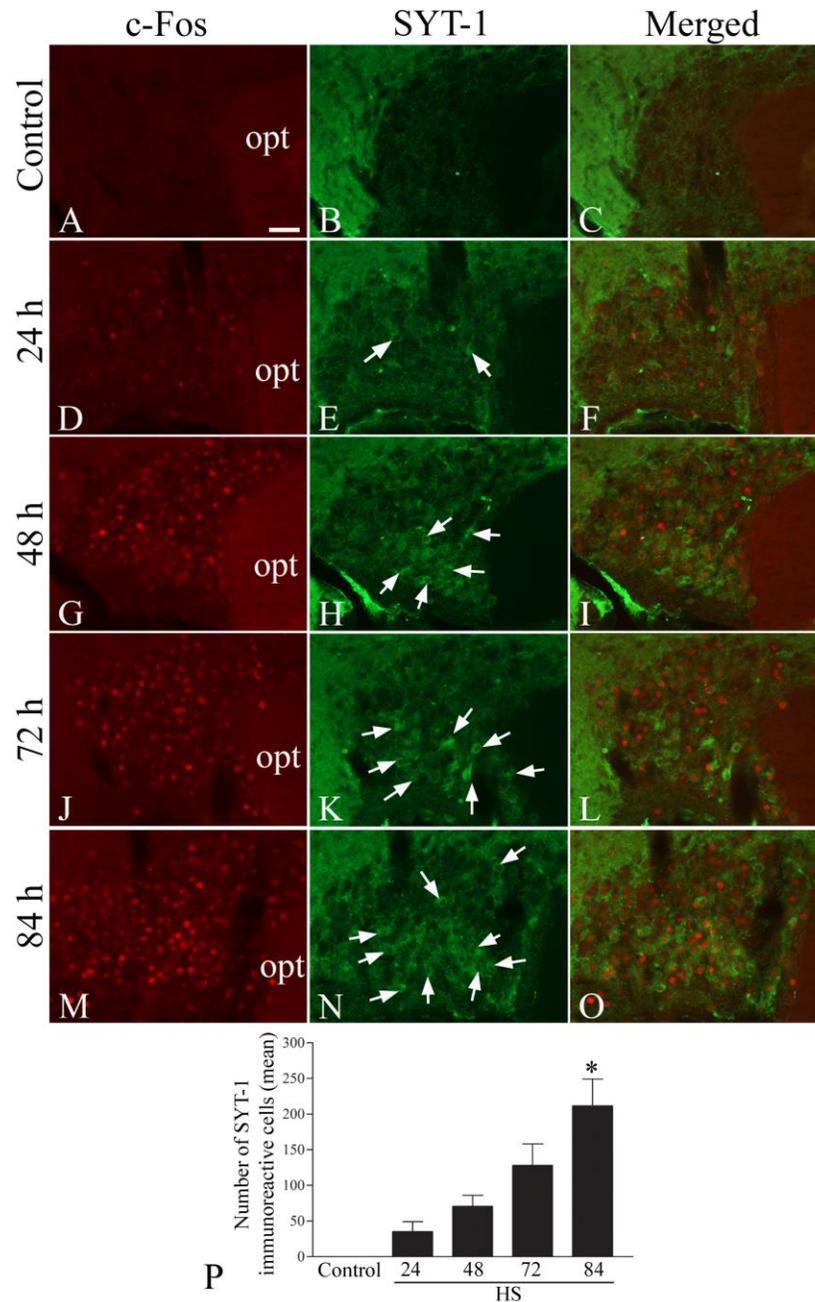
Figure 6: Activation of c-Fos and expression of synaptotagmin-1 (SYT-1) in the neurons of the hypothalamic supraoptic nucleus (SON) after salt loading.
Fluorescence photomicrographs showing (A, D, G, J, M) c-Fos (red) and (B, E, H, K, N) SYT-1 (green) immunoreactivity in the SON of (A-C) control and hypertonic saline (HS) treatment for (D-F) 24, (G-I) 48, (J-L) 72, and (M-O) 84 h. (C, F, I, L, O) Merged photomicrographs show c-Fos expression in SYT-1 immunoreactive neurons in the SON. Note SYT-1-immunoreactivity in the cell bodies of SON (arrows in E, H, K, N) after salt loading. (P) Semi-quantitative analysis of number of SYT-1-immunoreactive cells in the SON of control and salt loaded animals. opt, optic tract; III, third ventricle. Values represent mean ± SEM; *$P < 0.001$ *vs* control group (n = 3). Scale bar = 50 μm in A-O.

for 24 h resulted in appearance of isolated SYT-1-expressing cell bodies in the PVN (Fig. 5E, F) and SON (Fig. 6E, F). Compared to controls, a significant increase ($P < 0.05$) in the number of SYT-1-immunoreactive cell bodies was observed in the PVN (Fig. 5H, I) and SON (Fig. 6H, I) 48 h after the HS treatment. A further increase in the number of SYT-1-immunoreactive neurons was observed in the PVN and SON after 72 h (Fig. 5K, L and 6K, L) and 84 h (Fig. 5N, O and 6N, O) of salt loading. The number of SYT-1-immunoreactive neurons in the PVN and SON of rats treated with HS for 72 and 48 h was comparable ($P > 0.05$).

2.3.5 HS treatment-induced SYT-1 expression in the somatodendritic compartment of the magnocellular neurons

MAP2 antiserum has been used as a marker to localize the somatodendritic domain of neurons in the adult rodent brain [185,189–191]. Application MAP2 immunofluorescence resulted in labeling of the cortical (Fig. 7A) and hypothalamic (Fig. 7D) neurons. In control animals, MAP2 and SYT-1 double immunofluorescence showed SYT-1-immunoreactive presynaptic terminals around the MAP2-immunoreactive cell bodies in the cortex (Fig. 7A-C) and PVN (Fig. 7D-F). No SYT-1 immunoreactivity was observed in the cell bodies of the PVN and SON neurons in the control animals. Following the HS treatment, SYT-1 immunoreactivity was localized in the MAP2-immunreactive cell bodies of PVN and SON neurons (Fig. 7G-I).

The GAD-immunoreactivity has been demonstrated in the presynaptic terminals around VP cell bodies but not in the somata/dendrites after salt loading [192]. GAD immunofluorescence therefore served as presynaptic marker. Application of GAD and SYT-1 double immunofluorescence on the hypothalamic sections of salt-loaded rats showed a clear
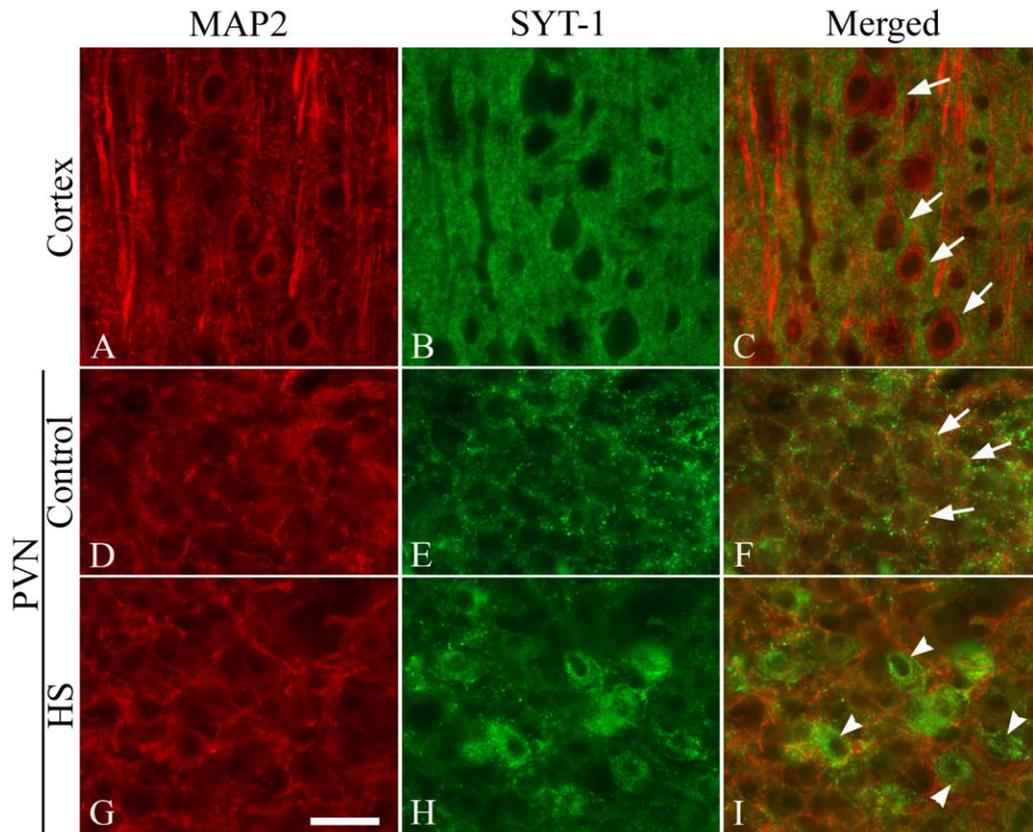
Figure 7: Synaptotagmin-1 (SYT-1) is recruited to the somatodendritic compartment of the hypothalamic neurons after salt loading.
Double immunofluorescence photomicrographs showing the association between (A, D, G) microtubule associated protein 2 (MAP2; red) and (B, E, H) SYT-1 (green) in the (A-C) cortex; and (D-I) hypothalamic paraventricular nucleus (PVN) of (D-F) control and (G-I) hypertonic saline (HS)-treated rats. SYT-1-immunoreactivity is seen in presynaptic terminals around the cell bodies in the cortex (arrows in C) and PVN of control rats (arrows in F). After HS-treatment, SYT-1-immunoreactivity is seen in the cell bodies of PVN (arrowheads in I). Scale bar = 20 µm.
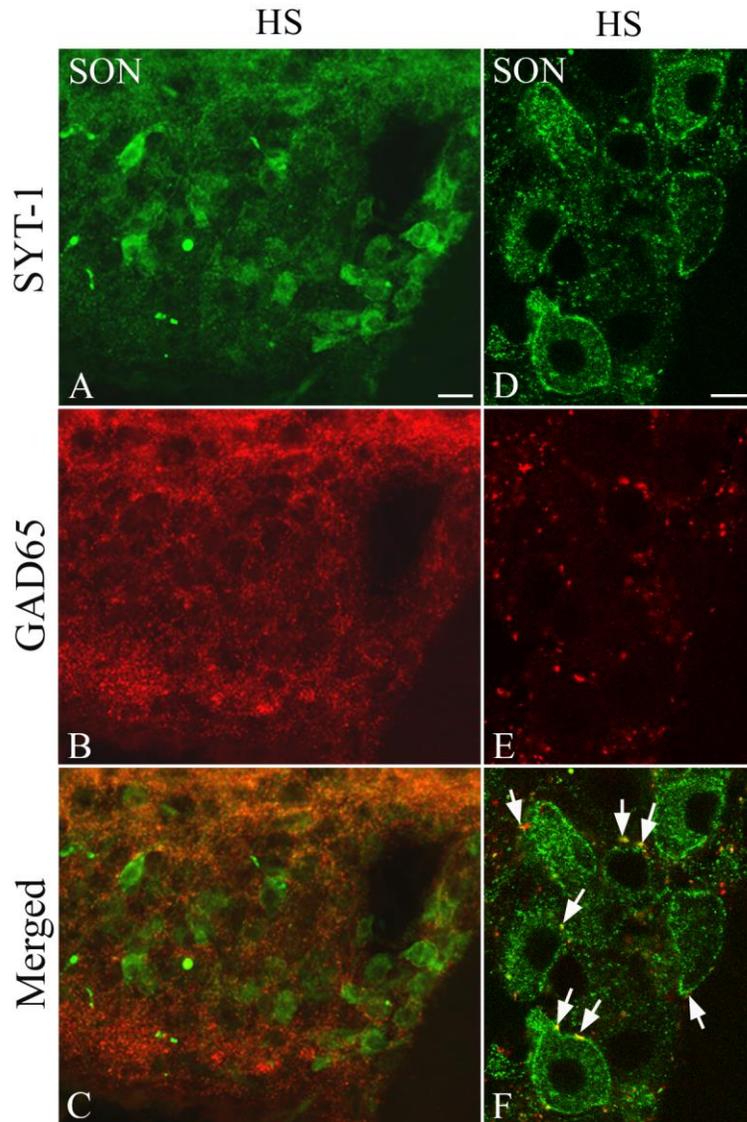
Figure 8: Synaptotagmin-1 (SYT-1) is expressed at presynaptic terminals and postsynaptically in the somatodendritic compartment of the hypothalamic neurons after salt loading.
Double immunofluorescence photomicrographs showing the association between (A, D) SYT-1 (green) and (B, E) glutamic acid decarboxylase (GAD, red) in the hypothalamic supraoptic nucleus (SON) of hypertonic saline (HS) loaded rats. (D-F) Confocal photomicrographs show the association between SYT-1 and GAD. Note the presence of GAD-immunoreactivity (arrows in F) in the presynaptic terminals around SYT-1-expressing cell bodies. Scale bar = 25 µm in A-C and 10 µm in D-F.

distinction between the presynaptic GAD-immunoreactive terminals and somata/dendritic SYT-1 (Fig. 8A-F).

2.3.6 SYT-1-immunoreactive neurons in the PVN and SON are hypophysiotropic

FG labelled neurons were observed in the PVN (Fig. 9A) and SON (Fig. 9D). Using double immunofluorescence labeling, all SYT-1-immunoreactive neurons in the PVN (Fig. 9A-C) and SON (Fig. 9D-F) showed retrograde accumulation of FG.

2.3.7 VP neurons in the SON and PVN express SYT-1 and SV2 after HS treatment

In the control rats, application of double immunofluorescence showed VP neurons in the PVN and SON, and SYT-1 in the presynaptic terminals around the VP cell bodies (Fig. 10A-C, G-I). After HS treatment, a great majority of SYT-1-immunoreactive cell bodies in the PVN (approximately 93 ± 3 %) (Fig. 10D-F) and SON (approximately 95 ± 4 %) (Fig. 10J-L) were VP-positive. Approximately 58 ± 4 % VP neurons in PVN and 43 ± 3 % VP neurons in SON showed SYT-1 immunoreactivity.

In the control rats, no SV2-containing cell bodies were observed in the PVN (Fig. 11A) and SON (Fig. 11G) and SV2-immunoreactivity was confined to the presynaptic terminals around VP cell bodies in the PVN and SON. HS treatment resulted in a dramatic appearance of SV2-immunoreactive cell bodies in the PVN (Fig. 11D) and SON (Fig. 11J). Application of VP and SV2 double immunofluorescence showed their co-localization in the cell bodies of PVN (Fig. 11D-F) and SON (Fig. 11J-L) after salt loading. Semi-quantitative analysis revealed, approximately 71 ± 4 % VP neurons in PVN and 58.4 ± 4 % VP neurons in SON co-expressed SV2 after 84 h salt loading.
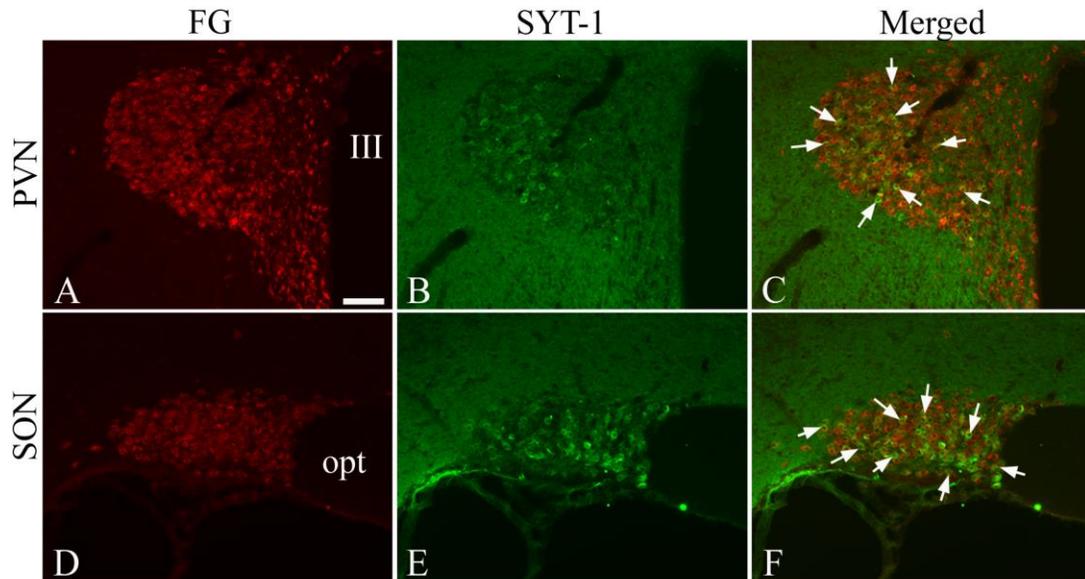
Figure 9: Synaptotagmin-1 (SYT-1) expressing magnocellular neurosecretory neurons in the hypothalamic paraventricular (PVN) and supraoptic (SON) nuclei are hypophysiotropic.
Double immunofluorescence photomicrographs showing the association between (A, D) fluoro-gold (FG, red) and (B, E) SYT-1 (green) in the (A-C) PVN and (D-F) SON neurons of hypertonic saline (HS) treated rats. A great majority of SYT-1-immunoreactive neurons in the PVN and SON retrogradely accumulated FG (arrows in C, F). opt, optic tract; III, third ventricle. Scale bar = 100 µm.
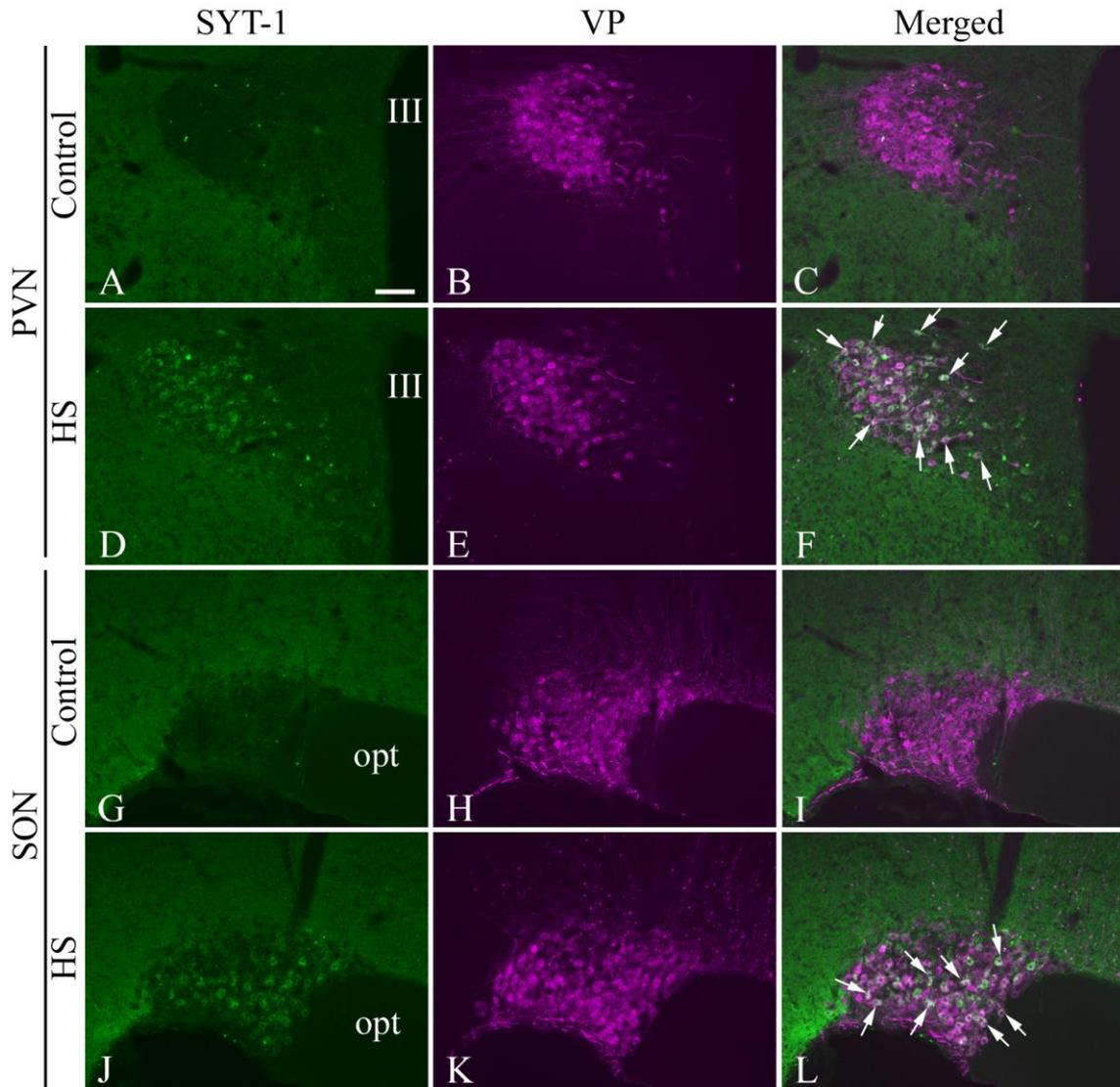
Figure 10: Somatodendritic compartment of the vasopressin (VP) neurons in the hypothalamic paraventricular (PVN) and supraoptic (SON) nuclei co-express synaptotagmin-1 (SYT-1) after salt loading.
Double immunofluorescence photomicrographs showing the association between (A, D, G, J) SYT-1 (green) and (B, E, H, K) VP (magenta) in the (A-F) PVN and (G-L) SON neurons of (A-C, G-I) control and (D-F, J-L) hypertonic saline (HS) treated rats. Note the co-expression of VP and SYT-1 (arrows) in the (F) PVN and (L) SON neurons after HS-treatment. opt, optic tract; III, third ventricle. Scale bar = 100 µm.
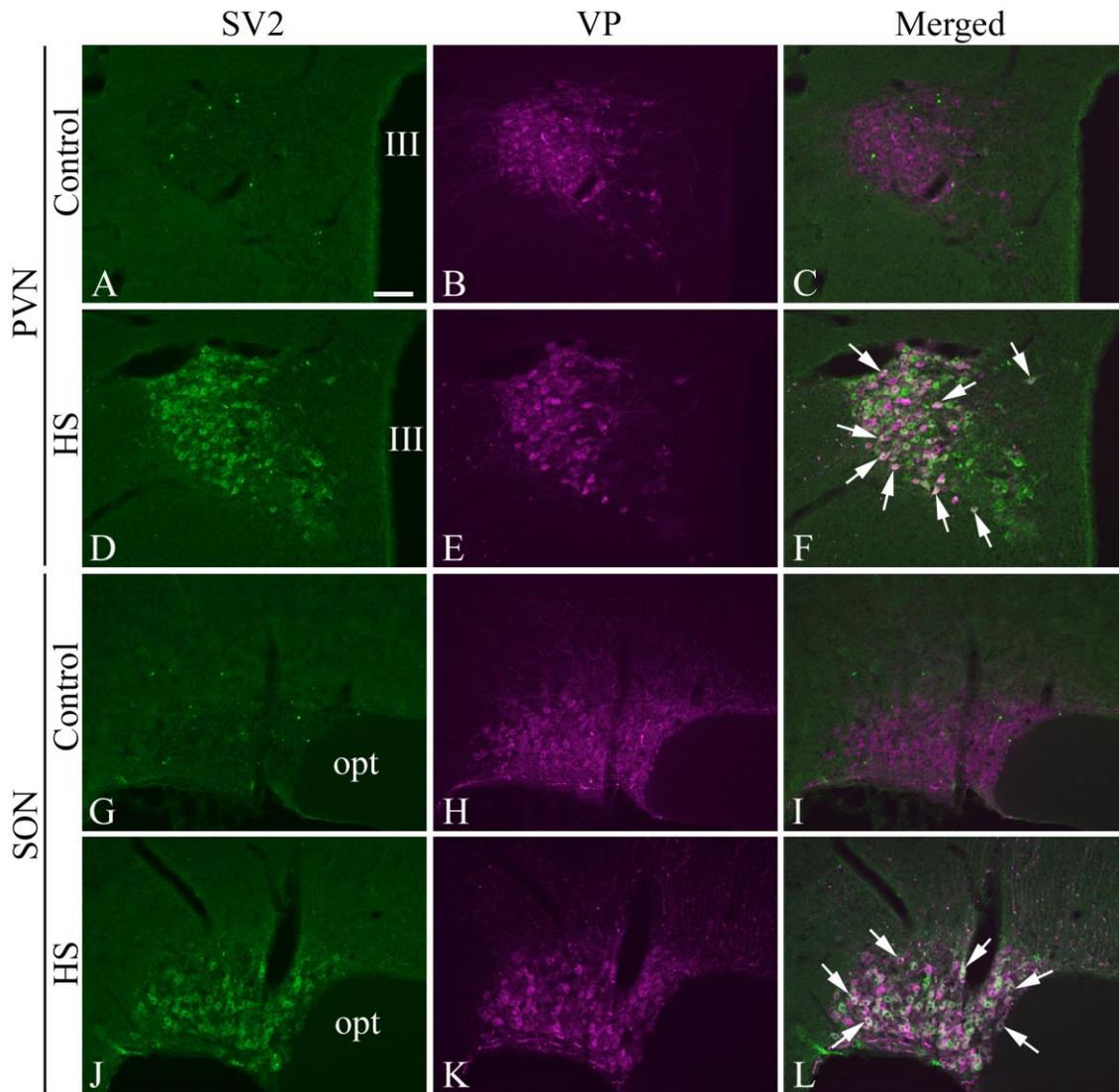
Figure 11: Somatodendritic compartment of the vasopressin (VP) neurons in the hypothalamic paraventricular (PVN) and supraoptic (SON) nuclei co-express synaptic vesicle protein-2 (SV2) after salt loading.
Double immunofluorescence photomicrographs showing the association between (A, D, G, J) SV2 (green) and (B, E, H, K) VP (magenta) in the (A-F) PVN and (G-L) SON neurons of (A-C, G-I) control and (D-F, J-L) hypertonic saline (HS) treated rats. Note the co-expression of VP and SV2 (arrows) in the (F) PVN and (L) SON neurons after HS-treatment. opt, optic tract; III, third ventricle. Scale bar = 100 µm.

2.3.8 SYT-1 neurons in the hypothalamus are equipped with TRPV3 ion channel

SYT-1-immunoreactive neurons were observed in the SON and magnocellular subdivisions of the PVN (Fig. 12). Double immunofluorescence showed co-localization of SYT-1 and TRPV3 in neurons of both these nuclei (Fig. 12A-C). Semi-quantitative analysis revealed approximately 73.65 ± 1 % SYT-1 neurons in SON and 74.50 ± 1 % SYT-1 immunoreactive neurons in PVN co-expressed TRPV3.

2.3.9 Organization of DA- and IST-containing systems in the preoptic area, tuberal region, and pituitary of *C. batrachus* and their relevance to neuroendocrine regulation

DA neurons were seen in the anterior (NPPa) (Fig. 13A-C) and posterior (NPPp) (Fig. 13F, G) subdivisions of the nucleus preopticus periventricularis (NPP). IST neurons were observed in the supraoptic (NPOso) (Fig. 14A, B) and paraventricular (NPOpv) (Fig. 14C, D) subdivisions of the nucleus preopticus (NPO). The axons of the DA neurons of NPPa (Fig. 13C-E) and IST neurons of NPO (Fig. 14K) project to the pituitary gland and innervate luteinizing hormone cells. DiI labeled cells were seen in the NPO as well as NPPa but no labeling was seen in neurons of NPPp (Fig. 15A-E). Application of TH-immunofluorescence showed 77% TH neurons of NPPa containing DiI (Fig. 15F-H) suggesting their hypophysiotropic nature. TH neurons in NPPp did not show retrograde accumulation of DiI (Fig. 15I-K).

2.3.10 Association between DA- and IST-containing systems in the preoptic area of

C. batrachus

Although no co-expression of DA and IST was seen in the neurons of preoptic area/
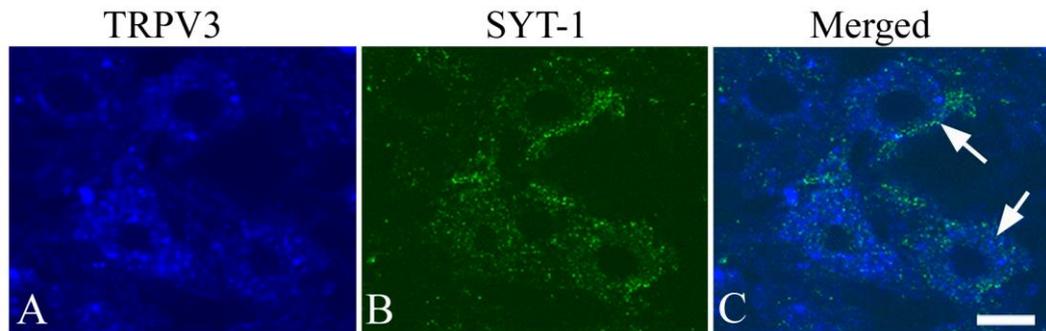
Figure 12: Synaptotagmin-1 (SYT-1) is up-regulated in TRPV3-equipped hypothalamic paraventricular (PVN) and supraoptic nuclei (SON) neurons after salt loading.
Confocal photomicrographs showing the association between (A) TRPV3 (blue) and (B) SYT-1 (green) in the magnocellular subdivision of the hypothalamic paraventricular (PVN) and supraoptic (SON) nuclei of rat treated with hypertonic saline (HS). (C) TRPV3-expressing neurons show SYT-1-immunoreactivity in the cell bodies (arrows) after HS treatment. Scale bar = 10 µm.

hypothalamus of *C. batrachus*, DA-axons of NPPp neurons seem to innervate IST neurons of NPO (Fig. 14C-F, I).

2.3.11 IST neurons in the NPO of *C. batrachus* are equipped with TRPV3

Application of anti-TRPV3 antiserum on the sections of the preoptic area and hypothalamus of *C. batrachus* has resulted in labeling of cell bodies and fibers. Distinct neurons were seen in the NPO (Fig. 16A) but no TRPV3 immunofluorescence was observed following application of the preadsorbed TRPV3 antiserum with control peptide (Fig. 16B, C). Isolated TRPV3-ir neurons were observed in the POA and NPPa (Fig. 16D, E) but several immunoreactive neurons were found in the NPOpv (Fig. 16F) as well as NPOso (Fig. 16G). TRPV3-ir fibers as well as cells were observed in the tuberal region of *C. batrachus* including nucleus lateralis tuberis, nucleus recessus lateralis and nucleus anterior tuberis ventral (Fig. 16H-N). Isolated TRPV3-ir fibers were observed in the pituitary gland (Fig. 16O). Using double immunofluorescence, none of the DA neurons in NPP showed co-expression of TRPV3 but a great majority of IST neurons in NPO were equipped with TRPV3 (Fig. 17A-I).

2.3.12 Oxytocin neurons in the PVN and SON of rat are equipped with TRPV3

Application of double immunofluorescence showed co-localization of oxytocin and TRPV3 in neurons of PVN (Fig. 18A-C) and SON (Fig. 18D-F) of rat. Using semi-quantitative image analysis approximately 88 and 75 % oxytocin neurons in the PVN and SON showed co-expression of TRPV3, respectively (Fig. 18C, F).
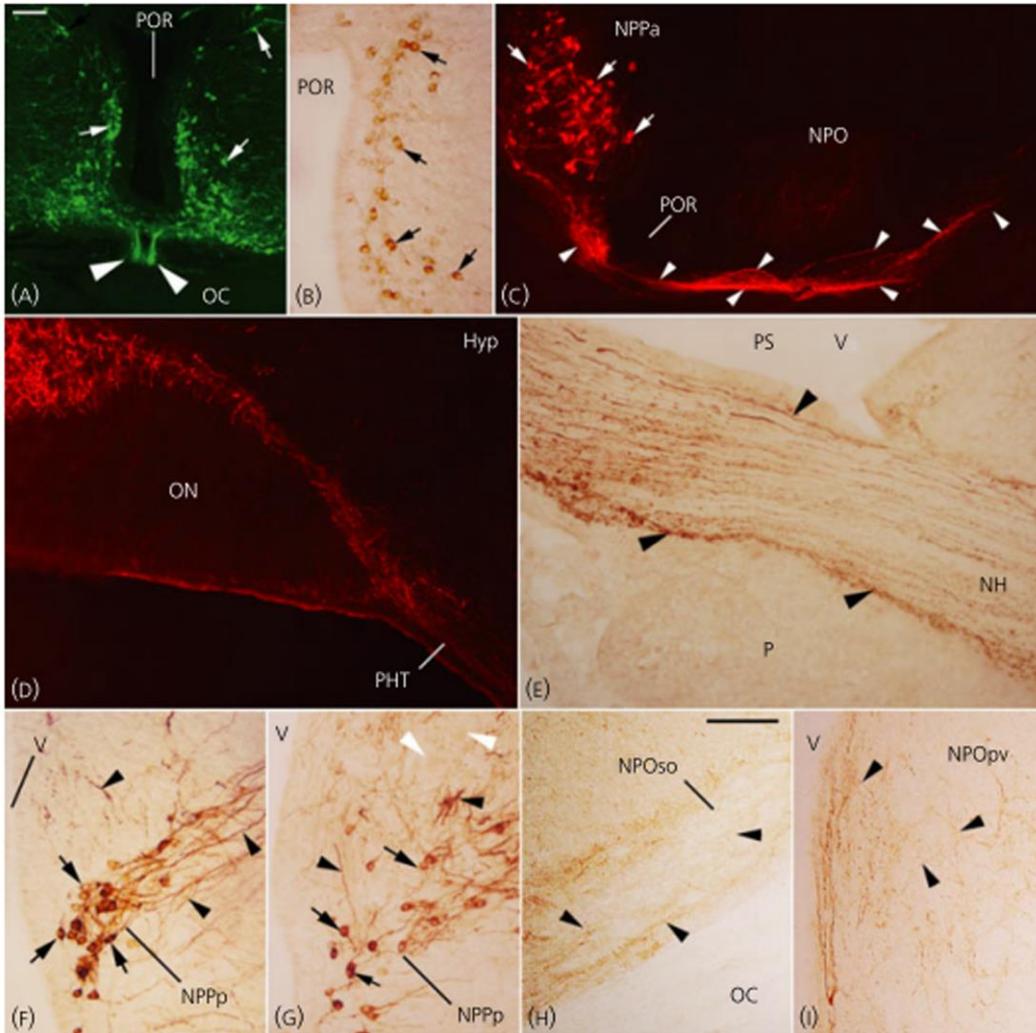
Figure 13: Photomicrographs of the preoptic area (POA) of *Clarias batrachus* showing the organization of tyrosine hydroxylase (TH)-immunoreactive neurones (arrows) and fibres (arrowheads).
(A) In the nucleus preopticus periventricularis anterior (NPPa), TH neurons and fibres are seen at the base of the POA and extending dorsally around the (B) preoptic recess (POR). (C) Sagittal section through the midline of the brain, showing TH in the NPPa associated with a thick bundle of TH axons that runs ventral to the (A, C) POR and (C) nucleus preopticus (NPO), and extends caudally towards the hypothalamus (Hyp). (D) The TH fibres swing over the optic nerve (ON) and enter into the preoptico-hypophyseal tract (PHT). Several TH-containing axons are visible running through the (E) pituitary stalk (PS) and neurohypophysis (NH) of the pituitary (P). Several TH neurones are visible in the (F) nucleus preopticus periventricularis posterior (NPPp) and are located just below the (G) NPO neurones (white arrowheads). Immunoreactive fibres are seen in the (H) supraoptic (NPOso) and (I) paraventricular (NPOpv) subdivisions of the NPO. OC, optic chiasm; V, ventricle. Scale bar = 25 µm (A–G) and 50 µm (H, I).
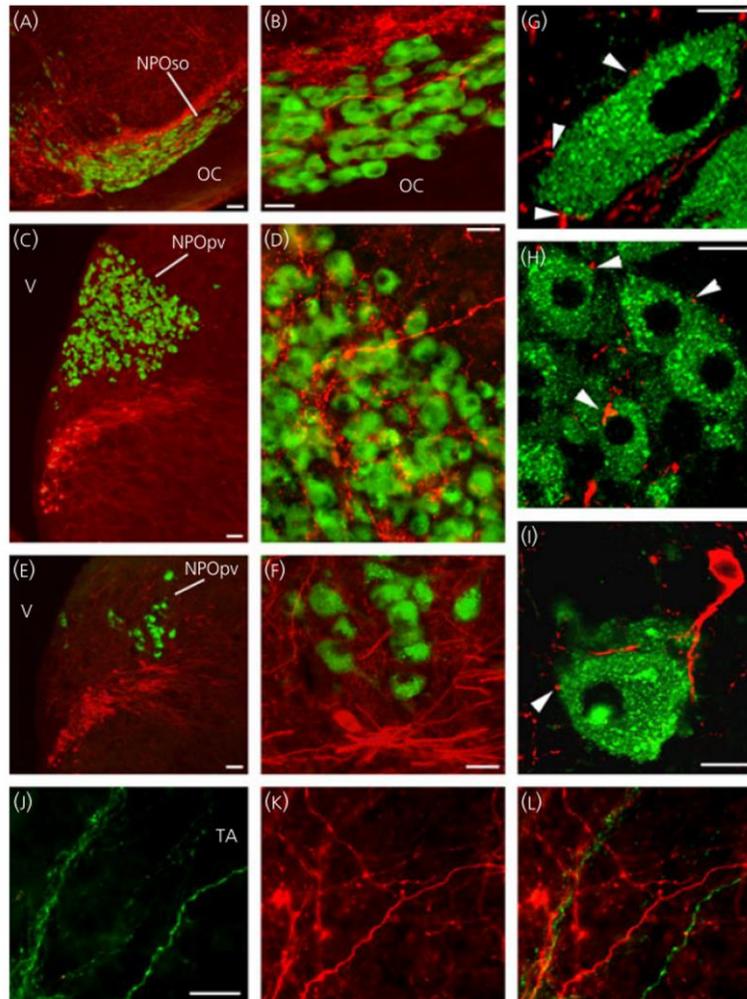
Figure 14: Association between between isotocin (IST) (green) and tyrosine hydroxylase (TH) (red) containing systems in the preoptic area (POA) of *Clarias batrachus*.

Low magnification photomicrographs are shown on the left (A, C, E) and their magnified view is shown on the right (B, D, F). Several TH-immunoreactive fibres are seen in the vicinity of isotocin neurones in the (A, B) supraoptic (NPOso) and (C-F) paraventricular (NPOpv) subdivisions of the nucleus preopticus (NPO). Cell bodies of few TH- immunoreactive neurones in the nucleus preopticus periventricularis anterior (NPPa) are seen in close association with isotocin neurones in the (A, B) NPOso. The TH-immunoreactive axons of the nucleus preopticus periventricularis posterior (NPPp) project towards the isotocin neurones in the (C) NPOpv, and associated with the isotocin neurones (D). Caudally, axons of the TH-immunoreactive neurones of the NPPp project towards the isotocin neurones in the (E, F) NPOpv. Confocal images (G–I) showing the association between TH-containing axons (red) and isotocin neurones (green) in the (G) NPOso and (H, I) NPOpv. The TH-containing boutons are seen on the isotocin neurones in each subdivision (arrowheads). A TH-containing neurone in the NPPp is seen in close association with an isotocin neurones in the (I) NPOpv. In the (J-L) tuberal area (TA), no colocalisation of isotocin (J) and TH (K) is seen. OC, optic chiasm. Scale bar = 25 µm.
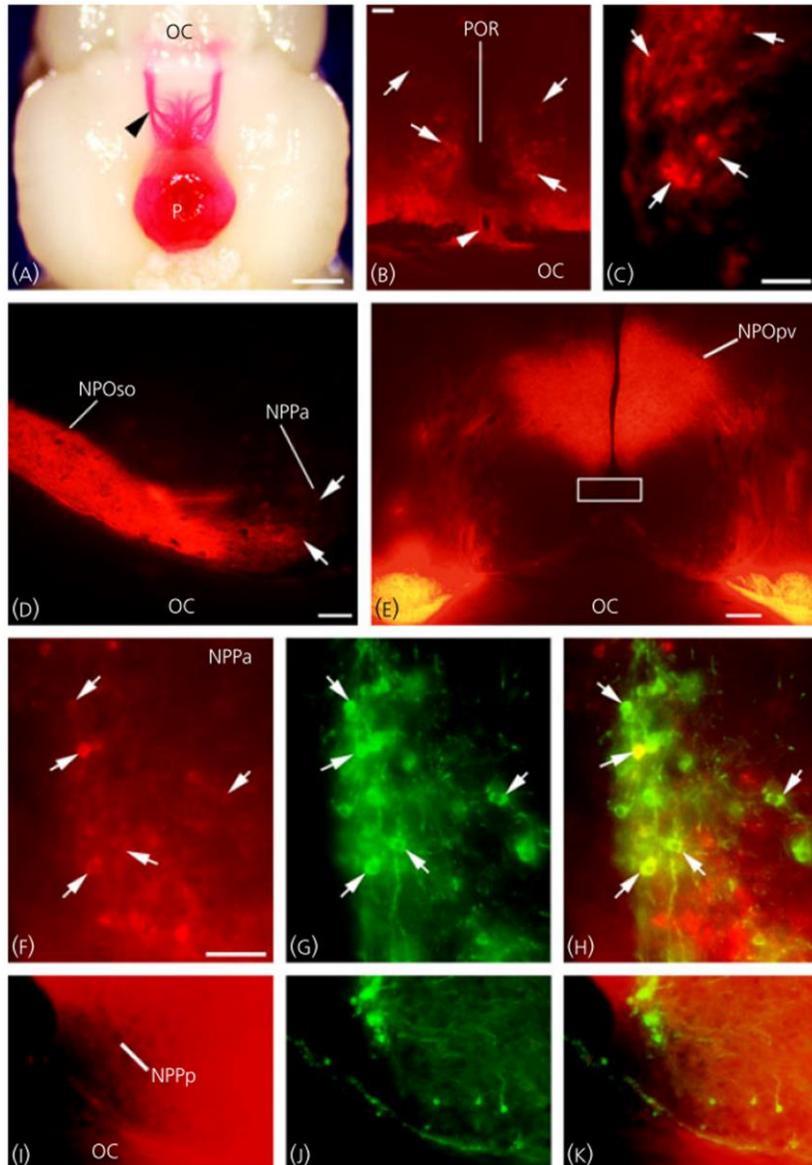
Figure 15: Retrograde neuronal tracing from the pituitary (P) and tyrosine hydroxylase (TH)-containing hypophysiotrophic neurons in the preoptic area (POA) of *Clarias batrachus*.

Example of 1,1'-dioctadecyl-3,3,3',3'-tetramethylindocarbocyanine perchlorate (DiI) injection in the (A) pituitary and retrograde transport towards the POA (arrowhead). Several retrogradely labelled neurones (arrows) are seen in the (B–D) nucleus preopticus periventricularis anterior (NPPa) around the preoptic recess (POR). A bundle of retrogradely labelled fibres (arrowhead) is seen on the ventral side of the (B) POA. In the nucleus preopticus (NPO), Intense DiI fluorescence is visible in the (D) supraoptic (NPOso) and (E) paraventricular (NPOpv) subdivisions. Beneath the NPOpv, no DiI labelled cell bodies are seen in the (E) nucleus preopticus periventricularis posterior (NPPp) (square). In the NPPa, several (F) DiI (red) and (G) TH-containing (green) neurones are seen. The majority of the TH-containing neurones in this subdivision of the NPP are hypophysiotrophic and appear yellow as a result of colour mixing (arrows, H). In the (I) NPPp, no DiI labelled neurones are visible, although several (J) TH-containing neurones are observed in this region. None of the (K) TH-containing neurones in this region are hypophysiotrophic. OC, optic chiasm. Scale bar = 1 mm (A); 25 µm (B–K).
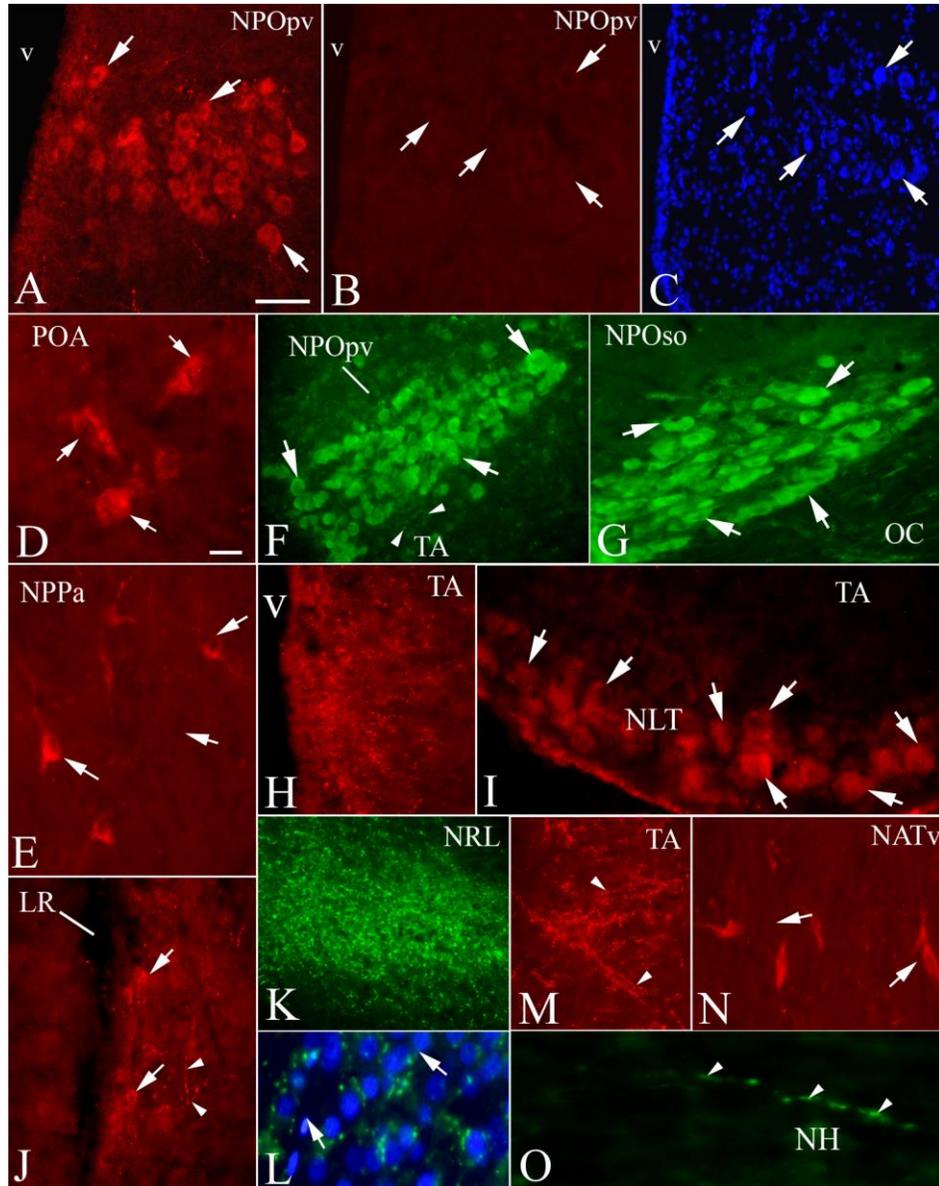
Figure 16: Organization of TRPV3-immunoreactive elements in the preoptic area (POA), tuberal area (TA), and pituitary of *Clarias batrachus*.
Photomicrographs showing TRPV3-immunoreactive cells (arrows) and fibers (arrowheads) in the (A) paraventricular subdivision of the nucleus preopticus (NPOpv), (B, C) no TRPV3 immunofluorescence was observed in NPOpv following application of the TRPV3 antiserum preadsorbed with control peptide. Isolated TRPV3 immunoreactive cell were observed in (D) preoptic area (POA) and (E) nucleus preopticus periventricularis anterior (NPPa). TRPV3-immunoreactive neurons are seen in the (F) NPOpv and (G) supraoptic subdivision of the NPO (NPOso). In the (H-N) tuberal area (TA), TRPV3 immunoreactive fibers and cells are seen in the (I) nucleus lateralis tuberis (NLT). TRPV3-ir cells and fibers are also seen around (J) lateral recess (LR), in the (K, L) nucleus recessus lateralis (NRL), and (N) nucleus anterior tuberis ventral. TRPV3-ir fibers are seen entering into the (O) neurohypophysis (NH) of the pituitary (P). v, ventricle. Scale bar = 50 µm in A-C, E-O and 25 µm in D.
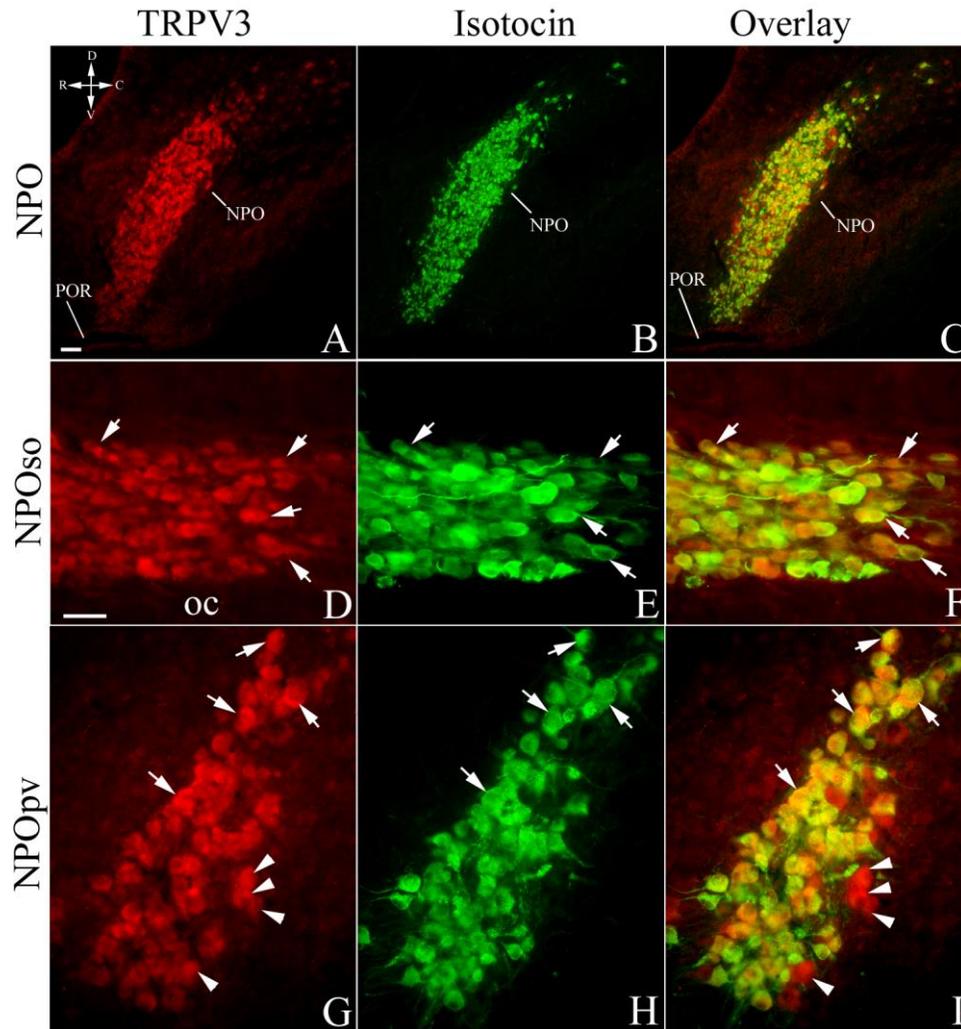
Figure 17: Isotocin (IST) neurons in the nucleus preopticus (NPO) of *Clarias batrachus* co-express TRPV3.
Fluorescence photomicrographs showing the association between (A, D, G) TRPV3 (red) and (B, E, H) IST (green) in the (A-C and G-H) paraventricular (NPOpv) and (D-F) supraoptic (NPOso) subdivisions of NPO. Majority of IST neurons in NPO co-express TRPV3 (arrows). Scale bar = 50 µm (A-C & D-I).
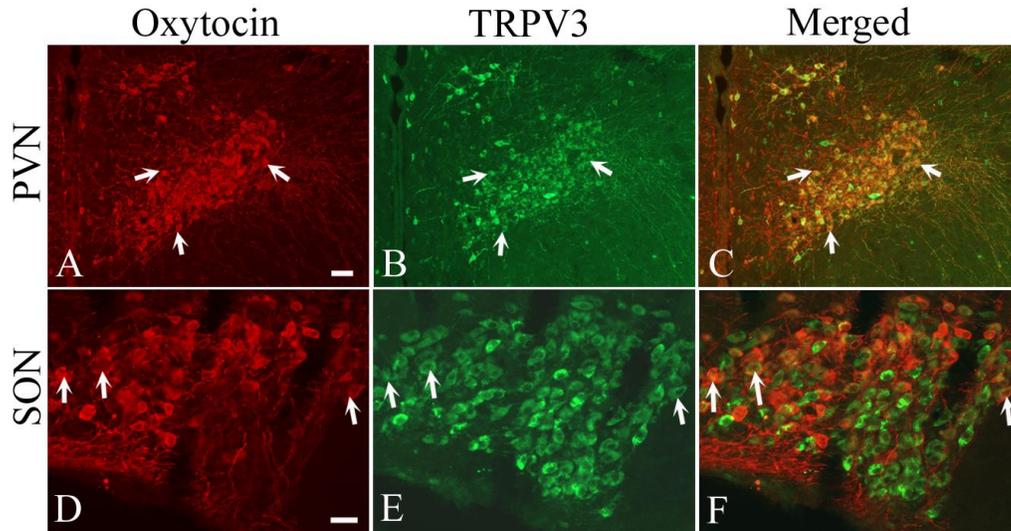
Figure 18: Oxytocin neurons in the hypothalamic paraventricular (PVN) and supraoptic (SON) nuclei co-express TRPV3.
Fluorescence photomicrographs showing the association between (A, D) oxytocin (red) and (B, E) TRPV3 (green) in the (A-C) PVN and (D-F) SON of rat. Note a majority of oxytocin neurons co-expressing TRPV3 (arrows) in the (C) PVN and (F) SON. Co-localized cells appear yellow due to color mixing. Scale bar = 50 µm.

2.4 DISCUSSION

A great majority of the VP neurons in the PVN and SON seem to be equipped with TRPV3 ion channel and these neurons respond to hyperosmotic stimulation. The results suggest that TRPV3 may serve as potential regulator of the VP neurons. In addition to the axonal release, hypothalamic VP and oxytocin neurons are known to engage in the somatodendritic release of these neuropeptides [160,161,164,180]. In the magnocellular neurons, the neurohormone is packed into the LDCVs, which undergoes regulated exocytosis from the axon terminals as well as somata/dendrities [161,164]. Similar to that seen at axon terminals, the SNARE complex has been suggested to play a role in a calcium-dependent regulated exocytosis of LDCVs somatodendritically [165]. Using immunofluorescence, while the expression of SNARE proteins *viz.* VAMP-2, SNAP-25, and syntaxin were observed in the axon terminals of VP and oxytocin neurons; CAPS-1 and munc-18 were localized in the somata/dendrites of these neurons [165]. Although crucial in the exocytosis process, the Ca^{2+} sensor and turbocharger of synaptic vesicle exocytosis, SYT-1 seem to remained confined to the presynaptic terminals around VP or oxytocin cell bodies [165]. Not only in the normal rat, but also in the lactating and post-natal day 8 rats, when there is enhanced somatodendritic peptide release, the somata/dendrites of VP or oxytocin neurons lack VAMP-2 and SYT-1 immunoreactivity, and these proteins were seen in the presynaptic terminals around the cell bodies [165]. In the present study, SYT-1-immunoreactivity was observed in the presynaptic terminals around VP cell bodies in the SON and PVN of the normal, untreated rats. Hypertonic NaCl treatment is known to stimulate axonal as well as somato/dendritic secretion of VP [164]. We observed that the chronic hypertonic NaCl treatment has resulted in the appearance of these proteins in the somata/dendrites of the PVN and SON neurons. Approximately 43 and 58 % VP neurons in the

SON and PVN, respectively co-expressed SYT-1 after hypertonic NaCl treatment and all SYT-1-expressing neurons were hypophysiotropic. The study demonstrates that during hyperosmotic stimulation, a subpopulation of the VP neurons in the SON and PVN recruits SYT-1, and may engage in somatodendritic release. In addition to SYT-1, expression of another important protein, SV2 was observed in cell bodies of the SON and PVN neurons after chronic salt loading. SV2 is a unique modulator of Ca^{2+}-mediated neurotransmitter release [173], regulates the amount of synaptotagmin recruitment in the synaptic vesicles [177], and play a role in maturation of primed vesicles into a Ca^{2+}- and synaptotagmin-responsive state [175]. Presence of SV2 in the cell bodies of the SON and PVN may serve as novel candidate in the exocytosis of vesicles from somata/dendrites of these neurons during salt-loading. In the present study, c-Fos served as reliable marker for neuronal activation following HS treatment. Previously, c-Fos has been used as marker for identifying the effect of HS on VP neurons [193]. c-Fos activation in VP neurons of SON and PVN may suggest the treatment was effective in inducing osmotic shock.

The expression of SNARE proteins in the cell bodies of TRPV3-expressing VP neurons hint at potential significance of TRPV3 ion channel in the somatodendritic release of VP. The results suggest that the TRPV3-immunoreactive neurons in the hypothalamus are hypophysiotropic and the channels seem to mediate osmotic influences. During chronic hypertonic NaCl treatment, the SYT-1-expressing VP neurons may also participate in the axonal release of VP. This is based upon the FG neuronal tracing study. We observed that the SYT-1-expressing neurons in the SON and PVN contained retrograde accumulation of FG. Since a majority of the SYT-1-expressing neurons in the SON and PVN contained VP after chronic salt loading, we suggest that VP neurons, which are engaged in the somatodendritic secretion, may

Chapter 2

also release the neurohormone from the axon terminals in posterior pituitary for systemic effects. Although VP neurons in SON and PVN were uniformly activated by hypertonic saline, only a subpopulation of VP neurons in these nuclei seems to be capable of somatodendritic release of VP during hyperosmotic challenge. Previously, i.p. hypertonic NaCl treatment resulted in instantaneous increase in VP levels in the blood whereas the dendritic VP release seem to be delayed by >1 h but lasted longer [164,194]. We observed the appearance of SYT-1 or SV2-immunoreactivity 24-48 h after oral hypertonic NaCl treatment, which further intensifies 72-84 h of salt-loading. While we do not know the reasons for the delay in expression of SYT-1 immunoreactivity in VP neurons after hypertonic NaCl treatment, it is possible that the VP neurons might be expressing low levels of SYT-1, which is difficult to detect by immunofluorescence.

The hypothalamic oxytocin and VP neurons are known to be equipped with other TRPV channels. The VP neurons in the hypothalamus of rodents express TRPV1 [15,92] and TRPV2 [12], whereas oxytocin neurons in the hypothalamus of macaque co-express TRPV2 [13]. In TRPV1$^{-/-}$ mice, the VP neurons in SON did not respond to hypertonic saline [92] and the temperature-induced increase in neuronal firing in VP neurons was attenuated following treatment with TRPV1 inhibitor or mice lacking TRPV1 [14]. While TRPV4 inhibits VP secretion [159], neuronal number of TRPV2-expressing VP neurons in the SON and PVN increases with elevated plasma VP levels associated with bile duct ligation [11]. More than two fold increase in the TRPV2 and TRPV4 mRNA expression with concomitant 4-fold increase in VP expression was observed [11]. We suggest that TRPV3 along with other TRPV channels might play a role in regulation of VP secretion.

The hyperosmotic stimulation-induced activation of TRPV1 in the magnocellular neurons in SON seem important for the somatodendritic release of VP [158,195]. Although studies have proposed the somatodendritic release of neuropeptides form the magnocellular VP and oxytocin neurons, precise mechanism regulating this process is not well established. We observed SYT-1 expression in cell bodies of VP neurons. Using retrograde neuronal tracing, the SYT-1 expressing neurons in the hypothalamus seem hypophysiotropic, suggesting engagement of a neuron in both axon terminal as well as somatodendritic neurohormone secretion. Double immunofluorescence study showed co-expression of SYT-1 and TRPV3 in neurons of PVN and SON after HS. In addition to the axonal release, the magnocellular vasopressin neurons release the neurohormone from somatodendritc compartment and the process is highly Ca^{2+} dependent [165]. The expression of SNARE proteins in somatodendritic compartments of TRPV3-expressing VP neurons hint at potential significance of these ion channels in high calcium surges necessary during this process.

Although the presence of TRPV3 ion channel in PVN and SON neurons further substantiates the significance of TRPV subfamily of ion channels in neuroendocrine regulation, it has indeed added to the complexity of the regulatory mechanism. While the neurons expressing TRPV1 were observed in PVN and SON of mice [81,196], TRPV2- and TRPV4-expressing neurons were also observed in these nuclei [11–13]. The VP and oxytocin neurons in the hypothalamus co-express TRPV1, TRPV2, and TRPV4, and their role in the regulation of these neurons have been suggested [11–14]. TRPV3 is not directly gated by vanilloid or endocannabinoid (anandamide) but can regulate the activity of TRPV1 by forming heterodimer with this channel [5,197]. The heteromeric channel constructs show altered characteristics from the homotetramers [198]. In the TRPV1::TRPV3 concatamer, both the subunits are functional

[96]. The channel formed by the TRPV1::TRPV3 concatamers showed a distinct single-channel conductance and temperature threshold compared to their respective homotetramers. It has been suggested that the channel formed from TRPV1::TRPV3 might be a new species [198]. TRPV1 is also known to form heterodimer with TRPV2 in the dorsal root ganglion neurons but its functional significance is not known [199]. It is interesting to note that the SON neurons which were insensitive to the treatment of TRPV1 agonist, capsaicin at 24 °C responded to the same concentration of the drug when the temperature was raised to 36 °C, the activation threshold temperature of TRPV3 [15]. The authors suggested that the osmoreceptor expressed on SON neurons may be a heteromultimer. We speculate that TRPV1 and TRPV3 may co-assemble, form heterodimer, and function as osmosensor on VP neurons.

The regulation of oxytocin and VP neurons seem complex since these neurons express receptors for oxytocin and VP, respectively [161]. While oxytocin neurons are equipped with oxytocin receptors, activation of these receptors resulted in elevated intracellular Ca^{2+} and dendritic oxytocin secretion [161,200]. The secretion of VP from the neurons is regulated by plasma osmolality and during increased activity, the coordination between VP neurons may distribute secretory load across the VP-secreting cells [201]. Similar to oxytocin neurons, the VP neurons express VP receptors but unlike oxytocin neurons, the auto-regulatory mechanism of VP is more complex [161,202]. While the central VP infusion results in decreased plasma VP levels in dogs [203], VP released from the somata/dendrites regulates the activity of SON VP neurons by auto-inhibitory mechanism [204]. The VP released from the somata/dendrites during hyperosmotic challenge might provide as efficient and non-exhaustive mechanism controlling systemic VP secretion [205]. McKinley and McAllen [206] suggested that such conservation mechanisms may be executed during declining systemic release of vasopressin. The VP content

in the posterior pituitary showed depletion during the prolonged salt-loading [207,208]. Yue et al. [182] studied the effect of chronic hyperosmotic treatment for 1-5 days on VP peptide hnRNA expression in the SON, its concentrations in the plasma, and rate of depletion from the neural lobe in the pituitary. While the VP hnRNA levels in the SON increased 1 day after salt-loading and was maintained at this level during the entire duration of salt-loading, the peptide levels in the neural lobe significantly decreased after each day of salt-loading [182].

The VP neurons express both VP, V1a and V2 receptors and the dendritically released peptide seem to act positively on its dendrites *via* V2 receptors to further enhance somatodendritic VP secretion [206]. In contrast, the dendritically released VP is known to act *via* V1a receptors on VP neurons excitability and inhibit the spiking activity and systemic release [163,164,206]. We observed that a sub-population of VP neurons in the SON and PVN expressed SYT-1 during osmotic stimulus. The VP released from the somata/dendrites of SYT-1-expressing neurons may act on its own dendrites *via* V2 receptors for sustained VP release from its somata/dendrites as well as from the axon terminals. In addition, somatodendritically released VP may act on the neighboring non-SYT-1-expressing VP neurons *via* V1a receptors and inhibit secretion of VP from the axon terminals. A proposed mechanism of somatodendritic release of VP from hypothalamic neurons and regulation of VP secretion from the axon terminals during osmotic challenge is shown in Figure 19.

IST is a nonapeptide and is a teleost homolog of mammalian oxytocin. In mammals, neurosecretory oxytocin neurons are present in the PVN and SON whereas in teleost the IST neurons reside in the NPO in preoptic/hypothalamic region. Although IST neurons were seen in the NPO of *C. batrachus*, the organization of these neurons seems comparable to oxytocin neurons in PVN and SON of rat. Unlike other teleosts, the NPO of *C. batrachus* has two distinct

subdivisions. In mammals, PVN and SON contain oxytocin neurons, and these neurons seem homologous to NPOpv and NPOso of *C. batrachus*. Although TRPV3-ir was observed in DA neurons in the SN and VTA of rat, the DA neurons of NPP of *C. batrachus* seem to be devoid of TRPV3. The DA neurons in NPPa were hypophysiotropic but those in the NPPp did not project to the pituitary. These neurons play a role in regulation of LH cells and reproduction in teleosts [188]. Similar to the PVN and SON of rat, IST neurons in NPOpv and NPOso showed co-expression of TRPV3. The results suggest that TRPV3 ion channel-expressing elements are widely organized in the brain of *C. batrachus*. Similar to rat the IST neurons expressing TRPV3 in the hypothalamus of a distant vertebrate species suggest its evolutionary significance in neuroendocrine regulations.
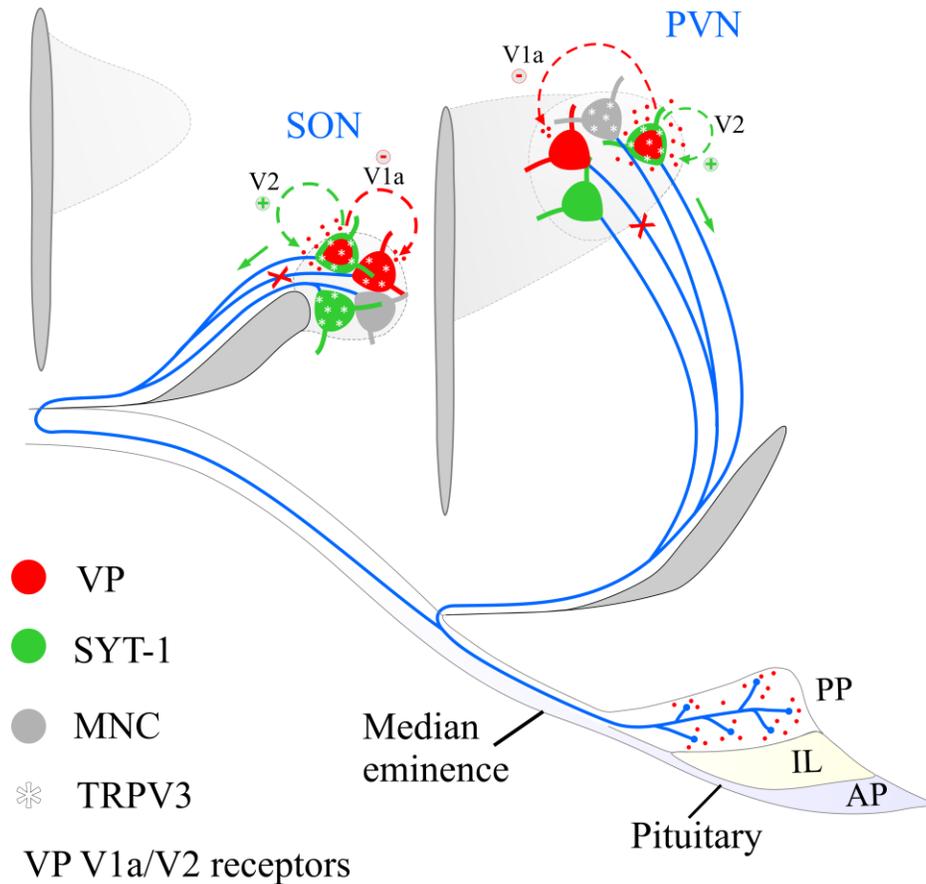
Figure 19: Proposed mechanism of regulation of vasopressin (VP) neurons in the hypothalamic paraventricular (PVN) and supraoptic nuclei (SON) during hyperosmotic challenge.
Schematic showing the proposed mechanism of regulation of VP secreting magnocellular neurosecretory cells (MNC) in the PVN and SON. The VP neurons (red) in the PVN and SON project to the posterior pituitary and secrete the peptide through the axon terminals for systemic effects. The somatodendritic compartment of a subpopulation of VP neurons in the PVN and SON express synaptotagmin-1 (SYT-1; green)/synaptic vesicle-2 (SV2; green) proteins during chronic salt loading. During chronic salt loading, the SYT-1 expressing VP (red/green) neurons may engage in the somatodendritic release of the peptide; and *via* V2 receptors may further enhance somatodendritic and systemic VP secretion. The somatodendritically released VP may act *via* V1a receptors and inhibit the VP neurons which do not express the essential components of the vesicular exocytosis machinery during hyperosmotic challenge. This may reduce the activity of VP neurons to secrete the peptide from axon terminals which serve as an important component of the regulatory system for more efficient and non-exhaustive control of systemic VP secretion during chronic salt loading. Essentially, the SYT-1 activity is highly $[Ca^{2+}]_i$ dependent and the members of TRPV *viz.* TRPV3 calcium channels are present on VP or SYT-1 positive neurons. The increased calcium surge during salt overloading therefore may activate TRPV3 ion channel for nonapeptide release. AP; anterior pituitary, IL; intermediate lobe; PP; posterior pituitary.

CHAPTER 3

TRPV3 in the ventral tegmental area (VTA) of rat: role in modulation of the mesolimbic-dopamine reward pathway

3.1 INTRODUCTION

Compared to other tissues, the gene for TRPV3 is predominantly expressed in the brain [5] but its relevance in the nervous system is still unclear. TRPV3 mRNA expression has been detected in the substantia nigra (SN) [4]. An important group of dopamine (DA) neurons resides adjacent to the SN in the VTA. Although, at molecular level the neurons in SN and VTA share certain similarities [4,209], these are anatomically and functionally distinct. While SN is a part of the basal ganglia and has a role in the motor and emotional control [210], the VTA DA neurons projecting to the nucleus accumbens shell (Acb shell) serve an important purpose in the mesolimbic-reward circuitry [22,23] and considered the best characterized, reward pathway in the brain [24,25,210–213]. TRPV channels are emerging as novel players in the modulation of mesolimbic DA neurons. Capsaicin, a TRPV1-agonist, has been implicated in the modulation of mesolimbic DA neurons, but the pathway seems to be *via* presynaptic glutamate release [17]. The monoterpenoids, thymol and carvacrol, are active ingredients of oregano and serve as TRPV3-agonists [18,19], and the role of carvacrol in DAergic neurotransmission and reward has recently been suggested [20,21]. While these observations hint at a putative role of TRPV3 in the modulation of DAergic system, the underlying mechanisms and nature of TRPV3-elements driving the mesolimbic-DA reward pathway are not known.

In a pilot study, we observed TRPV3 mRNA expression and TRPV3-immunoreactive neurons in the VTA. We therefore hypothesized that TRPV3 might be involved in the regulation of DA neurons of the VTA and mesolimbic-reward pathway. We investigated the role of TRPV3 in modulating mesolimbic-DAergic system and in processing reward. We first determined whether DA neurons in the VTA co-express TRPV3 and project to the Acb shell using retrograde neuronal tracing. Since TRPV3 is a Ca^{2+} permeable ion channels therefore we determined whether a TRPV3-agonist is capable of altering $[Ca^{2+}]_i$ activity in *ex vivo* midbrain

slices. Next, we employed an operant conditioning paradigm for food reward to explore whether intra-pVTA infusion of a TRPV3-agonist influences the mesolimbic-DAergic pathway controlling food reward. Although VTA-derived DAergic terminals release DA in the Acb shell and may simultaneously bind to DA D_1 and D_2 receptors in this region, differential and opposing effects mediated *via* these receptor subtypes have been suggested in other reward behaviors [214]. To explore the DA receptor subtypes mediating TRPV3 response, DA D_1- or D_2-like receptor antagonists were infused into the Acb shell followed by an intra-pVTA TRPV3-agonist, and motivational behavior was assessed.

3.2 MATERIALS AND METHODS

3.2.1 Animals

Adult, male, Wistar rats (230-250 g) were used in this study. The animals were acclimatized to the standard environmental conditions for at least one week and given food and water *ad libitum*. All experimental protocols were reviewed and approved by the Institutional Animal Ethics Committees (IAEC) at NISER and R.T.M. Nagpur University under the control of Committee for the Purpose of Control and Supervision of Experiments on Animals (CPCSEA), New Delhi, India.

3.2.2 Total RNA isolation and RT-PCR analysis

Rats (n = 4) were deeply anaesthetized, decapitated, brains were dissected out and frozen on dry ice. From the slice of midbrain, VTA was isolated using a tissue biopsy punch (Integra Miltex). After isolating VTA, the sections were fixed in 4 % paraformaldehyde and processed for TH immunohistochemistry using 3,3'-diaminobenzidine (DAB)/hydrogen peroxide (H_2O_2). From the VTA tissue, total RNA was isolated using TRIZOL reagent (Invitrogen). Using high-capacity cDNA reverse transcription kit (Invitrogen), first stand cDNA was synthesized. cDNA was amplified for 35 cycles using Phusion® High-Fidelity DNA Polymerase (NEB). N-terminal fragment was amplified with primer pair specific to exon/exon junction 7/8 of rat TRPV3 (forward: ACCCCATCCAATCCCAACAGTCC; reverse: CAGGGGCGTCTCACCAAAATAG). For C-terminal fragment, primer pair (forward: CGACGCGGTGCTGGAGCTCAA; reverse: CCATTCCGTCCACTTCACCTCGT) was adopted as described previously [4]. TH was amplified using primers (forward: TTCTTGAAGGAGCGGACTGG; reverse: GGTCAGCCAACATGGGTACA).

Annealing temperatures of 57 °C was used for the amplification of TH, and N- and C-terminal regions of TRPV3. The PCR products were electrophoresed on 1 % agarose gel, and image of the gel was acquired and edited in Adobe Photoshop. The N-terminal (~514 bp) fragment was excised from gel and purified for DNA sequencing.

3.2.3 Immunofluorescence

Animals (n = 3) were deeply anaesthetized and perfused transcardially with phosphate buffered saline (PBS), followed by 4 % paraformaldehyde in phosphate buffer (PB). Brains were removed, post-fixed in the same fixative and cryoprotected. Serial 25µm thick coronal sections through the rostro-caudal extent of midbrain were cut on a cryostat (Leica) to obtain four sets of free-floating sections in PBS.

Single immunofluorescence labeling: Immunofluorescence was employed as described earlier [188]. Sections through the rostro-caudal extent of the VTA were incubated in polyclonal rabbit anti-TRPV3 antiserum (1:5000) followed by biotinylated anti-rabbit IgG (Vector Laboratories, 1:400) and avidin-biotin-peroxidase complex (Vector, 1:1000). The immunoreaction was amplified using biotin-tyramide (BT) amplification kit (NEN Life Sciences, Boston, MA) and visualized using DTAF-avidin (Jackson Immunoresearch, 1:300). A set of serial sections through the rostro-caudal extent of the Acb were processed for TRPV3-immunofluorescence as described above.

Double immunofluorescence labeling: Sections through the rostro-caudal extent of the VTA of each rat were incubated in a mixture of mouse monoclonal anti-TH antibody (1:1000)

and polyclonal rabbit anti-TRPV3 antiserum (1:5000) overnight at 4°C. TRPV3 immunofluorescence was amplified as described above. For visualization of TH, sections were incubated in AlexaFluor 594-conjugated anti-mouse IgG (Invitrogen, 1:500). Sections were rinsed in PBS, and mounted with VECTASHIELD^{TM} mounting medium.

3.2.4 Retrograde neuronal tracing

To determine whether TRPV3 channels are associated with the DA neurons in pVTA that project to the Acb shell, the retrograde neuronal tracer, cholera toxin-β subunit (CtB), was iontophoresced into the Acb shell (n = 6) as described previously [215], with minor modifications. Coordinates for the Acb shell [from the bregma anterior-posterior (AP): + 1.7 mm; medio-lateral (ML): 0.75 mm; and dorso-ventral (DV): -7.2 mm] were adopted from Paxinos and Watson [150]. After 10 days, the animals were perfused transcardially and the sites of CtB injection in the Acb were localized using goat polyclonal CtB antiserum (1:500) 24 h at 4°C followed by DyLight 488-conjugated donkey anti-goat IgG (Jackson Immunoresearch; 1:300). A rostro-caudal series VTA sections of the animals with CtB injections localized into the Acb shell (n = 3) were further processed for triple immunofluorescence using polyclonal goat anti-CtB (1:500) and rabbit anti-TRPV3 (1:2500) antisera, and monoclonal mouse anti-TH (1:1000) antibodies, followed by incubation in secondary antibodies (DyLight 488 for TRPV3, AlexaFluor 594 for TH, and CtB was detected using BT amplification followed by AMCA-avidin).

3.2.5 Calcium imaging of midbrain slices containing VTA

Non-ratiometric calcium imaging of acute midbrain slices was employed as described

previously with minor modifications [4,216–218]. Animals (n = 6) were deeply anaesthetized,

decapitated, and brains were transferred to aCSF (NaCl 119 mM; KCl 2.5 mM; $MgSO_4.7H_2O$ 1.3

mM; $CaCl_2$ 2 mM; NaH_2PO_4 1 mM; $NaHCO_3$ 26 mM; Glucose 11 mM) saturated with 95 % O_2

and 5 % CO_2. A tissue block containing midbrain was mounted on the Vibratome (VT 1200,

Leica) in sucrose slicing solution (NaCl 119 mM; KCl 2.5 mM; $MgSO_4.7H_2O$ 7 mM; $CaCl_2$ 0.5

mM; NaH_2PO_4 1 mM; $NaHCO_3$ 26 mM; Glucose 11 mM; Sucrose 228 mM; Ascorbic acid 0.1

mM) saturated with 95 % O_2 and 5 % CO_2. Coronal slices (200 µm) were collected in aCSF,

loaded with 4 µM calcium indicator, Fluo-4 AM [219] for 30 min, and processed for

desertification for ~30 min. Slices were rinsed with artificial cerebrospinal fluid (aCSF),

observed under LSM780 confocal microscope (Carl Zeiss), and the region of interest was

focused. TRPV3 single channel opening probability has been shown to be upregulated with

increase in temperature from 25 to 37 °C [9]. To avoid temperature-induced activation of the

channel, TRPV3-agonist treatment was performed at ~25.5 °C. In the incubation chamber, the

slices were treated with the TRPV3 agonist, thymol (300 µM) in ≤ 0.05 % DMSO as vehicle.

This dose of thymol was used in a previous study [19]. Series of images were captured with

ZEN2011 software (Carl Zeiss) and processed using LSM Image viewer and Adobe Photoshop

CS4.

3.2.6 Image analysis

Images were captured with an AxioCam digital camera (Carl Zeiss). In double-labelled

sections, regions of interest were double exposed by switching the filter sets for DTAF and

AlexaFluor 594. Using Adobe Photoshop CS4 (Adobe Systems, Inc., San Jose, CA), images

were adjusted for size and superimposed to get a composite image of the same field. Association

between TH and TRPV3 in the VTA was analyzed under a confocal laser scanning microscope (LSM-780, Carl Zeiss). Using a 63X objective, images were captured and analyzed using Zeiss LSM image analysis software, and adjusted for brightness and contrast using Adobe Photoshop CS4 software. Using CorelDraw12 software, different subdivisions of the VTA were demarcated to depict TH/TRPV3 double-labelled neurons.

Semi-quantitative image analysis to determine the percentage of TH/TRPV3 double labelled neurons in the VTA was performed as described previously [220]. Similarly, the percentage of CtB labelled neurons in pVTA co-expressing TH and TRPV3 was also determined. The subdivisions of the VTA were identified based on the landmarks such as the mammillary and interpeduncular nuclei [220,221]. By switching the filter sets, (i) TH/TRPV3 double labelled neurons in different subdivisions of the VTA, and (ii) CtB/TH/TRPV3 labelled neurons in the pVTA were counted, the percentage was determined for each animal and the data expressed as the mean ± SEM.

3.2.7 Stereotaxic surgery for intra-pVTA and -Acb shell drug administration

Intra-Acb shell or -pVTA cannulation and injection was performed as reported previously [222,223]. Briefly, the rats were anesthetized with an intraperitoneal injection of a mixture containing ketamine (Themis Medicare Ltd., India; 90 mg/kg) and xylazine (Indian Immunologicals Ltd., India; 10 mg/kg). Under stereotaxic control, stainless steel guide cannulae [224] were implanted either in the Acb shell and/or pVTA [coordinates with respect to the bregma, Acb shell: AP +1.7 mm, ML 0.75 mm, DV -6.5 mm; and pVTA: AP -5.8 mm, ML 1.8 mm, DV -8.5 mm at the angle of 10° to the vertical] [150] . The cannulae were secured above the site of injection with stainless steel screws and dental cement, and the injector was designed

to project 0.5 mm below the guide cannula. Post-surgical care was taken during the recovery period. The rats were allowed to recover from surgery for 7 days and subjected to training in the operant chamber for behavioral assays.

3.2.8 Food pellet self-administration in an operant chamber

All the animals used for analyzing the behavioral effects of TRPV3-agonist on reward were trained to press the active lever for delivery of the sweet pellet. As described previously [222], the food pellet self-administration protocol was conducted on satiated rats in an operant conditioning chamber (Coulbourn Instruments, USA). The operant chamber consisted of the standard two lever (active and inactive) system mounted on the same wall 13 cm apart and 15 cm above the grid floor. This precluded the possibility of accidental lever pressings because of the general locomotor activation [223]. The house light (2W) was mounted on the wall opposite to the levers, and a cue light was placed above the active lever. The chamber was equipped with an automatic food dispenser. The hopper and motor driven food dispenser were mounted in between the two levers on the same wall. Pressing each, active lever activated the motor-driven automatic sweet pellet dispenser, delivered a sweet pellet and illuminated the cue light for 5 sec. The inactive lever had no such response [fixed ratio 1 (FR1)]. A 45 mg sweet food pellet (Mayon's Pharmaceuticals, India) was used as a reinforcer [222]. The training sessions were conducted for 30 min each day for each rat. After each session, they were returned to the home cage and provided with food *ad libitum*. The animals were trained over a week and those showing a stable response (~ 25-30 lever press/30 min session, for consecutive three sessions) were considered as trained. The trained animals were treated with different pharmacological agents and 15 min after last treatment; they were subjected to behavioral experimentation. All

the injections were given in freely moving animals using a microprocessor controlled syringe pump (BASi, West Lafayette, IN). The specific experiments are described below.

Effect of intra-pVTA TRPV3 agonist and inhibitor on active lever pressings: For intra-pVTA administration, thymol (Sigma, USA) and isopentenyl pyrophosphate (IPP, Echelon Biosciences) were used. Thymol has previously been used as TRPV3-agonist [18,19]. To validate the specificity and exclude the possibility of any off target effects of the agonist, TRPV3-inhibitor, IPP was used [130,225]. Thymol was dissolved in dimethyl sulfoxide (DMSO) as a stock solution. The stock solution was further diluted in aCSF such that the final concentration of DMSO was less than 0.05 % in both vehicle as well as thymol-treated groups. IPP was dissolved in aCSF. The rats trained in operant chamber were randomly divided in different groups (n = 8-10/group), as described previously [222] and subjected to the intra-pVTA injection of (i) vehicle, 0.5 µl/rat, (ii) TRPV3 agonist, thymol (40-160 ng/rat), (iii) TRPV3 inhibitor, IPP (25-100 ng/rat).

Effect of intra-Acb shell DA D_1- or D_2-like receptor antagonists on intra-pVTA thymol-induced active lever pressings: To determine whether the activation of TRPV3 in the pVTA produces reward *via* DAergic neurotransmission to the Acb, we first determined the effect of DA D_1 (SCH 23390, Sigma) or D_2 (sulpiride, Sigma)-like receptor antagonists on active lever presses. Both agents were dissolved in aCSF. In initial studies, rats trained in the operant chambers were subjected to the intra-Acb injection (0.5 µl) of either (i) aCSF, (ii) SCH 23390 (1-3 µg), or (iii) sulpiride (4-8 µg) (n = 8-10/group). Based on the dose of SCH 23390 and sulpiride to alter active lever presses, a second set of experiments was conducted. The intra-

pVTA thymol-induced active lever pressing response was studied in the animals pretreated with SCH 23390 or sulpiride (intra-Acb shell). The animals in each group (n = 8-10/group) received either (i) aCSF intra-Acb shell followed by vehicle intra-pVTA, (ii) SCH 23390 (1 µg) intra-Acb shell followed by vehicle intra-pVTA, (iii) SCH 23390 (1 µg) intra-Acb shell followed by thymol (160 ng) intra-pVTA, (iv) sulpiride (4 µg/rat) intra-Acb shell followed by vehicle intra-pVTA, and (v) sulpiride (4 µg/rat) intra-Acb shell followed by thymol (160 ng) intra-pVTA. Fifteen minutes following the injections, animals were studied in the operant chamber.

3.2.9 Open field test (OFT)

Locomotor activity was monitored using an open field test (OFT), as described earlier [223]. Briefly, the animals in each group were administered vehicle, thymol, IPP, SCH 23390 or sulpiride. Fifteen minutes thereafter, animals were individually placed in the centre of the OFT apparatus and the numbers of ambulations measured during a 30 min test period. Data was pooled and the mean ± SEM calculated.

3.2.10 Verification of cannula placement

Following the behavioural analysis, animals were euthanized and the brains were sectioned on cryostat. The sections were processed for the cresyl violet staining and examined under a light microscope to confirm the placement of guide cannula in the Acb shell and pVTA. The data from animals with incorrect placement were excluded from the study and only data from animals with correct cannula placements were used for further analysis. Examples of the cannulae targeted to the Acb shell and pVTA, or placed outside are shown in Fig. 7.

3.2.11 Statistical analysis

Sample size was chosen based on previously published reports [220,223]. The number of animals included in the analysis is given in the description of each figure. Data was analyzed with Graphpad Prism software (Graphpad Software, CA, USA). For comparison between two groups, Student's t-test was performed whereas in the experiments that involved three or more groups, statistical analysis was carried out using one-way ANOVA, followed by post-hoc Bonferroni's multiple comparison test. No adjustments were employed for multiple comparisons. All the data are expressed as mean ± SEM, statistical tests were two-tailed, and *P* < 0.05 was considered statistically significant. The data from animals (n = 28) with incorrect cannula placement were excluded from the study and only the data from animals with correct cannula placements were used for further analysis.

3.3 RESULTS

3.3.1 TRPV3 expression in the VTA

Tissue containing VTA (Fig. 1A) demonstrated expression of both N- and C-terminal fragments of TRPV3 mRNA as well as TH mRNA by RT-PCR (Fig. 1B), suggesting presence of the full-length TRPV3 in the VTA. Sequencing of the N-terminal fragment matched with that of the rat TRPV3 cDNA. TRPV3 antiserum labelled distinct cell bodies in the VTA (Fig. 1C) whereas replacement of the antiserum with normal serum did not produce any signal (Fig. 1D). The presence of TRPV3 in the cells of SN (Fig. 1E) served as a positive control.

3.3.2 TH neurons in the VTA co-express TRPV3

In view of the occurrence of TRPV3 in the VTA, we further explored the neuroanatomical organization of TRPV3-immunoreactive neurons in the VTA and its association with DA neurons in this region. The VTA has three distinct subdivisions *viz*., anterior (aVTA), posterior (pVTA), and tail (tVTA) [220]. TRPV3-immunoreactive neurons were identified in all three subdivisions of the VTA (Fig. 2A-C). Compared to aVTA and tVTA, majority of the TRPV3 neurons were identified in the pVTA. Double-labeling immunofluorescence revealed colocalization of TRPV3 and TH in neurons in each subdivision of the VTA (Fig. 2D-I). Of the total TH/TRPV3 double labelled neurons, approximately 34.4 ± 2.2 % neurons resided in the aVTA, 59.3 ± 2.2 % in the pVTA, whereas only a small fraction (6.3 ± 1.4 %) was detected in the tVTA (Fig. 2J). In the pVTA, approximately 68.4 ± 3.2 % TH neurons were TRPV3 positive, whereas 82 ± 2.6 % of the TRPV3 neurons were TH-immunoreactive. Data analysed using one way ANOVA revealed that a great majority of TH/TRPV3 double labelled neurons reside in the pVTA ($P < 0.0001$).
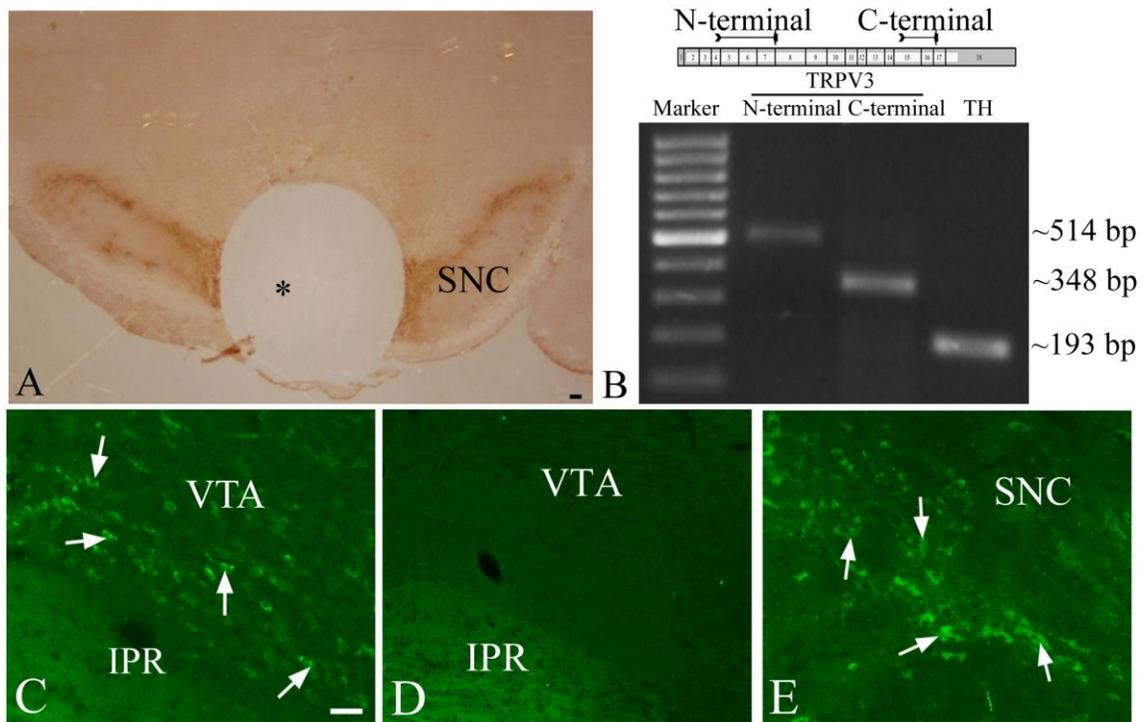
Figure 1: TRPV3 expression in the ventral tegmental area (VTA) of rat.
(A) Coronal section through midbrain of rat showing punched tissue containing VTA (asterisk) isolated for RT-PCR analysis. Substantia nigra, compact part (SNC) is intact as depicted with tyrosine hydroxylase (TH) immunoreactivity. (B) Schematic representation of the full length TRPV3 mRNA transcript, and N- and C-terminal primers pair site used for TRPV3 RT-PCR. Note expression of N- and C-terminal fragments of TRPV3 and TH mRNA in VTA. (C) TRPV3 labelled neurons are seen in the VTA (arrows) but (D) following replacement of the TRPV3 antiserum with normal serum, no immunoreactivity is observed in this region. (E) SNC TRPV3-labelled neurons (arrows), served as positive control. IPR, interpeduncular nucleus, rostral subnucleus. Scale bar = 100 µm in A, 25 µm
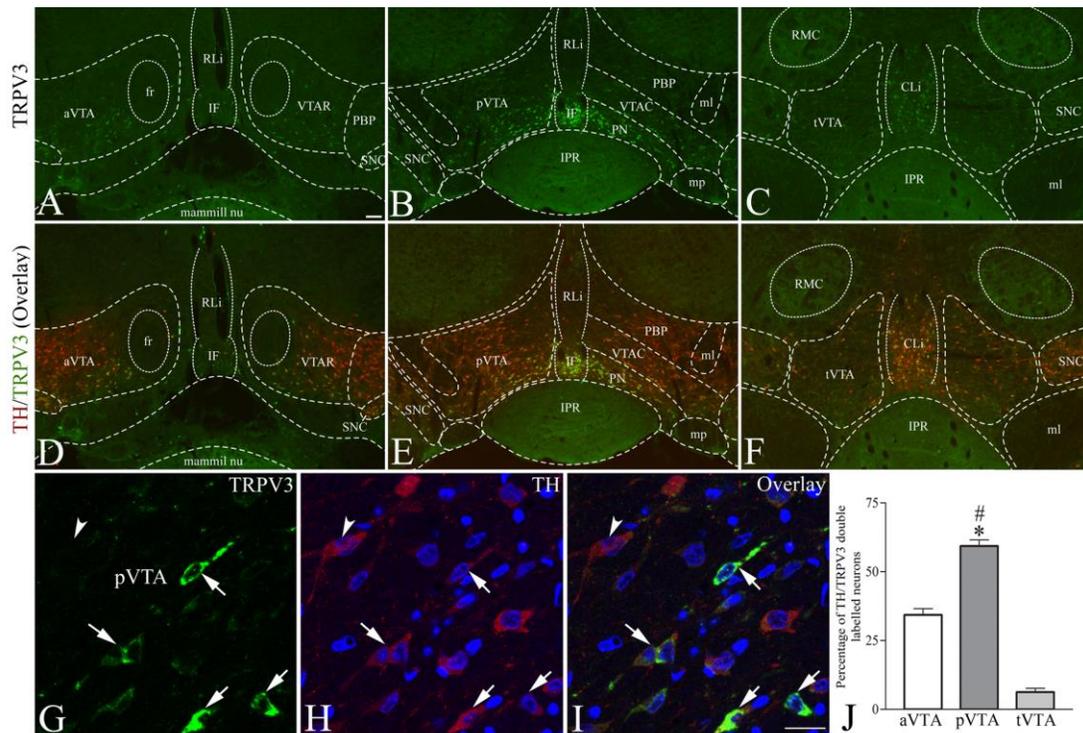
Figure 2: Dopamine neurons in the ventral tegmental area (VTA) express TRPV3.
Organization of (A-C) TRPV3 (green), and (D-F) tyrosine hydroxylase (TH, red) neurons expressing TRPV3 (yellow) in different subdivisions of VTA [anterior VTA (aVTA), posterior VTA (pVTA) and tail VTA (tVTA)]. (G-I) Confocal photomicrographs of pVTA showing TH neurons (red) with TRPV3 immunofluorescence (green) (arrows). The nucleus of the neurons appears blue due to DAPI. TH neurons not expressing TRPV3 are also seen (arrowhead). (J) Semi-quantitative image analysis of the VTA showing percentage of double-labelled neurons. Compared to other subdivisions, the majority of the TH/TRPV3 double-labelled neurons concentrate in the pVTA. Displayed values in J are mean ± SEM. Data was analysed using one-way ANOVA followed by post-hoc Bonferroni's multiple comparison test. *$P < 0.001$ and #$P < 0.0001$ compared to aVTA and tVTA, respectively (n = 3). CLi, caudal linear nucleus of the raphe; fr, fasciculus retroflexus; IF, interfascicular nucleus; IPR, interpeduncular nucleus, rostral subnucleus; mammil. nu., mammillary nucleus; ml, medial lemniscus; mp, mammillary peduncle; PBP, parabrachial pigmented nucleus of the VTA; PN, paranigral nucleus of the VTA; RLi, rostral linear nucleus of the raphe; RMC, red nucleus, magnocellular part; SNC, substantia nigra, compact part; VTAC, ventral tegmental area, caudal part; VTAR, ventral tegmental area, rostral part. Scale bar = 100 µm in A-F, 10 µm in G-I.

3.3.3 TRPV3-expressing TH neurons in the pVTA project to the Acb shell

Following iontophoretic injection of CtB into the Acb shell (Fig. 3A-F), the majority (83.7 ± 4.4 %) of the retrogradely labelled neurons in pVTA contained TH, as expected based on the literature [226]. Of the TRPV3-expressing TH neurons in pVTA, 68 ± 5.5 % accumulated CtB (Fig. 3G-J), providing an anatomical basis to evaluate the role of TRPV3 in reward mechanisms.

3.3.4 TRPV3-agonist up-regulates [Ca^{2+}]$_i$ activity in the pVTA

To determine the functional significance of TRPV3 cation channels on DA neurons in the pVTA, non-ratiometric [Ca^{2+}]i imaging was employed following activation of TRPV3 by thymol, a known TRPV3-agonist [18,19]. No difference in mean fluorescence intensity was observed following treatment with vehicle (≤ 0.05 % DMSO) or prior to the application of agonist (Fig. 4A and C). Treatment with thymol (300 µM), however, resulted in a rapid increase in [Ca^{2+}]$_i$ activity in pVTA neurons (Student's t-test, $P < 0.001$; Fig. 4B and C).

3.3.5 TRPV3 modulates the mesolimbic-DA reward pathway

Intra-pVTA thymol and IPP alters active lever pressings in an operant chamber: Intra-pVTA administration of vehicle did not alter the normal active lever press counts and served as control (Fig. 5A-D). However, administration of the TRPV3 agonist, thymol, *via* the same route, dose-dependently increased the number of active lever pressings ($P < 0.0001$; Fig. 5A-C). While the higher doses of thymol (80 or 160 ng/rat) significantly increased the number of active lever pressings ($P < 0.01$ with 80 ng and $P < 0.0001$ with 160 ng), a lower dose (40 ng/rat) was
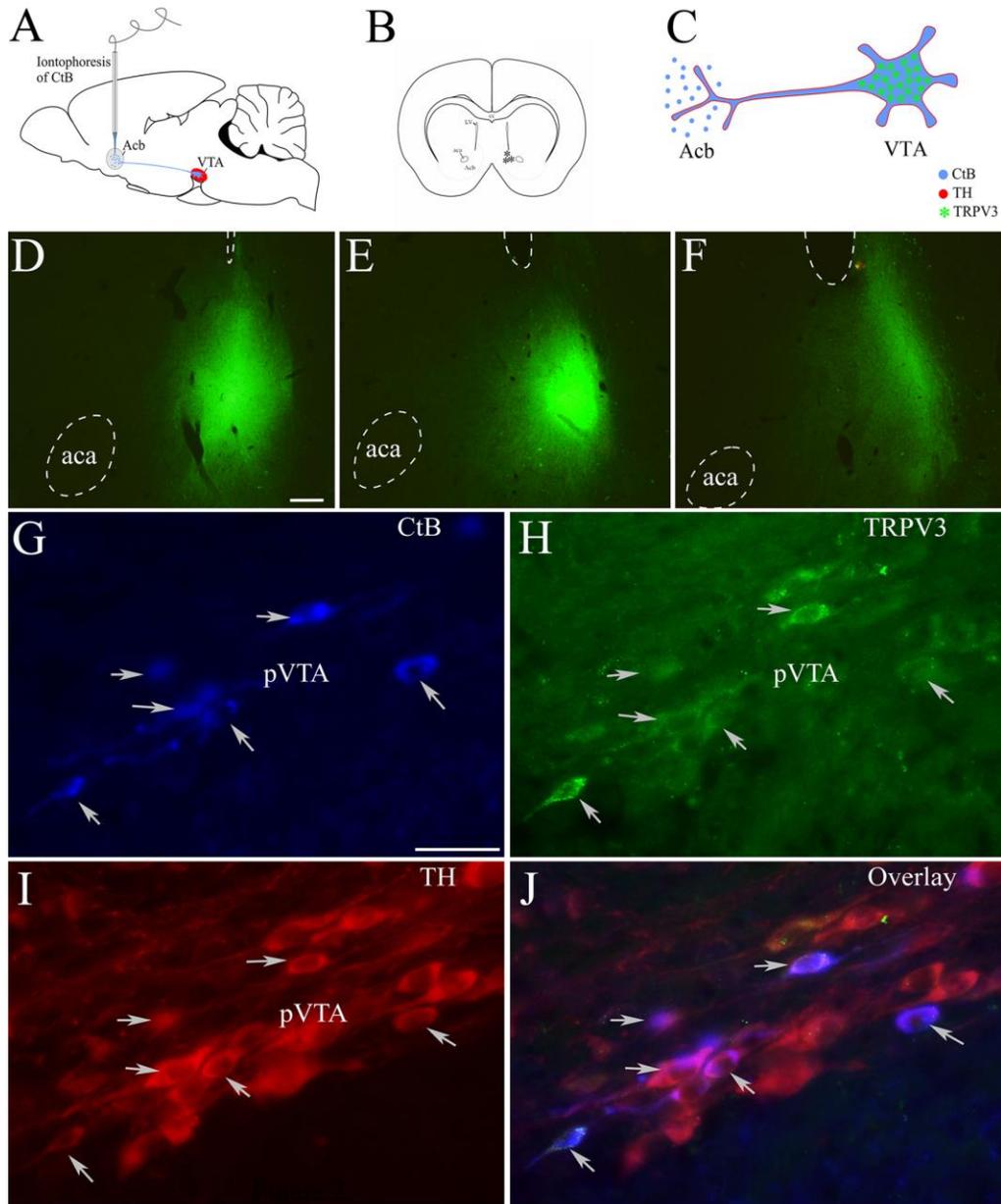
Figure 3: TRPV3-expressing dopamine neurons in the ventral tegmental area (VTA) project to the nucleus accumbens (Acb) shell.

Schematic of the brain showing (A) a micropipette targeted at the Acb for iontophoretic injection of the retrograde tracer, cholera toxin beta subunit (CtB), and (B) locations of the CtB injection (asterisks in B). (C) Schematic of a tyrosine hydroxylase (TH) neuron (red) in the VTA equipped with TRPV3 (green) contains retrogradely transported CtB (blue) from the Acb shell. (D-F) Fluorescence photomicrographs showing sites of injection of CtB in three different animals. The injection site was located using CtB antiserum followed by AlexaFluor-488-conjugated secondary antibody. Photomicrographs showing (G) CtB (AMCA), (H) TRPV3 (AlexaFluor-488), and (I) TH (AlexaFluor-594) neurons in the pVTA. (J) Majority (68 ± 5.5 %; n = 3) of the TRPV3-expressing TH neurons in pVTA contain CtB (arrows). aca, anterior commissure; cc, corpus callosum; LV, lateral ventricle. Scale bar = 200 µm in D-F and 25 µm in G-J.
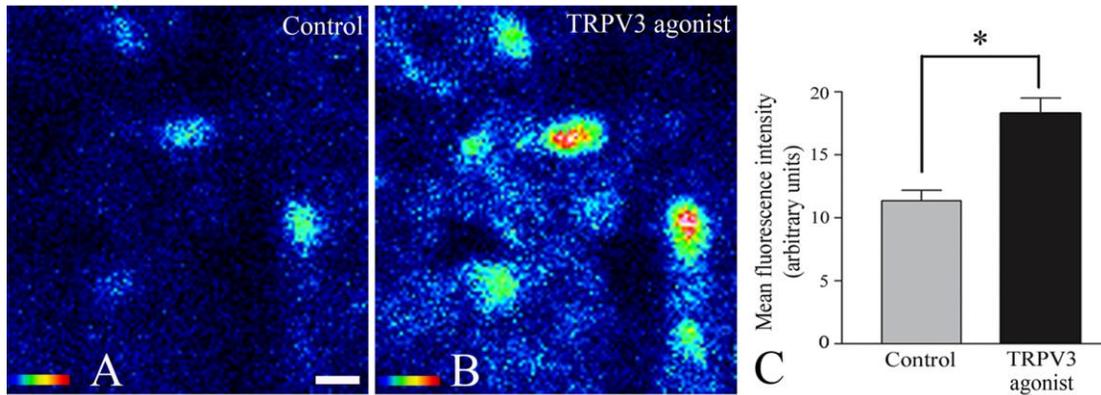
Figure 4: TRPV3-agonist increases [Ca^{2+}]$_i$ activity in the ventral tegmental area (VTA).
Photomicrographs of midbrain slices containing the posterior VTA (pVTA) loaded with the calcium indicator, Fluo-4 AM (A) before and (B) after treatment with the TRPV3-agonist, thymol. Fluorescence intensity scales are shown in the left lower corners. (C) Semi-quantitative image analysis shows the effect of thymol on mean fluorescence intensity in the cells. Displayed values are mean ± SEM. Data was analysed using Student's t-test. *$P < 0.001$ *vs* control. Scale bar = 20 µm.

ineffective ($P > 0.05$). Due to incorrect cannula placements, 4 animals were excluded from the statistical analysis of this experiment. In contrast, intra-pVTA administration of the TRPV3 inhibitor, IPP, resulted in a significant decrease in active lever press counts ($P < 0.001$; Fig. 5A, B and D), and was also dose dependent ($P < 0.01$ with 50 ng/rat and $P < 0.001$ after 100 ng/rat). A lower dose of IPP (25 ng/rat) had no effect on the number of active lever pressings (Fig. 5D). Inactive lever press counts following intra-pVTA TRPV3-agonist or the inhibitor were comparable to the control rats. From the statistical analysis of this experiment, 4 animals were excluded due to incorrect cannula placements.

Intra-Acb DA D_1- or D_2-like receptor antagonists alters active lever pressings in an operant chamber: Compared to aCSF controls, treatment with the DA D_1-like receptor antagonist, SCH 23390, at doses of 2 and 3 µg/rat, caused a significant reduction in the active lever press counts ($P < 0.001$; Fig. 5E-G). No effect was seen with the 1 µg/rat dose. Due to incorrect cannula placements, 8 animals were excluded from the statistical analysis of this experiment. Similarly, sulpiride, a DA D_2-like receptor antagonist, at doses of 6 and 8 µg/rat, resulted in significant reduction in the number of active lever pressings ($P < 0.001$; Fig. 5E, F and H), whereas there was no effect with a 4 µg/rat dose. From the statistical analysis of this experiment, 4 animals were excluded due to incorrect cannula placements.

In the open field test, the control, thymol, IPP (intra-pVTA), and SCH 23390- or sulpiride- (intra-Acb shell) treated groups showed 108.1 ± 6.1, 118.4 ± 3.1, 101.4 ± 3.42, 106.6 ± 4.3 or 98.5 ± 6.3 ambulations, respectively. No significant differences were found across the treatment and control groups ($P > 0.05$).

Effect of intra-Acb shell DA D_1- or D_2-like receptor antagonists on thymol-induced active lever pressings in an operant chamber: To further test whether thymol-induced active lever pressings in an operant chamber is mediated by DA release in the Acb, separate groups of rats received DA D_1- or D_2-like receptor antagonists into the Acb shell followed by thymol into the pVTA, and the response to press the active lever and self-administer food pellets was analysed (Fig. 6). Control rats received aCSF (intra-Acb shell) and vehicle (intra-pVTA) (Fig. 6 A-D). Compared to controls, rats treated with aCSF (intra-Acb shell) followed by thymol (intra-pVTA) showed significant increase ($P < 0.001$) in the active lever presses, whereas treatments with intra-Acb shell SCH23390 (Fig. 6C) and sulpiride (Fig. 6D) followed by intra-pVTA vehicle had no effect. Compared to the animals treated with aCSF (intra-Acb shell) followed by thymol (intra-pVTA), administration of SCH 23390 (1 µg/rat, intra-Acb shell) (Fig. 6C) and sulpiride (4 µg/rat, intra-Acb shell) (Fig. 6D) significantly reduced ($P < 0.0001$ for SCH 23390 and $P < 0.05$ for sulpiride) the thymol-induced increase in active lever presses. Due to incorrect cannula placements, 8 animals were excluded from the statistical analysis of this experiment.
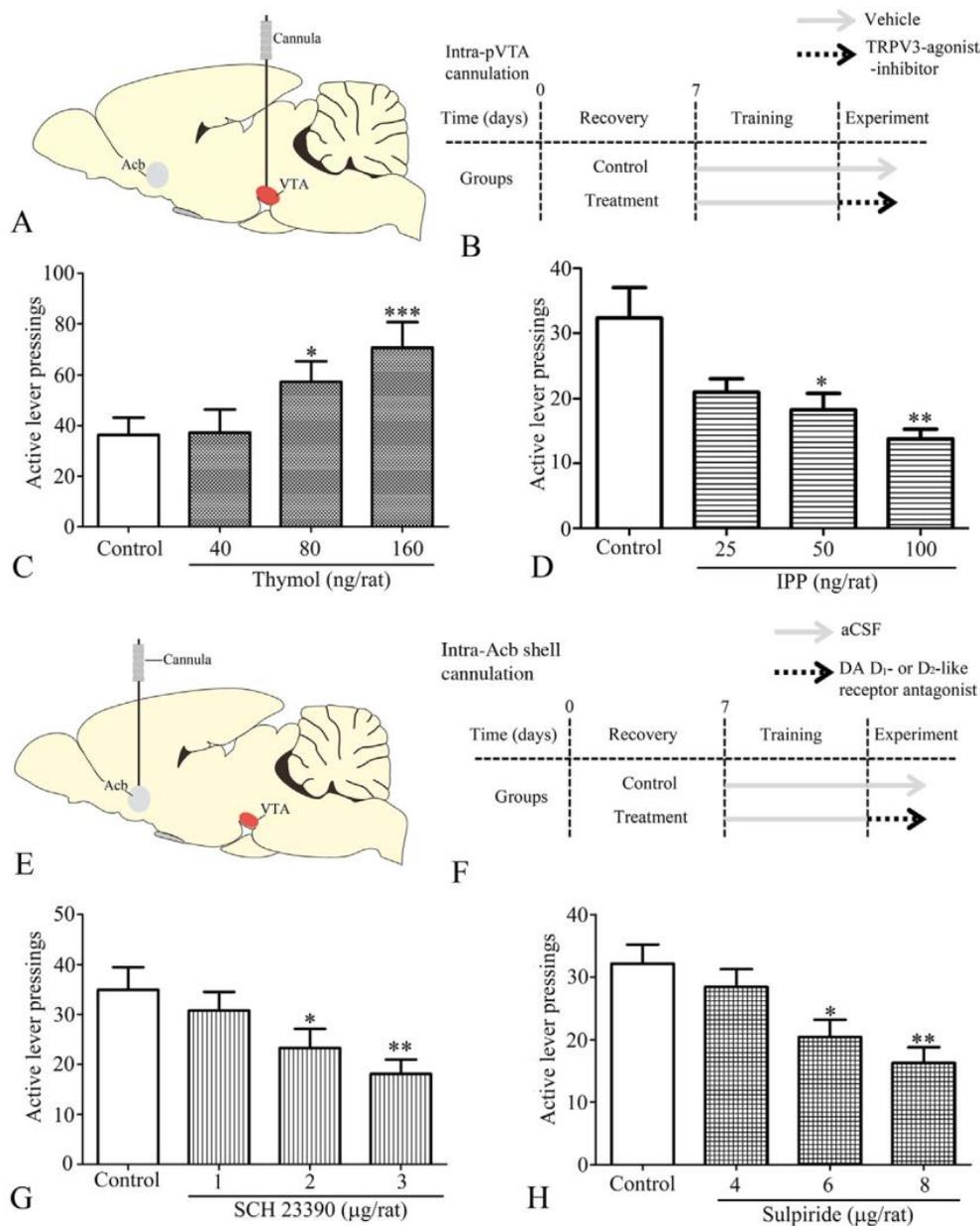
Figure 5: Effect of TRPV3-agonist or inhibitor, and dopamine (DA) D₁ - or D₂ -like receptor antagonists on active lever pressings in an operant chamber.
Diagrammatic representation of a sagittal view of rat brain showing a cannula in the (A) ventral tegmental area (VTA) or (E) nucleus accumbens shell (Acb shell). The experimental design for (B) intra-pVTA or (F) intra-Acb shell drug administrations and their effect on active lever pressings. Graphic representations showing the effect of intra-posterior VTA (pVTA) administration of (C) TRPV3-agonist, thymol (n = 9/group) or (D) TRPV3-inhibitor, isopentenyl pyrophosphate (IPP) (n = 8/group); and intra-Acb shell administration of DA (G) D₁ -like receptor antagonist, SCH 23390 (n = 10/group) or (H) D₂ -like receptor antagonist, sulpiride (n = 8/group), on active lever pressings in an operant chamber. Displayed values are mean ± SEM. Data was analysed using one-way ANOVA followed by post-hoc Bonferroni's multiple comparison test. *$P < 0.01$, **$P < 0.001$, ***$P < 0.0001$ *vs* respective control group.
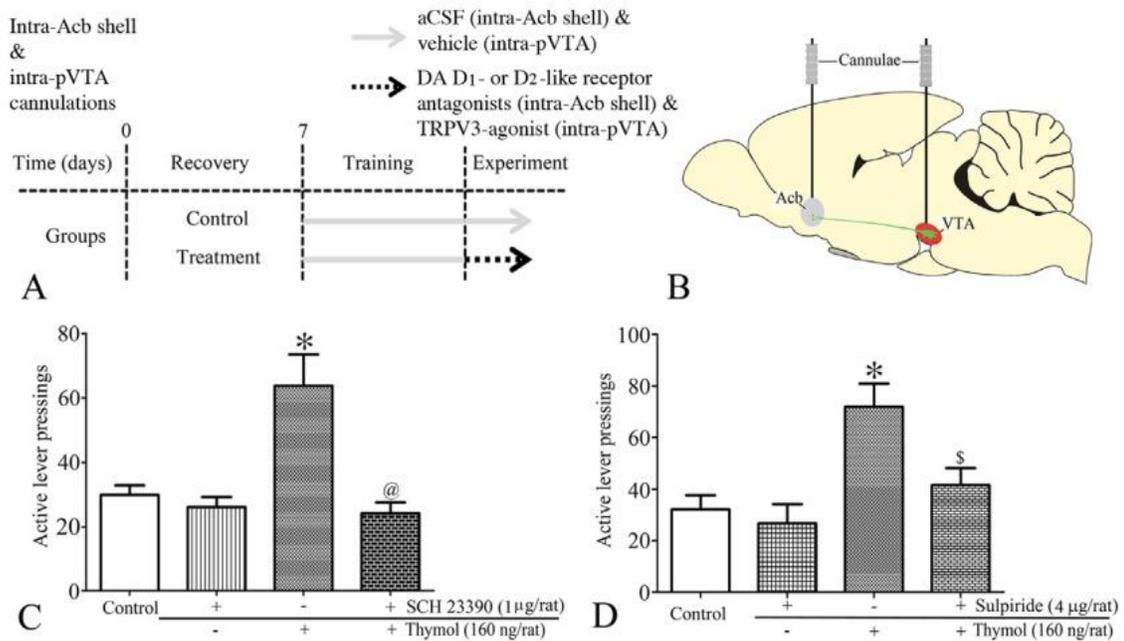
Figure 6: TRPV3 modulates the mesolimbic-dopamine reward pathway.
(A) Experimental design and (B) a schematic of the sagittal view of rat brain showing cannulae in the ventral tegmental area (VTA) and nucleus accumbens (Acb) for administration of TRPV3-agonist and dopamine (DA) D_1 - or D_2 -like receptor antagonists, respectively. Effect of intra-Acb shell DA (C) D_1 -like receptor antagonist, SCH 23390 or (D) D_2 -like receptor antagonist, sulpiride on intra-posterior VTA (pVTA) thymol-induced increase in active lever press counts in the operant chamber. Pre-treatment with SCH 23390 or sulpiride significantly attenuates the thymol-induced active lever pressings. Data was analysed using one-way ANOVA followed by post-hoc Bonferroni's multiple comparison test. n = 8/group; $*P < 0.001$ *vs* control, and $@P < 0.0001$ and $\$P < 0.05$ *vs* respective dose of thymol. Displayed values are mean ± SEM.
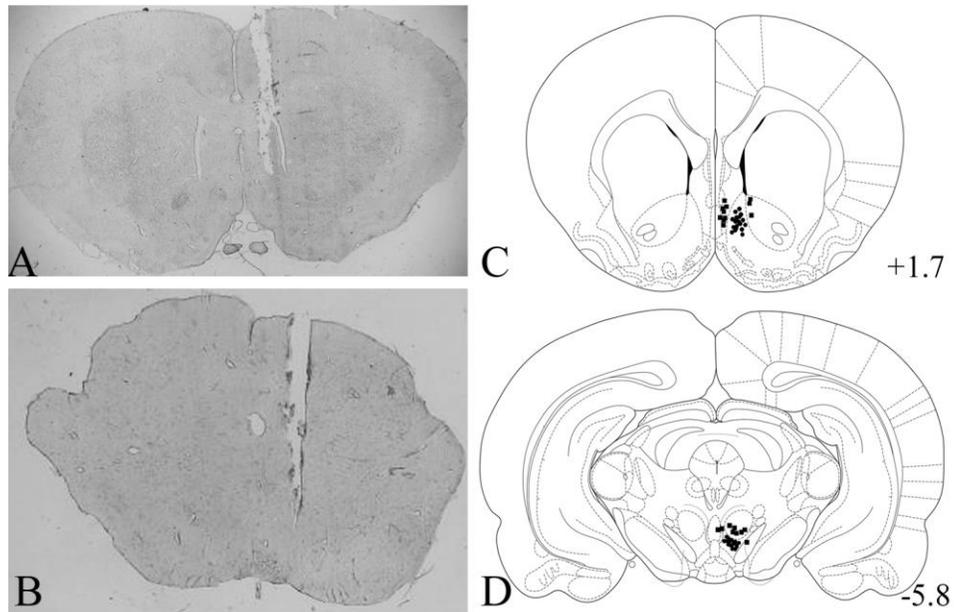
Figure 7: Placement of cannulae.
Photomicrographs of the coronal sections through the rat brain showing placement of cannulae in the (A) nucleus accumbens (Acb) and (B) posterior ventral tegmental area (pVTA). (C, D) The schematics of the rat brain adapted from the rat brain atlas [150] showing site of injections. (C) Acb (+1.7 mm) and (D) pVTA (-5.8 mm) from bregma showing examples of the cannula placements (filled circles). The filled squares represent cannulae placed outside the target (n = 28) and were excluded from the analysis.

3.4. DISCUSSION

Information triggered by the psychoactive agents, drugs of abuse or natural rewards such as food and sex invariably converge on the mesolimbic reward pathway [213,227–231]. These rewarding stimuli are known to modulate DA neurons in the VTA directly, or *via* presynaptic glutamatergic terminals as well as GABAergic interneurons [213,229,232]. Yet another interesting aspect of the system is the demonstrated rise in temperature of the reward processing mesolimbic substrates by a class of drugs of abuse, or even under conditions of natural reward [6]. Temperature, endocannabinoids, and active ingredients of chilli/spices such as capsaicin, thymol, and carvacrol, which activate TRPV-channels, may also serve as potential modulators of DA neurons [6,17,21,233]. There has been a steady increase in the number of studies on the thermosensitive TRPV channels as potential regulators of mesolimbic-DA neurons. TRPV1 regulates mesolimbic-DA neurons by facilitating glutamate release from the presynaptic terminals [17]. Herein, we demonstrate the role of TRPV3, a channel gated by temperature within the physiological range and uniquely sensitive around 37 °C, in the direct modulation of the mesolimbic-DA reward pathway. DA-producing neurons of VTA co-express TRPV3, indicating that these neurons are equipped with these channels and their activation with specific agonists to TRPV3 modulated food reward. We suggest that TRPV3-channels may serve as important regulator of DA neurons in the VTA and may constitute crucial component of the mesolimbic-DA reward circuitry. Due to limitations of the tissue punching technique, the possibility that the excised VTA tissue might also contain the adjoining area of the midbrain cannot be excluded. However, application of TRPV3 antisera showed discrete localization of TRPV3 in VTA. Additional experiments showed increased active lever pressings and enhanced $[Ca^{2+}]_i$ activity in VTA neurons following TRPV3-agonist treatment. Therefore, the evidence

supports expression of these ion channels in the VTA, co-expression in DA neurons, and their functional significance in the modulation of the mesolimbic-DA reward pathway.

Information about the role of TRPV channels in the regulation of mesencephalic DA neurons is limited. The TRPV1-agonist, capsaicin, can act presynaptically, facilitates glutamate release, and can increase neuronal firing of DA neurons [17,234]. While intra-VTA microinjection of capsaicin transiently enhances DA release in the Acb, both neuronal firing of DA neurons and its release in Acb can be reduced by treatment with a TRPV1-antagonist, iodoresineferatoxin [17]. Although TRPV1-induced activation of DA neurons would appear to occur at the level of VTA [17], others have reported the presence of TRPV1-immunoreactivity in the prefrontal cortex and Acb [235,236]. These results suggest that TRPV1 may also regulate DA release directly at the site where the neurotransmitter exerts its action to precipitate reward. In another study, TRPV1 was transgenically expressed in the midbrain DA neurons (SN and VTA) of mice [7]. In these mice, capsaicin increased locomotor activity, but the treatment was ineffective in modulating food reward [7]. Marinelli et al. [234] speculated the involvement of other capsaicin-insensitive TRPV channels in the modulation of DAergic neurons in the midbrain.

In our study, no TRPV3-immunoreactive neurons were identified in the Acb, but intra-pVTA injection of a TRPV3-agonist elicited active lever presses in operant chambers for food reward. In view of this observation, the role of TRPV3 to modulate the mesolimbic-DA pathway at the level of the pVTA is suggested. This is further supported by expression of TRPV3-mRNA and -protein, and increased $[Ca^{2+}]_i$ activity in the pVTA following activation of TRPV3. Due to technical limitations, it is difficult to comment on the DAergic phenotype of the activated neurons. However, based upon the observation that 68.4 ± 3.2 % of the TH neurons in pVTA

express TRPV3 and thymol is a specific agonist of TRPV3 [19], we speculate that the thymol-induced increase in $[Ca^{2+}]_i$ activity observed in the cells in VTA are likely DA neurons.

The monoterpenoid, thymol and carvacrol, serve as TRPV3-agonists [18,19]. Rats given injections of thymol directly into the pVTA were avidly engaged in active lever pressings. The lever press-potentiating activity of thymol may be attributed to the stimulation of TRPV3, since it was reversed by TRPV3-inhibitor, IPP. IPP serves as selective inhibitor of TRPV3 since the carvacrol-induced increase in the unitary Ca^{2+} influx in endothelial cells from pial arteries and cerebral parenchymal arterioles is inhibited by this agent [225]. In addition, the effect of the TRPV3-agonist on Ca^{2+} response in a heterologous expression system, cultured sensory neurons, and epidermal keratinocytes was blocked by pre-treatment with IPP [130]. Therefore, we presume that the pre-treatment with IPP may also block the thymol-induced active lever pressings. Further, we did not find any locomotor stimulating effect following the intra-pVTA thymol treatment. The thymol-induced increase in active lever pressing activity suggests reward and may not be attributed to the general locomotory activation. Thymol-induced increase in active lever pressings further suggests that TRPV3 activation may trigger release of DA into the Acb. This possibility was supported by demonstrating that antagonizing DA receptors in the Acb shell with SCH 23390 and sulpiride prior to activation of TRPV3 in the pVTA with thymol, led to a significant reduction in agonist-induced active lever pressings. Along these lines, it is interesting to note that the administration of carvacrol, modulates DAergic neurotransmission and increases DA levels in prefrontal cortex [20,21]. In addition, a positive reinforcing effect of carvacrol has been suggested [21]. Carvacrol and thymol are present in the flavour enhancing spices like oregano. They may therefore serve like a modulator of the reward value of the food

spiced with these substances by enhancing the palatability and inducing reward by acting on VTA DA neurons *via* TRPV3.

Using retrograde neuronal tract tracing study, we observed ~68 % of DA neurons in the pVTA projecting to the Acb shell were equipped with TRPV3. The projections of neurons in VTA have been extensively studied in rodents using classical as well as the recent viral mediated neural tract techniques [226,237,238]. Swanson [226] observed that ~80% VTA DA neurons project to Acb. Our results are also supported by recent studies demonstrating pVTA as a major Acb projecting VTA subregion [239,240]. This region has been shown to harbor the highest percentage of retrogradely labeled mesoaccumbal neurons [238]. Although other subdivisions of VTA have also been shown to contribute in mesoaccumbal projections, these regions provide minimal innervations to Acb as compared to pVTA [239,240]. In addition to Acb shell, the core region of Acb is also known to receive inputs from the VTA. For example, the caudal linear nucleus of the raphe (CLi) region has been shown to innervate mainly the Acb core [238]. Similar to pVTA, the paranigral (PN) and rostral VTA (rVTA) also innervate different regions of Acb but they contained only few retrogradely labeled neurons as compared to pVTA [238]. In the present study, since the CtB injections were localized into the Acb shell with minimal spread, majority of the pVTA DA neurons accumulated CtB whereas aVTA and tVTA subdivisions of VTA were devoid of retrogradely labeled neurons. We, therefore, suggest that the TRPV3-expressing DA neurons in pVTA may serve as major axonal projecting center to Acb and contribute to the mesolimbic-DA reward pathway. Using tract tracing studies, recently [238] have analyzed an interesting aspect of the VTA-Acb pathway. These authors demonstrated that both DAergic as well as non-DAergic neurons in VTA, contribute to Acb innervation, these neuronal populations were intermingled, and equal proportion of DA and non-DA neurons in

VTA project to given Acb subdivision. Since we observed ~ 83% of TRPV3 neurons were TH-immunoreactive, we suggest that the majority of the DAergic neurons involved in the regulation of mesolimbic pathways might be under the control of TRPV3.

DA plays crucial and overlapping roles in natural reward and drugs of abuse induced reinforcing/rewarding behavior and treatment with DA receptor antagonists has been suggested to block these behaviors [232,241,242]. Although the precise role of DAergic system and the receptor mediating food reward is not well understood [243], the involvement of both DA D_1 and D_2 type receptors in DA-mediated reward [244], particularly in ghrelin-induced food reward behavior [242], has been demonstrated. Feeding increases the extracellular levels of DA in Acb [243]. The VTA-derived DAergic terminals release DA in the Acb which may simultaneously bind to all DA receptors in this region and activate both D_1 and D_2 receptors to modulate food reward and reinforcement [242,244]. Our observation that both receptor subtypes mediate thymol-induced active lever pressings is in agreement with these reports.

Available evidence and the present study suggest that the significance of TRPV channels in the VTA is to function as novel regulators of the mesolimbic-DA reward pathway. A schematic of the mesolimbic-DA pathway and proposed mechanism for TRPV channels driving the circuitry is shown in Figure. 8. Capsaicin is present in chilli peppers, and carvacrol and thymol are active ingredients of the oregano spices [21] and serve as flavour enhancers. Zotti et al. [21] suggested that the ingestion of dietary carvacrol might induce reward. Both capsaicin and carvacrol cross the blood brain barrier [21,245], and may directly act on TRPV channels [246] in the VTA to modulate DAergic neurotransmission [19,21]. Since thymol and carvacrol are isomers [18], thymol may also cross the blood brain barrier. Both these agents seem to activate TRPV3 in similar fashion [18]. DA neurons in the VTA express TRPV3 and the action

of this agent seems to be at the level of VTA. Although a range of natural compounds serve as modulators of TRPV3, this is the only TRPV channel for which the endogenous modulators have not been described [97]. Phosphatidylinositol 4,5-bisphosphate [PI(4,5)P2] and 17(R)-resolvin D1 have been proposed as probable endogenous modulators of TRPV3 [97,247]. In addition, farnesyl pyrophosphate and isopentenyl pyrophosphate, produced in the mevalonate pathway, have also been suggested to modulate this channel [97,130,247]. Bang et al. [247] suggested that farnesyl pyrophosphate serve as endogenous activator of TRPV3. However, pharmacological manipulation of TRPV3 in the brain might be complex. It can act as an agonist for several nuclear hormone receptors [248]. The authors have demonstrated that farnesyl pyrophosphate act as agonist of the glucocorticoid receptors (GR). It is impotant to note that the dopamine neurons in VTA are equipped with GR [249]. In the present study, we used thymol as TRPV3 agonist since treatment with farnesyl pyrophosphate may activate dopamine neurons in VTA and the action might be mediated via GR as well as TRPV3, and it would be difficult to assess the involvement of TRPV3. Several GPCRs activate TRPV1 via phospholipase C [2]. Similarly, TRPV3 has also been suggested to function with such receptor species. This is supported by the evidence in HEK293 cells expressing the human muscarinic receptor type 1 and transfected with mTRPV3 [19]. The addition of the muscarinic agonist in the presence of carvacrol to these cells greatly enhanced TRPV3 currents [19].

The neural pathway processing natural reward is also a target for drugs of abuse and control addictive behaviors [213]. Endocannabinoids (anandamide and N-Arachidonoyl dopamine) serve as TRPV1-agonists and act on presynaptic terminals on DA neurons in the SN facilitating glutamate release [233]. A similar mechanism of action of endocannabinoids on the VTA DA neurons is speculated. Drugs of abuse such as cocaine have been shown to increase the

temperature of mesolimbic substrates [6], and may take control of the circuitry by elevating the temperature and activating TRPV-channels. Taken together, we propose that TRPV channels in the VTA may serve as novel molecular determinants for processing specific reward and potential targets to control overeating and addictive behaviors.
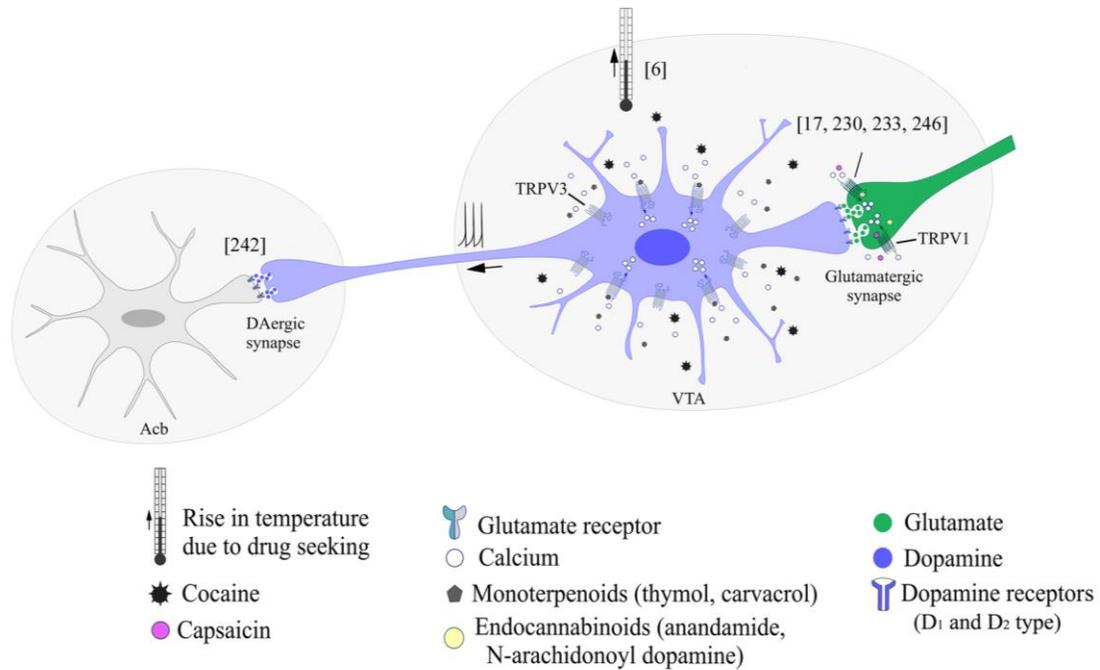
Figure 8: VTA-Acb DAergic pathway and proposed mechanism of modulation of the VTA DA neurons by TRPV ion channels.

DA neuron (blue) in the VTA innervate neurons in the Acb (grey). Neurons in the Acb express either DA D_1- or D_2- or both receptor subtypes, and play a role in food reward. The glutamatergic axon terminal (green) innervating the VTA DA neuron is equipped with TRPV1. Capsaicin and endocannabinoids serve as specific TRPV1 agonists. Similar to capsaicin, endocannabinoids may also act on the presynaptic glutamatergic terminals to facilitate glutamate release onto DA neurons and stimulate DA neurotransmission to the Acb. As DA neurons in the VTA are equipped with TRPV3-channels, monoterpenoids (thymol and carvacrol) may stimulate DA neurons and modulate the mesolimbic-DA reward pathway. Cocaine may increase the temperature of the mesolimbic substrates and hijack the reward circuitry *via* thermosensitive TRPV channels.

CHAPTER 4

Expression of TRPV3 in the cerebellum of rat: significance in motor coordination

4.1 INTRODUCTION

Coordinated motor functions including movements of eyes and limbs, defense mechanism, balance, and regulation of physiological activities are some of the key functions controlled by the cerebellum [250]. Purkinje neurons are important component of the cerebellum. In the human brain, these neurons have been suggested as one of the largest neurons [251]. These neurons are located in a row throughout the cerebellar border of granular and the molecular layer [252]. These cells serve as integrative center for sensory inputs and provide output for downstream actions [253]. Calcium homeostasis is necessary for Purkinje cells survival as well for sensory and its cellular activity [254]. The disrupted intracellular calcium homeostasis in Purkinje cells due to altered voltage-gated calcium currents or genes encoding Ca^{2+} channel subunits lead to calcium-related neuronal dysfunctions like ataxia and altered motor activites [255,256].

Purkinje cells show complex trimodal firing pattern *viz.* tonically firing, bursting, and silent modes [156]. The spontaneous trimodal activity of Purkinje cells is sensitive to temperature and age dependent [156]. In *ex vivo* slices of cerebellum, a 3 °C decrease in temperature from 35 °C resulted in loss of firing in Purkinje cells [156]. These cells are equipped with high voltage activated (HVA) *viz.* P/Q type, L-type and N-type, and low voltage activated (LVA) *viz.* T- and R-type calcium channels for range of cellular functioning ranging from development to synaptic firing [257–263]. In addition to the classical voltage-activated calcium channels, cerebellar Purkinje neurons are also equipped with other types of calcium channels *viz.* ligand gated calcium channels like AMPA [264] and NMDA [265] receptors.

Recently, the mRNA analysis showed the presence of transcripts for TRP ion channels in the cerebellum [68]. TRP melastatin-3 (TRPM3) and TRP canonical-1 (TRPC1) are reported at

glutamatergic parallel fiber-purkinje cell synapse (PR-PCs) and these channel proteins have been shown to generate slow excitatory postsynaptic conductance (EPSC) [266]. These channels also modulates the release of the neurotransmitters [267,268]. Compared to others, TRPV channels showed lower expression in the cerebellum [68]. While the presence of TRPV1 has been demonstrated in the Purkinje neurons of mouse using immunohistochemisty [269]; mRNA analysis showed the expression of other TRPV ion channels in the cerebellar tissue [68]. Whether the neuronal elements in the cerebellum also express TRPV2-6, however has remained unexplored.

Unlike other members in the TRPV subfamily, TRPV3 is gated by temperature between 31-39 °C [8,9] and is uniquely sensitive around 37 °C [9]. Interestingly, the effect of temperature on the synaptic activity in the cerebellar neurons and animal behavior has been studied in the goldfish [270]. In body cooling and heating experiments as well as when temperature of the cerebellum was elevated by thermode, initial hyperactivity and enhancement of reflexes was observed [270]. Similarly, the rat cerebellar neurons *ex vivo* were spontaneously active and cooling at 18 °C resulted in reduced neuronal activity [271]. As described in chapter 1, we observed TRPV3 mRNA expression in the cerebellum of rat and the Purkinje cells seem to be equipped with TRPV3-immunoreactivity. We therefore characterized TRPV3-expressing Purkinje neurons in further details and studied the role of these ion channels in the control of motor coordination.

4.2 MATERIALS AND METHODS

4.2.1 Animals

Adult, male, Wistar rats (250-280 g) were used in this study. Animals were maintained in temperature controlled room (22 ± 1 °C) with light between 6:00 and 18:00 h, and access to water and food *ad libitum*. All the experimental procedures were approved by the Institutional Animal Ethics Committees (IAEC) at NISER, Bhubaneswar and Department of Pharmaceutical Sciences, Nagpur University, Nagpur.

4.2.2 Tissue preparation and immunofluorescence

Animals were anesthetized with ketamine (100 mg/ml) and xylazine (10 mg/ml) and perfused, transcardially with 100 ml of phosphate buffer saline (PBS, 0.2 M, pH-7.4) followed by 4 % paraformaldehyde (PFA) in phosphate buffer (0.1 M, pH-7.4). Brain were dissected out and post-fixed overnight in 4 % PFA at 4 °C. Brains (n = 3) were cryoprotected in 25 % sucrose solution in PBS followed by 4 sets of 25 µm thick coronal sections were cut on cryostat.

For TRPV3 immunofluorescence, biotin-tyramide (BT) amplification protocol was employed as described in chapter 1. One set of cerebellar sections from each animal (n = 3) were rinsed in PBS and treated with 0.5 % Triton X-100 in PBS for 20 min. Sections were incubated in 3 % normal horse serum in PBS for 30 min and incubated overnight at 4 °C in polyclonal rabbit anti-TRPV3 antiserum. The immunoreaction was amplified and visualized using DTAF-avidin (Jackson Immunoresearch).

Double immunofluorescence was employed to determine whether Purkinje neurons in the cerebellum co-express TRPV3. One set of coronal sections through the rostro-caudal extent of

the cerebellum of each animal (n = 3) were rinsed in PBS, treated with 0.5 % triton X-100 in PBS for 20 min, and immersed 3 % normal horse serum for 30 min. Sections were incubated overnight at 4 °C in a mixture of polyclonal rabbit anti-TRPV3 antiserum (1:5000) and mouse calbindin D28k (1:500) antibody. TRPV3 was amplified using BT amplification as described above and visualized using DTAF-avidin. Calbindin D28k was visualized using AlexaFluor-549 conjugated anti-mouse IgG (Invitrogen, 1:500). After rinsing in PBS, sections were mounted on glass slides, coverslipped with mounting medium containing DAPI (Vector), and observed under an AxioImager M2 fluorescence microscope (Carl Zeiss). Images were captured, adjusted for brightness and contrast and merged using Adobe Photoshop CS4 software.

4.2.3 Stereotaxic surgery for intra-cerebellum drug administration

Intra-cerebellum cannulation and injection was performed as reported previously [222,223]. Briefly, the rats were anesthetized with an intraperitoneal injection of a mixture containing ketamine (Themis Medicare Ltd., India; 90 mg/kg body weight) and xylazine (Indian Immunologicals Ltd., India; 10 mg/kg body weight). Under stereotaxic control, the stainless steel guide cannulae [224] were implanted bilaterally in the cerebellum using coordinates AP: -11.6, DL: ± 2.3, DV: - 4.6 [150]. The cannulae were secured above the site of injection with stainless steel screws and dental cement, and the injector was designed to project 0.5 mm below the guide cannula. Post-surgical care was taken during the recovery period. The rats were allowed to recover from surgery for 7 days and subjected to training for behavioral assays.

4.2.4 Intra-cerebellum TRPV3 agonist and inhibitor administration

For intra-cerebellum administration, thymol (Sigma, USA) and isopentenyl pyrophosphate (IPP, Echelon Biosciences) were used. Thymol has previously been used as TRPV3-agonist [18,19,149]. IPP serves as TRPV3-inhibitor [130,225]. Thymol was dissolved in dimethyl sulfoxide (DMSO) as a stock solution. The stock solution was further diluted in aCSF such that the final concentration of DMSO was less than 0.05 % in both vehicle as well as thymol-treated groups. IPP was dissolved in aCSF as described in Chapter 3. The rats were randomly divided in different groups (n = 6), as described previously [222] and subjected to the intra-cerebellum injection of (i) vehicle (0.5 µl/side/rat); (ii) thymol (0.5 µl/side/rat); (iii) IPP (0.5 µl/side/rat). The animals were subjected to toe footprint analyses, locomotor activity, and open field test as described below.

4.2.5 Behavioral assays

Toe Footprint analyses: To quantify the gait abnormalities, method described by Klapdor et al [272] was employed. Briefly, the rats were allowed to walk on an inclined gangway (100 cm x 12 cm x 10 cm with 30° inclination) leading to a darkened enclosure. The gangway was lined with white paper and the fore- and hind-paws of the animals were dipped in two different non-toxic watercolors to monitor the footprints. The walking pattern was recorded twice for each animal, after which the colors were washed off; wet areas were dried and returned to their cages. The footprints were analyzed for parameters *viz.* footprint length and stride length.

Locomotor count using actophotometer: Locomotor activity was monitored in rats with an actophotometer (Centroniks Electronic, India) of 38 cm diameter and 16 cm height, equipped with photocells that automatically recorded the movements of rat [273]. Any movement of the rat that interrupted photo beams was recorded as a motor count. Each rat was injected aCSF or drug intra-cerebellar in their home cages and placed in the actophotometer 15 min after treatment. Spontaneous locomotor activity of each rat was measured for 10 min. Animals were used only once and after each test the actophotometer grid floor was carefully cleaned. The data are expressed as mean number of counts per 10 min.

Number of crossovers using open field test (OFT): Although OFT is used to study the anxiety-like behavior in rodents, it is also a routinely employed, and validated animal paradigm to the number of crossovers to assess walking pattern in the animals [149]. Each rat was placed at the center of the open field apparatus designed as previously described [274,275]. The field consists of a circular arena divided into 60 squares of 10 x 10 cm each. The entire arena was provided with a 75 cm high aluminum walls at the periphery. A 60 W light bulb was positioned 90 cm above the center of the arena, and provided the only source of illumination in the testing room. Each animal was placed in the center of the open field apparatus, and the number of crossovers was measured during a 5 min period. A line crossing was counted when all four paws of animal crossed over the line. After each exposure, floor of the apparatus was wiped, cleaned to remove excreta and pheromones.

4.2.6 Image and statistical analysis

Tissue sections of cerebellum immunolabelled with TRPV3 antiserum and calbindin

D28k were observed under the fluorescence microscope. The images were captured and prcessed as described in chapter 1.

Data was analyzed using GraphPad Prism software (Graphpad Software, CA, USA). For comparison between the groups, statistical analysis was carried out using one-way ANOVA, followed by post-hoc Bonferroni's multiple comparison test. No adjustments were employed for multiple comparisons. All the data are expressed as mean ± SEM, statistical tests were two-tailed, and $P < 0.05$ was considered significant.

4.3 RESULTS

4.3.1 TRPV3 expression in the cerebellum

RT-PCR analysis revealed TRPV3 mRNA expression in the cerebellum. Details are given in chapter 1. Using TRPV3 specific antiserum moderately immunoreactive cells and fibers were observed in the cerebellum (Fig. 1A-C). Double-labelled immunofluorescence revealed the colocalization of TRPV3 and calbindin D28k (Fig. 1D-F) in the Purkinje cells. All the calbindin D28k-positive Purkinje cells were TRPV3-immunoreactive (Fig. 1G-I).

4.3.2 TRPV3 controls motor coordination

Effect of intra-cerebellum thymol and IPP on gait patterns: Animals infused with aCSF, IPP, and thymol; and were tested for gait abnormalities. Splayed paws and movement incoordination (wobbling gait) was observed in all the rats which received IPP (Fig. 2) No significant change was observed ($P > 0.05$) in the gait parameters between the controls (aCSF-treated) and thymol-treated rats. The footprint and the stride lengths were significantly affected in the animals treated with IPP. Compared to controls, the stride length; the distance between the two successive hind limb prints, was significantly decreased ($P < 0.001$) (Fig. 2B). The footprint length, measured as the distance from the heel to the tip of the third digit of the hind limb, was significantly increased ($P < 0.001$) in IPP-treated animals (Fig. 2C).

Effect of thymol and IPP on locomotor counts and number of crossovers: The locomotor activity was measured in rats using actophotometer following aCSF, IPP, or thymol treatments. Compared to the aCSF treated control rats, IPP administered directly into the cerebellum

significantly decreased the locomotor counts (Fig. 3A, ($P < 0.001$). Thymol treatment did not alter the normal locomotor activity (Fig. 3A; $P > 0.05$).

Rats were administered aCSF, IPP, or thymol and subjected to OFT, where the number of ambulation (crossovers) was measured. Compared to aCSF-treated rats, IPP decreased the number of crossovers from 168.30 ± 5.1 to 56.8 ± 6.7 (Fig. 3B; $P < 0.001$). The numbers of crossovers in the thymol-treated rats were significantly more as compared to that of the IPP treated rats (Fig. 3B; $P < 0.001$).
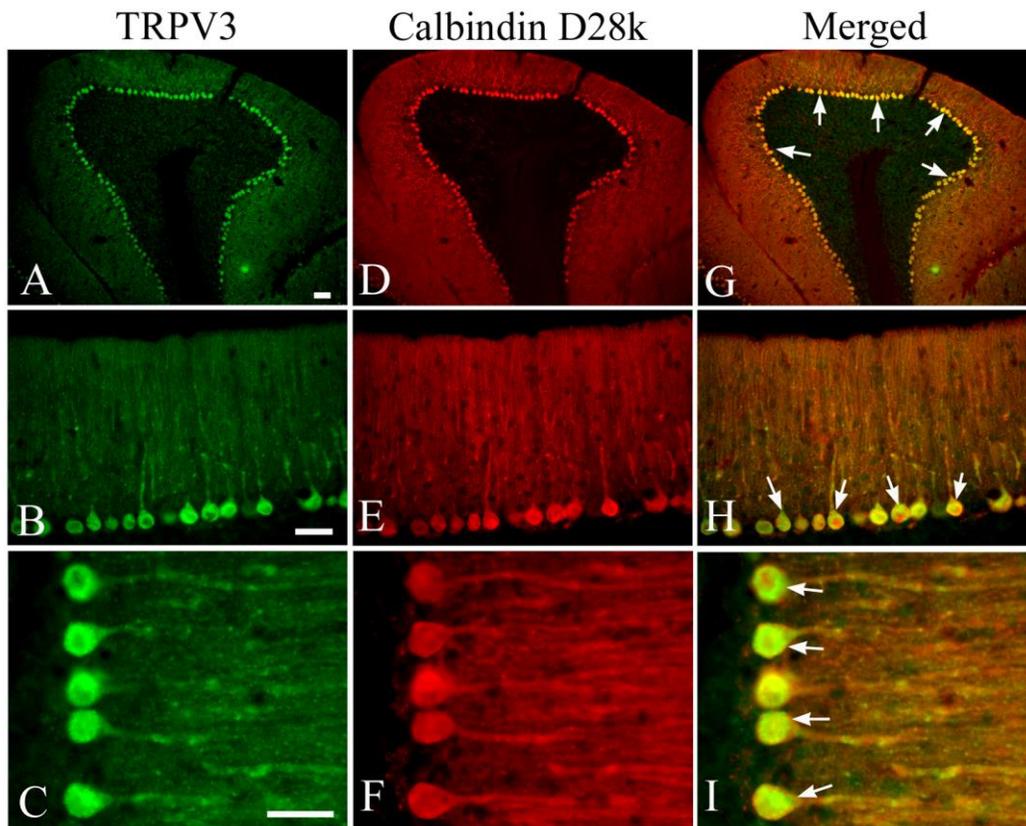
Figure 1: TRPV3-immunoreactivity in the cerebellum of rat.
Fluorescence photomicrographs showing (A-C) TRPV3 (green) and (D-F) calbindin D28K (red) immunoreactivity in the cerebellum. (G-I) TRPV3 and calbindin D28K are colocalized in the Purkinje neurons. Colocalized Purkinje neurons appear yellow due to color mixing (arrows). Scale bar = 50 µm.
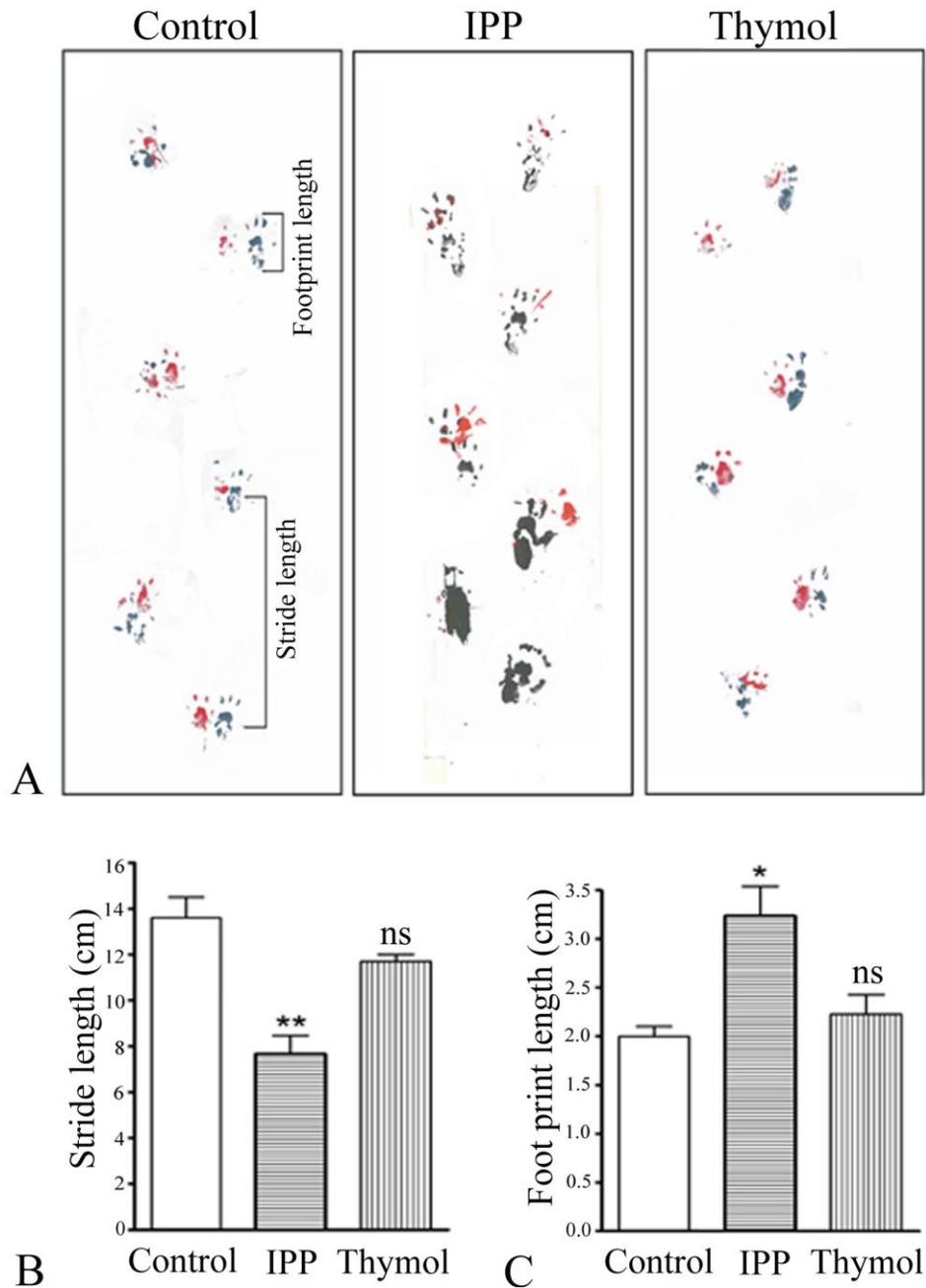
Figure 2: Intra-cerebellar TRPV3-inhibitor alter footprint and stride length.
(A) Footprint pattern and stride length of rats infused with either intra-cerebellum vehicle, TRPV3 inhibitor isopentenyl pyrophosphate (IPP), or TRPV3 agonist, thymol. Paw patterns were assessed for (B) stride length and (C) footprint length. Note significantly wider footprint and reduced stride length after IPP administration. ns, non-significant; *$P < 0.01$ and **$P < 0.001$ *vs* control. Displayed values are mean ± SEM.
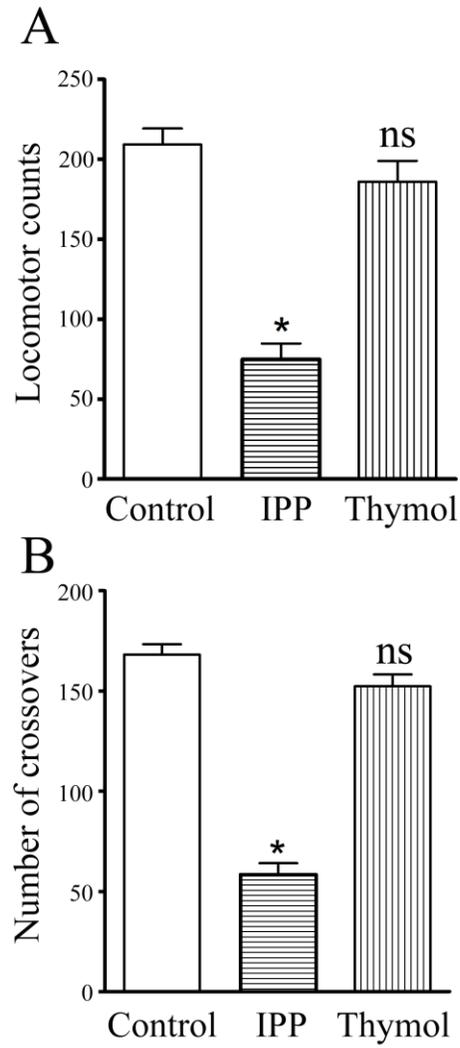
Figure 3: Intra-cerebellar TRPV3-inhibitor decreases locomotor activity.
The motor performance of animals is significantly impaired after infusion of TRPV3 inhibitor, isopentenyl pyrophosphate (IPP) (intra-cerebellum). Bar graphs show (A) the decrease in locomotor counts and (B) inability of animals to walk. Vehicle and agonist-infused animals did not show such effects. ns, non-significant; *$P < 0.001$ *vs* control. Displayed values are mean ± SEM.

4.4 DISCUSSION

In this study we have explored the presence and role of TRPV3 in the cerebellum of rat. Purkinje neurons showed TRPV3-immunoreactivity. While the treatment with TRPV3-inhibitor, IPP produced gait abnormalities, intra-cerebellum TRPV3-agonist, thymol had no effect on this behavior. Based upon these observations, we suggest that the Purkinje neurons in the cerebellum of rat are equipped with TRPV3 ion channel which may contribute to the regulation of motor coordination.

While the expression of non-selective TRPV (1-6) ion channels has been demonstrated in the cerebellum [68], information about the neuroanatomical organization and functional significance of TRPV3 in the cerebellum is still not available. Using RT-PCR, we observed low level of TRPV3 expression in the cerebellum of rat (Please see chapter 1). The results are in agreement with previous findings showing TRPV3 mRNA expression in the cerebellum [68]. Using double immunofluorescence, all Purkinje neurons were also TRPV3-immunoreactive. Purkinje cells serve as the important computational units of the cerebellum and the recent reports have underscored the significance of TRP channels in the modulation these neurons [68,266]. The presence of TRPC1 in glutamatergic parallel fiber-purkinje cell synapse (PR-PC) and its significance in motor coordination has recently been described [68,266].

To characterize the role of TRPV3 ion channel in the Purkinje cell function, we analyzed gait abnormalities of the adult wild-type rats based upon the pattern of their footprints. Control rats displayed a normal alternating gait along a straight line. The rats which were given with IPP intra cerebellum, however displayed gait with broader width and abnormal step patterns. Further, the assessment of motor coordination by other behavioral tests, we observed that the inhibition of TRPV3 with IPP severely affected the ability of the animal to maintain their

balance to walk across the beam and displayed reduced cross over in OFT apparatus. Heterozygous *Mwk* mice (Mwk$^{-/+}$) for TRPC3 displayed similar results in ataxic mouse mutants [155]. Based on these reports and our observations, we suggest that the TRP channels may serve as novel modulators of cerebellar functions.

Purkinje cells are unique, since they are intrinsically active and generate action potentials even in the absence of synaptic stimulus [276,277]. Few reports suggested that these cells fire at defined rate [276–278], whereas a more complex neuronal firing has also been observed [279]. Womack and Khodakhah [156] reported an intrinsic, trimodal pattern of activity in these cells which is independent of glutamatergic and GABAergic synaptic inputs. The trimodal pattern of activity is prominent at the maturation stage of the cerebellum and remained high during adult stages [156]. Purkinje cells develops an extensive dendritic tree till postnatal 3rd week [250], thereby strengthening of the motor coordination becomes more efficient [250]. Given the increasing importance of TRP ion channels in cerebellar function [266], the highly dynamic cellular arborization, and calcium-dependent functional aspect of Purkinje neurons [255,256], we speculate that TRPV3 ion channel may play a similar role.

Another interesting aspect of the trimodal pattern of firing in the Purkinje cells is that these neurons are sensitive to changes in temperature. The spontaneous firing at 35 °C ceases by a decrease in temperature by 3 °C [258]. Unlike other members in the TRPV-subfamily, TRPV3 is gated by temperature between 31-39 °C [8,9]. Expression of TRPV3 in temperature sensitive Purkinje neurons seems important in the modulation of these neurons. This is supported by previous *in vivo* studies demonstrating the effect of elevated temperature on motor reflex in the goldfish [270], and the experiments conducted *in vitro* system showing the effect of temperature

on Purkinje cell firing [271]. We speculate that the TRPV3 ion channel in Purkinje cells may acts as intrinsic molecular switch to alter their mode of activity necessary for motor functions.

SUMMARY AND CONCLUSIONS

From the available evidence and present study, TRPV3 seem to be the most widely distributed and discretely organized TRP ion channel in the brain of rat. To our knowledge this is the first study demonstrating a detailed neuroanatomical organization of TRPV3-expressing elements in the brain. Based upon the differential localization of TRPV3 in the preoptic area, hypothalamus, midbrain and brainstem, we suggest that TRPV3 in the brain may control a range of neural functions including food reward, neuroendocrine regulation, and motor coordination. Neuroanatomical organization of TRPV3-immunoreactive elements in the brain of rat was comparable with that of the mice. The neuroanatomical maps showing discrete localization of TRPV3 in the brain of these model animals would help in designing further experiments delineating the functional significance of this ion channel in the brain.

TRPV3-equipped elements were abundantly expressed in the hypothalamus of rat, and two important neuroendocrine centers in the hypothalamus *viz.* hypothalamic paraventricular (PVN) and supraoptic (SON) nuclei showed TRPV3-immunoreactive neurons. A great majority of the vasopressin (VP) neurons in these nuclei were equipped with TRPV3. The VP neurons in the PVN and SON are known to secrete this peptide in the posterior pituitary, and VP acts on kidney to conserve water [280]. Our retrograde neuronal tracing study suggests that the TRPV3-equipped neurons are hypophysiotropic; and TRPV3-equipped VP neurons respond to the hyperosmotic challenge. In addition to TRPV3, the VP and oxytocin neurons in the hypothalamus are also known to co-express TRPV1, TRPV2, and TRPV4, and their role in the regulation of these neurons is suggested [2,11–13]. It is interesting to note that the SON neurons which were insensitive to the treatment of TRPV1 agonist, capsaicin at 24 °C responded to the same concentration of the drug when the temperature was raised to 36 °C [15]. We therefore

suggest that the osmoreceptor expressed on PVN and SON neurons may be a hetero-multimer formed by TRPV1 and TRPV3.

In addition to the axonal secretion, the magnocellular VP and oxytocin neurons also secrete these nonapeptides through their somata/dendrites and exerts extra-synaptic actions in the brain. Such somatodendritic secretion of the nonapeptides has been suggested to modulate behavior and the action seems to be long lasting [164]. Release of these neuropeptides from the somatodendritic compartment of the PVN and SON neurons has also been suggested important in the coordination/synchronization with other neurons in these nuclei [281]. The magnocellular neurons are equipped with two types of synaptic vesicles *viz*. the small clear core and large dense core vesicles (LDCVs). While the small clear core vesicles are present at the axon terminals of these neurons, the LDCVs are distributed at axon terminals as well as in the somata/dendrities [164]. Although the regulatory SNARE proteins are essential to modulate the Ca^{2+}-mediated exocytosis of the synaptic vesicles, the somatodendritic compartment of the magnocellular neurons seem to lack the component of the regulatory SNARE complex essential for exocytosis [161,165]. As previously demonstrated [161,186], we observed the presence of synaptic vesicle 2 (SV2) and synaptotagmin-1 (SYT-1) -immunoreactivity in the presynaptic terminals in the hypothalamus of normal, untreated rats, but show that hyperosmotic challenge recruits SYT-1 and SV2 proteins to somata/dendrites of VP neurons in the PVN and SON. Not all but ~58 % VP neurons in the PVN and 43 % in SON showed the co-expression of SYT-1 during salt loading. All the SYT-1 expressing VP neurons in PVN and SON were hypophysiotropic in nature. VP has auto-regulatory effect and the regulation of VP secretion is more complex [161,202]. The central injection of VP results in reduced plasma VP levels in dogs [203]. Ludwig and Leng [204] suggested that the VP released from the somata/dendrites regulates the

activity of SON VP neurons by auto-inhibitory mechanism. Thus, the VP released from the somata/dendrites during hyperosmotic challenge might provide an efficient and non-exhaustive mechanism controlling systemic VP secretion [205]. While the VP neurons are equipped with both VP V1a and V2 receptors, dendritically released peptide is believed to act positively on its own dendrites *via* V2 receptors and further enhance somatodendritic VP secretion [206]. In contrast, dendritically released VP acting on V1a receptors may inhibit the spiking activity and systemic release of VP [163,164,206]. We propose that VP released from the somata/dendrites of SYT-1-expressing neurons act on its own dendrites *via* V2 receptors for sustained VP release from its somata/dendrites, as well as from the axon terminals. In addition, somatodendritically released VP may act on adjacent non-SYT-1-expressing VP neurons *via* V1a receptors and inhibit secretion of VP from their axon terminals.

Occurrence of TRPV3 expressing neurons in the ventral tegmental area (VTA) in the midbrain of rat and role of these ion channels in the modulation of mesolimbic DA neurons is one of the interesting finding of my thesis. Guatteo et al. [4] observed the presence of TRPV3 mRNA in the midbrain tissue and demonstrated that the DA neurons in the substantia nigra (SN), a region adjacent to VTA, were thermosensitive. These neurons showed increased neuronal firing at 39 °C, which seems in the range of the activation threshold temperature of TRPV3. We observed several TRPV3-equipped neurons in the posterior VTA (pVTA) and 68 % of TRPV3-equipped DA neurons project to the nucleus accumebs shell (Acb Shell). Interestingly, the projections of DA neurons to Acb shell constitute the well characterized reward pathway and the release of DA in Acb shell produces reward [24,25]. Recent evidences have underscored the importance of TRPV channels in the regulation of mesolimbic DA reward pathway. The TRPV1 ions channel on presynaptic glutamatergic terminals in VTA responds to glutamate release in

response to capsaicin which has triggered neuronal firing of DA neurons [17,234]. Zotti et al. [21] suggested positive reinforcing effect of a TRPV3 agonist, carvacrol. TRPV3 expression in DA neuron increased $[Ca^{2+}]_i$ activity in the VTA neurons suggests that TRPV3 ion channel may serve as a direct modulator of mesolimbic DA neurons. Role of TRPV3 in driving the reward behavior was further demonstrated using operant conditioning, a well-established behavioral system to study reward. While the rats infused with TRPV3 agonist thymol directly into the pVTA showed positive reinforcing behavior, the response was inhibited by intra-pVTA infusion of TRPV3 inhibitor, isopentenyl pyrophosphate (IPP). Although the DA receptor subtypes employed to mediate the effect of increased DAergic tone during reward is not well established [243], recent study has demonstrated the involvement of both DA D_1- and D_2-like receptor for ghrelin-induced food reward [242]. Our observation on involvement of DA D_1- as well as D_2-receptors in mediating TRPV3-induced DAergic neurotransmission to Acb Shell is in agreement with this report. We proposed that the TRPV3 ion channel in VTA may serve as novel molecular determinant for processing specific reward and potential target to control overeating and addictive behaviors.

TRPV3 is expressed in the cerebellum and the Purkinje cells were TRPV3-immunoreactive. The observation is supported with a recent report demonstrating TRPV3 mRNA expression in the cerebellum [68]. The Purkinje neurons are major cell type in the cerebellum which receives the central inputs and control the motor functions. Interestingly, the effect of temperature on motor reflexes has been suggested [270]. Given the thermosensitive nature of TRPV3, the ions channel may play a regulatory role in cerebellum. We observed presense of TRPV3-immunoreactivity in Purkinje neurons and TRPV3 inhibitor, IPP infused intra-cerebellum altered motor coordination behavior of the rats. We suggest that TRPV3 ion

channel in cerebellum, may act as an intrinsic molecular switch to alter the neuronal activity of Purkinje neurons for motor functions.

The data presented in this thesis supports the previously suggested notion that the TRPV3 is predominantly a gene of the nervous system. The differential expression pattern in the brain, abundance in the hypothalamic region, localization in the VTA, and modulation of reward behavioral by pharmacological alteration of the channel activity suggests that TRPV3 might be a crucial driver of specific microcircuits in the brain. Given the close overlapping organization of TRPV3 and TRPV1 in the brain, we propose that TRPV3 ion channel might be coupled with TRPV1 or some other as yet undefined receptors in different brain regions and modulation of these receptors by neurotransmitters or endogenous signaling may differentially regulate neuronal response. From the study conducted on the brain of *C. batrachus*, we suggest that the regulation of oxytocin neurons by TRPV3 might be evolutionary conserved. Future studies are required to decipher the significance of TRPV3 ion channel in the brain and its endogenous modulation.

REFERENCES

1 Montell C (2001) Physiology, phylogeny, and functions of the TRP superfamily of cation channels. *Sci. STKE* **2001**, re1.

2 Kauer JA & Gibson HE (2009) Hot flash: TRPV channels in the brain. *Trends Neurosci.* **32**, 215–224.

3 Caterina MJ (2007) Transient receptor potential ion channels as participants in thermosensation and thermoregulation. *Am. J. Physiol. Regul. Integr. Comp. Physiol.* **292**, R64–R76.

4 Guatteo E, Chung KKH, Bowala TK, Bernardi G, Mercuri NB & Lipski J (2005) Temperature sensitivity of dopaminergic neurons of the substantia nigra pars compacta: involvement of transient receptor potential channels. *J. Neurophysiol.* **94**, 3069–3080.

5 Smith GD, Gunthorpe MJ, Kelsell RE, Hayes PD, Reilly P, Facer P, Wright JE, Jerman JC, Walhin J-P, Ooi L, Egerton J, Charles KJ, Smart D, Randall AD, Anand P & Davis JB (2002) TRPV3 is a temperature-sensitive vanilloid receptor-like protein. *Nature* **418**, 186–190.

6 Kiyatkin EA (2013) The hidden side of drug action: brain temperature changes induced by neuroactive drugs. *Psychopharmacology (Berl).* **225**, 765–780.

7 Güler AD, Lee H, Iida T, Shimizu I, Tominaga M & Caterina M (2002) Heat-evoked activation of the ion channel, TRPV4. *J. Neurosci.* **22**, 6408–6414.

8 Peier AM, Reeve AJ, Andersson DA, Moqrich A, Earley TJ, Hergarden AC, Story GM, Colley S, Hogenesch JB, McIntyre P, Bevan S & Patapoutian A (2002) A heat-sensitive TRP channel expressed in keratinocytes. *Science* **296**, 2046–2049.

9 Xu H, Ramsey IS, Kotecha SA, Moran MM, Chong JA, Lawson D, Ge P, Lilly J, Silos-Santiago I, Xie Y, DiStefano PS, Curtis R & Clapham DE (2002) TRPV3 is a calcium-permeable temperature-sensitive cation channel. *Nature* **418**, 181–186.

10 Horvath TL, Warden CH, Hajos M, Lombardi a, Goglia F & Diano S (1999) Brain uncoupling protein 2: uncoupled neuronal mitochondria predict thermal synapses in homeostatic centers. *J. Neurosci.* **19**, 10417–10427.

11 Nedungadi TP, Carreño FR, Walch JD, Bathina CS & Cunningham JT Region-specific changes in transient receptor potential vanilloid channel expression in the vasopressin magnocellular system in hepatic cirrhosis-induced hyponatraemia. *J. Neuroendocrinol.* **24**, 642–652.

12 Nedungadi T, Dutta M, Bathina C, Caterina M & Cunningham J (2012) Expression and distribution of TRPV2 in rat brain. *Exp. Neurol.* **237**, 223–237.

13 Wainwright A, Rutter AR, Seabrook GR, Reilly K & Oliver KR (2004) Discrete expression of TRPV2 within the hypothalamo-neurohypophysial system: Implications for regulatory activity within the hypothalamic-pituitary-adrenal axis. *J. Comp. Neurol.* **474**, 24–42.

14 Sharif-Naeini R, Ciura S & Bourque CW (2008) TRPV1 gene required for thermosensory transduction and anticipatory secretion from vasopressin neurons during hyperthermia. *Neuron* **58**, 179–185.

15 Moriya T, Shibasaki R, Kayano T, Takebuchi N, Ichimura M, Kitamura N, Asano A, Hosaka Y, Forostyak O, Verkhratsky A, Dayanithi G & Shibuya I (2015) Full-length transient receptor potential vanilloid 1 channels mediate calcium signals and possibly contribute to osmoreception in vasopressin neurones in the rat supraoptic nucleus. *Cell Calcium* **57**, 25–37.

16 Moussaieff A, Rimmerman N, Bregman T, Straiker A, Felder CC, Shoham S, Kashman Y, Huang SM, Lee H, Shohami E, Mackie K, Caterina MJ, Walker JM, Fride E & Mechoulam R (2008) Incensole acetate, an incense component, elicits psychoactivity by activating TRPV3 channels in the brain. *FASEB J.* **22**, 3024–3034.

17 Marinelli S, Pascucci T, Bernardi G, Puglisi-Allegra S & Mercuri NB (2005) Activation of TRPV1 in the VTA excites dopaminergic neurons and increases chemical- and noxious-induced dopamine release in the nucleus accumbens. *Neuropsychopharmacology* **30**, 864–870.

18 Vogt-Eisele AK, Weber K, Sherkheli MA, Vielhaber G, Panten J, Gisselmann G & Hatt H (2007) Monoterpenoid agonists of TRPV3. *Br. J. Pharmacol.* **151**, 530–540.

19 Xu H, Delling M, Jun JC & Clapham DE (2006) Oregano, thyme and clove-derived flavors and skin sensitizers activate specific TRP channels. *Nat. Neurosci.* **9**, 628–635.

20 Melo FHC, Moura BA, de Sousa DP, de Vasconcelos SMM, Macedo DS, Fonteles MM de F, Viana GS de B & de Sousa FCF (2011) Antidepressant-like effect of carvacrol (5-Isopropyl-2-methylphenol) in mice: involvement of dopaminergic system. *Fundam. Clin. Pharmacol.* **25**, 362–367.

21 Zotti M, Colaianna M, Morgese MG, Tucci P, Schiavone S, Avato P & Trabace L (2013) Carvacrol: From ancient flavoring to neuromodulatory agent. *Molecules* **18**, 6161–6172.

22 Ding ZM, Ingraham CM, Rodd ZA & McBride WJ (2015) The reinforcing effects of ethanol within the posterior ventral tegmental area depend on dopamine neurotransmission to forebrain cortico-limbic systems. *Addict. Biol.* **20**, 458–468.

23 Ikemoto S & Bonci A (2014) Neurocircuitry of drug reward. *Neuropharmacology* **76**, 329–341.

24 Phillips PE, Stuber GD, Heien ML, Wightman RM & Carelli RM (2003) Subsecond dopamine release promotes cocaine seeking. *Nature* **422**, 614–618.

25 Russo SJ & Nestler EJ (2013) The brain reward circuitry in mood disorders. *Nat. Rev. Neurosci.* **14**, 609–625.

26 Johnston D, Magee JC, Colbert CM & Cristie BR (1996) Active properties of neuronal dendrites. *Annu. Rev. Neurosci.* **19**, 165–186.

27 Yuste R & Tank DW (1996) Dendritic integration in mammalian neurons, a century after Cajal. *Neuron* **16**, 701–716.

28 Araki T & Otani T (1955) Response of single motoneurons to direct stimulation in toad's spinal cord. *J. Neurophysiol.* **18**, 472–485.

29 Coombs JS, Eccles JC & Fatt P (1955) The electrical properties of the motoneurone membrane. *J Physiol.* **28**, 291–325.

30 Frank K & Fuortes MG (1956) Stimulation of spinal motoneurones with intracellular electrodes. *J. Physiol.* **134**, 451–470.

31 Rall W (1960) Membrane potential transients and membrane time constant of motoneurons. *Exp. Neurol.* **2**, 503–532.

32 Rall W (1967) Distinguishing theoretical synaptic potentials computed for different soma-dendritic distributions of synaptic input. *J. Neurophysiol.* **30**, 1138–1168.

33 Rall W, Burke R, Smith T, Nelson P & Frank K (1967) Dendritic location of synapses and possible mechanisms for the monosynaptic EPSP in motoneurons. *J. Neurophysiol.* **30**, 1169–1193.

34 Hodgkin AL & Huxley AF (1952) Currents carried by sodium and potassium ions through the membrane of the giant axon of Loligo. *J. Physiol.* **116**, 449–472.

35 Hodgkin AL & Huxley A.F. (1952) The components of membrane counductance in the giant axon of Loligo. *J. Physiol.* **116**, 473–496.

36 Hodgkin AL & Huxley AF (1952) The dual effect of membrane potential on sodium conductance in the giant axon of Loligo. *J. Physiol.* **116**, 497–506.

37 Lipowsky R, Gillessen T & Alzheimer C (1996) Dendritic Na$^+$ Channels Amplify EPSPs in Hippocampal CA1 Pyramidal Cells. *J. Neurophysiol.* **76**, 2181–2191.

38 Magee JC, Christofi G, Miyakawa H, Christie B, Lasser-Ross N & Johnston D (1995) Subthreshold synaptic activation of voltage-gated Ca^{2+} channels mediates a localized Ca^{2+} influx into the dendrites of hippocampal pyramidal neurons. *J. Neurophysiol.* **74**, 1335–1342.

39 Purves D (2011) *Neuroscience*, Edition 5 Sinauer Associates, Incorporated.

40 Schwindt PC & Crill WE (1995) Amplification of synaptic current by persistent sodium conductance in apical dendrite of neocortical neurons. *J Neurophysiol.* **74**, 2220–2224.

41 Williams SR & Stuart GJ (2003) Role of dendritic synapse location in the control of action potential output. *Trends Neurosci.* **26**, 147–154.

42 Devaux JJ, Kleopa KA, Cooper EC & Scherer SS (2004) KCNQ2 is a nodal K$^+$ channel. *J Neurosci* **24**, 1236–1244.

43 Hille B (2001) *Ion Channels of Excitable Membranes*, Third Sinauer Associates, Inc.

44 Shepherd GM (2004) *The Synaptic Organization of the Brain* (5th Ed, ed.) Oxford University Press.

45 Cai X (2008) Unicellular Ca^{2+} signaling "toolkit" at the origin of metazoa. *Mol. Biol. Evol.* **25**, 1357–1361.

46 Berridge MJ, Bootman MD & Roderick HL (2003) Calcium signalling: dynamics, homeostasis and remodelling. *Nat. Rev. Mol. Cell Biol.* **4**, 517–29.

47 Bootman MD, Lipp P & Berridge MJ (2001) The organisation and functions of local Ca^{2+} signals. *J. Cell Sci.* **114**, 2213–2222.

48 Bootman MD (2012) Calcium signaling. *Cold Spring Harb. Perspect. Biol.* **4**, a011171.

49 Berridge MJ, Lipp P & Bootman MD (2000) The versatility and universality of calcium signalling. *Nat. Rev. Mol. Cell Biol.* **1**, 11–21.

50 Kinjo TG & Schnetkamp PPM (2005) Ca^{2+} Chemistry, Storage and Transport in Biologic Systems: An Overview. In *Voltage-Gated Calcium Channels* 2005th ed., pp. 1–11. Springer.

51 Clapham DE (2007) Calcium Signaling. *Cell* **131**, 1047–1058.

52 Grienberger C & Konnerth A (2012) Imaging Calcium in Neurons. *Neuron* **73**, 862–885.

53 Ramsey IS, Delling M & Clapham DE (2006) An introduction to TRP channels. *Annu. Rev. Physiol.* **68**, 619–647.

54 Montell C & Rubin GM (1989) Molecular characterization of the drosophila trp locus: a putative integral membrane protein required for phototransduction. *Neuron* **2**, 1313–1323.

55 Hardie RC & Minke B (1992) The trp gene is essential for a light-activated Ca^{2+} channel in Drosophila photoreceptors. *Neuron* **8**, 643–651.

56 Wheeler GL & Brownlee C (2008) Ca^{2+} signalling in plants and green algae - changing channels. *Trends Plant Sci.* **13**, 506–514.

57 Chang Y, Schlenstedt G, Flockerzi V & Beck A (2010) Properties of the intracellular transient receptor potential (TRP) channel in yeast, Yvc1. *FEBS Lett.* **584**, 2028–2032.

58 Matsuura H, Sokabe T, Kohno K, Tominaga M & Kadowaki T (2009) Evolutionary conservation and changes in insect TRP channels. *BMC Evol. Biol.* **9**, 228.

59 Venkatachalam K & Montell C (2007) TRP channels. *Annu. Rev. Biochem.* **76**, 387–417.

60 Montell C (2005) The TRP superfamily of cation channels. *Sci. STKE* **2005**, re3.

61 Pedersen SF, Owsianik G & Nilius B (2005) TRP channels: An overview. *Cell Calcium* **38**, 233–252.

62 Nilius B, Owsianik G, Voets T & Peters J A (2007) *Transient receptor potential cation channels in disease.*

63 Damann N, Voets T & Nilius B (2008) TRPs in Our Senses. *Curr. Biol.* **18**, R880–R889.

64 Clapham DE, Runnels LW & Strübing C (2001) The TRP ion channel family. *Nat. Rev. Neurosci.* **2**, 387–396.

65 Moran MM, Xu H & Clapham DE (2004) TRP ion channels in the nervous system. *Curr. Opin. Neurobiol.* **14**, 362–369.

66 Lu G, Henderson D, Liu L, Reinhart PH & Simon SA (2005) TRPV1b, a functional human vanilloid receptor splice variant. *Mol. Pharmacol.* **67**, 1119–1127.

67 Murakami M, Xu F, Miyoshi I, Sato E, Ono K & Iijima T (2003) Identification and characterization of the murine TRPM4 channel. *Biochem. Biophys. Res. Commun.* **307**, 522–528.

68 Kunert-Keil C, Bisping F, Krüger J & Brinkmeier H (2006) Tissue-specific expression of TRP channel genes in the mouse and its variation in three different mouse strains. *BMC Genomics* **7**, 159.

69 Clapham DE (2003) TRP channels as cellular sensors. *Nature* **426**, 517–524.

70 Zeilhofer HU, Kress M & Swandulla D (1997) Fractional Ca2+ currents through capsaicin- and proton-activated ion channels in rat dorsal root ganglion neurones. *J. Physiol.* **503 (Pt 1)**, 67–78.

71 Drews A, Loch S, Mohr F, Rizun O, Lambert S & Oberwinkler J (2010) The fractional calcium current through fast ligand-gated TRPM channels. *Acta Physiol.* **198**, Supplement 677.

72 Boisseau S, Kunert-Keil C, Lucke S & Bouron A (2009) Heterogeneous distribution of TRPC proteins in the embryonic cortex. *Histochem. Cell Biol.* **131**, 355–363.

73 Gees M, Colsoul B & Nilius B (2010) The role of transient receptor potential cation channels in Ca2+ signaling. *Cold Spring Harb. Perspect. Biol.* **2**, a003962.

74 Vennekens R, Owsianik G & Nilius B (2008) Vanilloid transient receptor potential cation channels: an overview. *Curr. Pharm. Des.* **14**, 18–31.

75 Nilius B & Owsianik G (2011) The transient receptor potential family of ion channels. *Genome Biol.* **12**, 218.

76 Nilius B, Droogmans G & Wondergem R (2003) Transient receptor potential channels in endothelium: solving the calcium entry puzzle? *Endothelium* **10**, 5–15.

77 Nilius B, Vriens J, Prenen J, Droogmans G & Voets T (2004) TRPV4 calcium entry channel: a paradigm for gating diversity. *Am. J. Physiol. Cell Physiol.* **286**, C195–C205.

78 Vriens, J., Appendino, G., Nilius B (2009) Pharmacology of Vanilloid Transient Receptor Potential Cation Channels. *Mol. Pharmacol.* **75**, 1262–1279.

79 Vennekens, R., Hoenderop, J.G., Prenen, J., Stuiver, M., Willems, P.H., Droogmans, G., Nilius, B., Bindels RJ (2000) Permeation and gating properties of the novel epithelial Ca^{2+} channel. *J. Biol. Chem.* **275**, 3963–3969.

80 Caterina MJ, Schumacher MA, Tominaga M, Rosen TA, Levine JD & Julius D (1997) The capsaicin receptor: a heat-activated ion channel in the pain pathway. *Nature* **389**, 816–824.

81 Cavanaugh DJ, Chesler AT, Jackson AC, Sigal YM, Yamanaka H, Grant R, O'Donnell D, Nicoll RA, Shah NM, Julius D & Basbaum AI (2011) Trpv1 reporter mice reveal highly restricted brain distribution and functional expression in arteriolar smooth muscle cells. *J. Neurosci.* **31**, 5067–77.

82 Cristino L, de Petrocellis L, Pryce G, Baker D, Guglielmotti V & Di Marzo V (2006) Immunohistochemical localization of cannabinoid type 1 and vanilloid transient receptor potential vanilloid type 1 receptors in the mouse brain. *Neuroscience* **139**, 1405–1415.

83 Mezey E, Tóth ZE, Cortright DN, Arzubi MK, Krause JE, Elde R, Guo A, Blumberg PM & Szallasi A (2000) Distribution of mRNA for vanilloid receptor subtype 1 (VR1), and VR1-like immunoreactivity, in the central nervous system of the rat and human. *Proc. Natl. Acad. Sci. U. S. A.* **97**, 3655–3660.

84 Roberts JC, Davis JB & Benham CD (2004) [3H]Resiniferatoxin autoradiography in the CNS of wild-type and TRPV1 null mice defines TRPV1 (VR-1) protein distribution. *Brain Res.* **995**, 176–183.

85 Tóth A, Boczán J, Kedei N, Lizanecz E, Bagi Z, Papp Z, Edes I, Csiba L & Blumberg PM (2005) Expression and distribution of vanilloid receptor 1 (TRPV1) in the adult rat brain. *Brain Res. Mol. Brain Res.* **135**, 162–168.

86 Hu J, Choo H & Ma S (2011) Infrared heat treatment reduces food intake and modifies

expressions of TRPV3-POMC in the dorsal medulla of obesity prone rats. *Int. J. Hyperth.* **27**, 708–716.

87 Lee JC & Choe SY (2014) Age-related changes in the distribution of transient receptor potential vanilloid 4 channel (TRPV4) in the central nervous system of rats. *J. Mol. Histol.* *45,497-505.*

88 Oldfield BJ, Badoer E, Hards DK & McKinley MJ (1994) Fos production in retrogradely labelled neurons of the lamina terminalis following intravenous infusion of either hypertonic saline or angiotensin II. *Neuroscience* **60**, 255–262.

89 Ludwig M, Sabatier N, Bull PM, Landgraf R, Dayanithi G & Leng G (2002) Intracellular calcium stores regulate activity-dependent neuropeptide release from dendrites. *Nature* **418**, 85–89.

90 Tobin VA, Douglas AJ, Leng G & Ludwig M (2011) The involvement of voltage-operated calcium channels in somato-dendritic oxytocin release. *PLoS One* **6**, e25366.

91 Harteneck C, Plant TD & Schultz G (2000) From worm to man: three subfamilies of TRP channels. *Trends Neurosci.* **23**, 159–166.

92 Sharif Naeini R, Witty MF, Séguéla P & Bourque CW (2006) An N-terminal variant of Trpv1 channel is required for osmosensory transduction. *Nat. Neurosci.* **9**, 93–98.

93 Kinsman B, Cowles J, Lay J, Simmonds SS, Browning KN & Stocker SD (2014) Osmoregulatory thirst in mice lacking the transient receptor potential vanilloid type 1 (TRPV1) and/or type 4 (TRPV4) receptor. *AJP Regul. Integr. Comp. Physiol.* **307**, R1092–R1100.

94 Hwang SJ, Burette A, Rustioni A & Valtschanoff JG (2004) Vanilloid receptor VR1-positive primary afferents are glutamatergic and contact spinal neurons that co-express neurokinin receptor NK1 and glutamate receptors. *J. Neurocytol.* **33**, 321–329.

95 Boulant JA (2000) Role of the Preoptic-Anterior Hypothalamus in Thermoregulation and Fever. *Clin Infect Dis* **31**, S157–S161.

96 Cheng W, Yang F, Liu S, Colton CK, Wang C, Cui Y, Cao X, Zhu MX, Sun C, Wang K & Zheng J (2012) Heteromeric heat-sensitive transient receptor potential channels exhibit distinct temperature and chemical response. *J. Biol. Chem.* **287**, 7279–7288.

97 Nilius B, Bíró T & Owsianik G (2014) TRPV3: time to decipher a poorly understood family member! *J. Physiol.* **592**, 295–304.

98 Shi DJ, Ye S, Cao X, Zhang R & Wang KW (2013) Crystal structure of the N-terminal ankyrin repeat domain of TRPV3 reveals unique conformation of finger 3 loop critical for channel function. *Protein Cell* **4**, 942–950.

99 Phelps CB, Wang RR, Choo SS & Gaudet R (2010) Differential regulation of TRPV1, TRPV3, and TRPV4 sensitivity through a conserved binding site on the ankyrin repeat domain. *J. Biol. Chem.* **285**, 731–740.

100 Grandl J, Hu H, Bandell M, Bursulaya B, Schmidt M, Petrus M & Patapoutian A (2008) Pore region of TRPV3 ion channel is specifically required for heat activation. *Nat. Neurosci.* **11**, 1007–1013.

101 Voets T, Droogmans G, Wissenbach U, Janssens A, Flockerzi V & Nilius B (2004) The principle of temperature-dependent gating in cold- and heat-sensitive TRP channels. *Nature* **430**, 748–754.

102 Voets T (2012) Quantifying and modeling the temperature-dependent gating of TRP channels. *Rev. Physiol. Biochem. Pharmacol.* **162**, 91–119.

103 Cao X, Yang F, Zheng J & Wang K (2012) Intracellular proton-mediated activation of TRPV3 channels accounts for the exfoliation effect of α-hydroxyl acids on keratinocytes. *J. Biol. Chem.* **287**, 25905–25916.

104 Chung MK, Lee H, Mizuno A, Suzuki M & Caterina MJ (2004) 2-Aminoethoxydiphenyl Borate Activates and Sensitizes the Heat-Gated Ion Channel TRPV3. *J. Neurosci.* **24**, 5177–5182.

105 Chung MK, Lee H, Mizuno A, Suzuki M & Caterina MJ (2004) TRPV3 and TRPV4 mediate warmth-evoked currents in primary mouse keratinocytes. *J. Biol. Chem.* **279**, 21569–21575.

106 Xiao R, Tian J, Tang J & Zhu MX (2008) The TRPV3 mutation associated with the hairless phenotype in rodents is constitutively active. *Cell Calcium* **43**, 334–343.

107 Moqrich, A., Hwang, S.W., Earley, T.J., Petrus, M.J., Murray, A. N., Spencer, K.S., Andahazy, M., Story G. M. & Patapoutian A (2005) Impaired thermosensation in mice lacking TRPV3, a heat and camphor sensor in the skin. *Science.* **307**, 1468–1472.

108 Nilius B & Bíró T (2013) TRPV3: A "more than skinny" channel. *Exp. Dermatol.* **22**, 447–452.

109 Cals-Grierson MM & Ormerod AD (2004) Nitric oxide function in the skin. *Nitric Oxide* **10**, 179–193.

110 Miyamoto T, Petrus MJ, Dubin AE & Patapoutian A (2011) TRPV3 regulates nitric oxide synthase-independent nitric oxide synthesis in the skin. *Nat. Commun.* **2**, 369.

111 Radtke C, Sinis N, Sauter M, Jahn S, Kraushaar U, Guenther E, Rodemann HP & Rennekampff HO (2011) TRPV channel expression in human skin and possible role in thermally induced cell death. *J Burn Care Res* **32**, 150–159.

112 Asakawa M, Yoshioka T, Matsutani T, Hikita I, Suzuki M, Oshima I, Tsukahara K, Arimura A, Horikawa T, Hirasawa T & Sakata T (2006) Association of a mutation in TRPV3 with defective hair growth in rodents. *J. Invest. Dermatol.* **126**, 2664–2672.

113 Borbíró I, Lisztes E, Tóth BI, Czifra G, Oláh A, Szöllosi AG, Szentandrássy N, Nánási PP, Péter Z, Paus R, Kovács L & Bíró T (2011) Activation of transient receptor potential vanilloid-3 inhibits human hair growth. *J. Invest. Dermatol.* **131**, 1605–1614.

114 Cheng X, Jin J, Hu L, Shen D, Dong X ping, Samie MA, Knoff J, Eisinger B, Liu ML, Huang SM, Caterina MJ, Dempsey P, Michael LE, Dlugosz AA, Andrews NC, Clapham DE & Xu H (2010) TRP channel regulates EGFR signaling in hair morphogenesis and skin barrier formation. *Cell* **141**, 331–343.

115 Xiao, R., Tian, J., Tang, J.& Zhu MX (2008) The TRPV3 mutation associated with the hairless phenotype in rodents is constitutively active. *Cell Calcium.* **43**, 334–343.

116 Lai-Cheong JE, Sethuraman G, Ramam M, Stone K, Simpson MA & McGrath JA (2012) Recurrent heterozygous missense mutation, p.Gly573Ser, in the TRPV3 gene in an Indian boy with sporadic Olmsted syndrome. *Br. J. Dermatol.* **167**, 440–442.

117 Lin Z, Chen Q, Lee M, Cao X, Zhang J, Ma D, Chen L, Hu X, Wang H, Wang X, Zhang P, Liu X, Guan L, Tang Y, Yang H, Tu P, Bu D, Zhu X, Wang K, Li R & Yang Y (2012) Exome sequencing reveals mutations in TRPV3 as a cause of Olmsted syndrome. *Am. J. Hum. Genet.* **90**, 558–564.

118 Huang SM, Lee H, Chung M-K, Park U, Yu YY, Bradshaw HB, Coulombe PA, Walker JM & Caterina MJ (2008) Overexpressed transient receptor potential vanilloid 3 ion channels in skin keratinocytes modulate pain sensitivity via prostaglandin E2. *J. Neurosci.* **28**, 13727–13737.

119 Mandadi S, Sokabe T, Shibasaki K, Katanosaka K, Mizuno A, Moqrich A, Patapoutian A, Fukumi-Tominaga T, Mizumura K & Tominaga M (2009) TRPV3 in keratinocytes transmits temperature information to sensory neurons via ATP. *Pflugers Arch.* **458**, 1093–1102.

120 Yamamoto-Kasai E, Imura K, Yasui K, Shichijou M, Oshima I, Hirasawa T, Sakata T & Yoshioka T (2012) TRPV3 as a therapeutic target for itch. *J Invest Dermatol.* **132**, 2109–2112.

121 Saito S, Fukuta N, Shingai R & Tominaga M (2011) Evolution of vertebrate transient receptor potential vanilloid 3 channels: Opposite temperature sensitivity between mammals and western clawed frogs. *PLoS Genet.* **7**.

122 Gracheva EO, Ingolia NT, Kelly YM, Cordero-Morales JF, Hollopeter G, Chesler AT, Sánchez EE, Perez JC, Weissman JS & Julius D (2010) Molecular basis of infrared detection by snakes. *Nature* **464**, 1006–11.

123 Viswanath V, Story GM, Peier AM, Petrus MJ, Lee VM, Hwang SW, Patapoutian A & Jegla T (2003) Opposite thermosensor in fruitfly and mouse. *Nature* **423**, 822–823.

124 Myers BR, Sigal YM & Julius D (2009) Evolution of thermal response properties in a cold-activated TRP channel. *PLoS One* **4**, e5741.

125 Moussaieff A & Mechoulam R (2009) Boswellia resin: from religious ceremonies to medical uses; a review of in-vitro, in-vivo and clinical trials. *J. Pharm. Pharmacol.* **61**, 1281–1293.

126 Paul M & Jauch J (2012) Efficient preparation of incensole and incensole acetate, and quantification of these bioactive diterpenes in Boswellia papyrifera by a RP-DAD-HPLC method. *Nat.Prod.Commun.* **7**, 283–288.

127 De Petrocellis L, Orlando P, Moriello AS, Aviello G, Stott C, Izzo AA & Di Marzo V (2012) Cannabinoid actions at TRPV channels: Effects on TRPV3 and TRPV4 and their potential relevance to gastrointestinal inflammation. *Acta Physiol.* **204**, 255–266.

128 Goldstein JL & Brown MS (1990) Regulation of the mevalonate pathway. *Nature* **343**, 425–430.

129 Bang S, Yoo S, Yang TJ, Cho H & Hwang SW (2010) Farnesyl pyrophosphate is a novel

pain-producing molecule via specific activation of TRPV3. *J. Biol. Chem.* **285**, 19362–19371.

130 Bang S, Yoo S, Yang TJ, Cho H & Hwang SW (2011) Isopentenyl pyrophosphate is a novel antinociceptive substance that inhibits TRPV3 and TRPA1 ion channels. *Pain* **152**, 1156–1164.

131 Hu HZ, Xiao R, Wang C, Gao N, Colton CK, Wood JD & Zhu MX (2006) Potentiation of TRPV3 channel function by unsaturated fatty acids. *J. Cell. Physiol.* **208**, 201–212.

132 Serhan CN, Hong S, Gronert K, Colgan SP, Devchand PR, Mirick G & Moussignac RL (2002) Resolvins: a family of bioactive products of omega-3 fatty acid transformation circuits initiated by aspirin treatment that counter proinflammation signals. *J. Exp. Med.* **196**, 1025–1037.

133 Ariel A & Serhan CN (2007) Resolvins and protectins in the termination program of acute inflammation. *Trends Immunol.* **28**, 176–183.

134 Lima-Garcia JF, Dutra RC, Da Silva K, Motta EM, Campos MM & Calixto JB (2011) The precursor of resolvin D series and aspirin-triggered resolvin D1 display anti-hyperalgesic properties in adjuvant-induced arthritis in rats. *Br. J. Pharmacol.* **164**, 278–293.

135 Bang S, Yoo S, Yang TJ, Cho H & Hwang SW (2012) 17(R)-resolvin D1 specifically inhibits transient receptor potential ion channel vanilloid 3 leading to peripheral antinociception. *Br J Pharmacol.* **165**, 683–692.

136 Ataullakhanov FI & Vitvitsky VM (2002) What determines the intracellular ATP concentration. *Biosci. Rep.* **22**, 501–511.

137 Lee H & Caterina MJ (2005) TRPV channels as thermosensory receptors in epithelial cells. *Pflugers Arch.* **451**, 160–167.

138 Zhu MX (2005) Multiple roles of calmodulin and other Ca^{2+}-binding proteins in the functional regulation of TRP channels. *Pflugers Arch.* **451**, 105–115.

139 Nilius B, Owsianik G & Voets T (2008) Transient receptor potential channels meet phosphoinositides. *Embo J* **27**, 2809–2816.

140 Akamatsu H, Makiura M, Yamamoto N, Yagami A, Shimizu Y & Matsunaga K (2006) The effect of fexofenadine on pruritus in a mouse model (HR-ADf) of atopic dermatitis. *J Int Med Res.* **34**, 495–504.

141 Biró T, Ko MC, Bromm B, Wei ET, Bigliardi P, Siebenhaar F, Hashizume H, Misery L, Bergasa N V, Kamei C, Schouenborg J, Roostermann D, Szabó T, Maurer M, Bigliardi-Qi M, Meingassner JG, Hossen MA, Schmelz M & Steinhoff M (2005) How best to fight that nasty itch - from new insights into the neuroimmunological, neuroendocrine, and neurophysiological bases of pruritus to novel therapeutic approaches. *Exp. Dermatol.* **14**, 225–40.

142 Neckermann G, Bavandi A & Meingassner JG (2000) Atopic dermatitis-like symptoms in hypomagnesaemic hairless rats are prevented and inhibited by systemic or topical SDZ ASM 981. *Br. J. Dermatol.* **142**, 669–679.

143 Imura K, Yoshioka T, Hikita I, Tsukahara K, Hirasawa T, Higashino K, Gahara Y, Arimura

A & Sakata T (2007) Influence of TRPV3 mutation on hair growth cycle in mice. *Biochem. Biophys. Res. Commun.* **363**, 479–483.

144 Yoshioka T, Imura K, Asakawa M, Suzuki M, Oshima I, Hirasawa T, Sakata T, Horikawa T & Arimura A (2009) Impact of the Gly573Ser substitution in TRPV3 on the development of allergic and pruritic dermatitis in mice. *J. Invest. Dermatol.* **129**, 714–722.

145 Luo J, Stewart R, Berdeaux R & Hu H (2012) Tonic inhibition of TRPV3 by Mg^{2+} in mouse epidermal keratinocytes. *J. Invest. Dermatol.* **132**, 2158–65.

146 Ahern GP, Brooks IM, Miyares RL & Wang XB (2005) Extracellular cations sensitize and gate capsaicin receptor TRPV1 modulating pain signaling. *J. Neurosci.* **25**, 5109–5116.

147 Kim SE, Patapoutian A & Grandl J (2013) Single Residues in the Outer Pore of TRPV1 and TRPV3 Have Temperature-Dependent Conformations. *PLoS One* **8**, e59593.

148 Huang SM, Li X, Yu Y, Wang J & Caterina MJ (2011) TRPV3 and TRPV4 ion channels are not major contributors to mouse heat sensation. *Mol. Pain* **7**. 37.

149 Singh U, Kumar S, Shelkar G, Yadhav M, Kokare D, Goswami C, Lechan R & Singru P (2016) Transient receptor potential vanilloid (TRPV3) in the ventral tegmental area of rat: Role in modulation of the mesolimbic-dopamine reward pathway. *Neuropharmacology* **110**, 198-210.

150 Paxinos G & Watson C (1998) *The rat brain in stereotaxic coordinates. Fourth edition*, 4th ed. Academic Press.

151 Ryan PJ, Ma S, Olucha-Bordonau FE & Gundlach AL (2011) Nucleus incertus-An emerging modulatory role in arousal, stress and memory. *Neurosci. Biobehav. Rev.* **35**, 1326–1341.

152 Williams KW & Elmquist JK (2012) From neuroanatomy to behavior: central integration of peripheral signals regulating feeding behavior. *Nat. Neurosci.* **15**, 1350–1355.

153 Lechan RM & Fekete C (2006) The TRH neuron: a hypothalamic integrator of energy metabolism. *Prog. Brain Res.* **153**, 209–235.

154 Kohno D, Gao HZ, Muroya S, Kikuyama S & Yada T (2003) Ghrelin directly interacts with neuropeptide-Y-containing neurons in the rat arcuate nucleus: Ca^{2+} signaling via protein kinase A and N-type channel-dependent mechanisms and cross-talk with leptin and orexin. *Diabetes* **52**, 948–956.

155 Becker EB, Oliver PL, Glitsch MD, Banks GT, Achilli F, Hardy A, Nolan PM, Fisher EM & Davies KE (2009) A point mutation in TRPC3 causes abnormal Purkinje cell development and cerebellar ataxia in moonwalker mice. *Proc. Natl. Acad. Sci. U. S. A.* **106**, 6706–6711.

156 Womack M & Khodakhah K (2002) Active contribution of dendrites to the tonic and trimodal patterns of activity in cerebellar Purkinje neurons. *J Neurosci* **22**, 10603–10612.

157 Güler AD, Rainwater A, Parker JG, Jones GL, Argilli E, Arenkiel BR, Ehlers MD, Bonci A, Zweifel LS & Palmiter RD (2012) Transient activation of specific neurons in mice by selective expression of the capsaicin receptor. *Nat. Commun.* **3**, 746.

158 Beitzel, C.S., Castillo, J., Valdez, M., Shahidzadeh, A., Spurgin, K., Calma, R., Curras-Collazo M (2010) TRPV1 channels contribute to hyperosmotic-induced release of vasopressin from somata and dendrites of magnocellular neuroendocrine cells in supraoptic

punches. *FASEB J* **24**, Supplement 627.8.

159 Mizuno A, Matsumoto N, Imai M & Suzuki M (2003) Impaired osmotic sensation in mice lacking TRPV4. *Am. J. Physiol. Cell Physiol.* **285**, C96–C101.

160 Bichet D. (2011) The posterior pituitary. In *The pituitary* (Melmed S, ed), 3rd ed., p. 261. Academic Press.

161 Tobin V, Leng G & Ludwig M (2012) The involvement of actin, calcium channels and exocytosis proteins in somato-dendritic oxytocin and vasopressin release. *Front. Physiol.* **3**, 261.

162 Morris JF & Pow DV (1991) Widespread release of peptides in the central nervous system: quantitation of tannic acid-captured exocytoses. *Anat. Rec.* **231**, 437–45.

163 Ludwig M (1998) Dendritic release of vasopressin and oxytocin. *J. Neuroendocrinol.* **10**, 881–895.

164 Ludwig M & Leng G (2006) Dendritic peptide release and peptide-dependent behaviours. *Nat. Rev. Neurosci.* **7**, 126–136.

165 Tobin V, Schwab Y, Lelos N, Onaka T, Pittman QJ & Ludwig M (2012) Expression of Exocytosis Proteins in Rat Supraoptic Nucleus Neurones. *J. Neuroendocrinol.* **24**, 629–641.

166 Custer KL, Austin NS, Sullivan JM & Bajjalieh SM (2006) Synaptic vesicle protein 2 enhances release probability at quiescent synapses. *J. Neurosci.* **26**, 1303–1313.

167 Buckley K & Kelly RB (1985) Identification of a transmembrane glycoprotein specific for secretory vesicles of neural and endocrine cells. *J. Cell Biol.* **100**, 1284–1294.

168 Crowder KM, Gunther JM, Jones TA, Hale BD, Zhang HZ, Peterson MR, Scheller RH, Chavkin C & Bajjalieh SM (1999) Abnormal neurotransmission in mice lacking synaptic vesicle protein 2A (SV2A). *Proc. Natl. Acad. Sci. U. S. A.* **96**, 15268–15273.

169 Bajjalieh SM, Frantz GD, Weimann JM, McConnell SK & Scheller RH (1994) Differential expression of synaptic vesicle protein 2 (SV2) isoforms. *J. Neurosci.* **14**, 5223–5235.

170 Tanner VA, Ploug T & Tao-Cheng JH (1996) Subcellular Localization of SV2 and Other Secretory Vesicle components in PC12 cells by an efficient method of preembedding EM immunocytochemistry for cell cultures. *J. Histochem. Cytochem.* **44**, 1481–1488.

171 Bragina L, Fattorini G, Giovedí S, Melone M, Bosco F, Benfenati F & Conti F (2012) Analysis of Synaptotagmin, SV2, and Rab3 Expression in Cortical Glutamatergic and GABAergic Axon Terminals. *Front. Cell. Neurosci.* **5**, 1–9.

172 Ferro-Novick S & Brose N (2013) Nobel 2013 Physiology or medicine: Traffic control system within cells. *Nature* **504**, 98.

173 Nowack A, Yao J, Custer KL & Bajjalieh SM (2010) SV2 regulates neurotransmitter release via multiple mechanisms. *Am. J. Physiol. Cell Physiol.* **299**, C960–C967.

174 Lazzell DR, Belizaire R, Thakur P, Sherry DM & Janz R (2004) SV2B regulates synaptotagmin 1 by direct interaction. *J. Biol. Chem.* **279**, 52124–52131.

175 Chang WP & Sudhof TC (2009) SV2 renders primed synaptic vesicles competent for Ca^{2+}-induced exocytosis. *J. Neurosci.* **29**, 883–897.

176 Chapman ER (2002) Synaptotagmin: a Ca^{2+} sensor that triggers exocytosis? *Nat. Rev. Mol. Cell Biol.* **3**, 498–508.

177 Yao J, Nowack A, Kensel-Hammes P, Gardner RG & Bajjalieh SM (2010) Cotrafficking of SV2 and synaptotagmin at the synapse. *J. Neurosci.* **30**, 5569–5578.

178 Neumann I, Russell JA & Landgraf R (1993) Oxytocin and vasopressin release within the supraoptic and paraventricular nuclei of pregnant, parturient and lactating rats: a microdialysis study. *Neuroscience* **53**, 65–75.

179 Chevaleyre V, Dayanithi G, Moos FC & Desarmenien MG (2000) Developmental regulation of a local positive autocontrol of supraoptic neurons. *J. Neurosci.* **20**, 5813–5819.

180 Bichet DG (2014) Central vasopressin: dendritic and axonal secretion and renal actions. *Clin. Kidney J.* **7**, 242–247.

181 Jacobsson G, Bean AJ & Meister B (1999) Isoform-specific exocytotic protein mRNA expression in hypothalamic magnocellular neurons: regulation after osmotic challenge. *Neuroendocrinology* **70**, 392–401.

182 Yue C, Mutsuga N, Sugimura Y, Verbalis J & Gainer H (2008) Differential kinetics of oxytocin and vasopressin heteronuclear RNA expression in the rat supraoptic nucleus in response to chronic salt loading in vivo. *J. Neuroendocrinol.* **20**, 227–232.

183 Arima H & Aguilera G (2000) Vasopressin and oxytocin neurones of hypothalamic supraoptic and paraventricular nuclei co-express mRNA for type-1 and type-2 corticotropin-releasing hormone receptors. *J. Neuroendocrinol.* **12**, 833–842.

184 Kádár A, Sánchez E, Wittmann G, Singru P, Füzesi T, Marsili A, Larsen P, Liposits Z, Lechan R & Fekete C (2010) Distribution of hypophysiotropic thyrotropin-releasing hormone (TRH)-synthesizing neurons in the hypothalamic paraventricular nucleus of the mouse. *J. Comp. Neurol.* **518**, 3948–3961.

185 Pennuto M, Bonanomi D, Benfenati F & Valtorta F (2003) Synaptophysin I controls the targeting of VAMP2/synaptobrevin II to synaptic vesicles. *Mol. Biol. Cell* **14**, 4909–4919.

186 Hrabovszky E1, Deli L, Turi GF, Kalló I & Liposits Z (2007) Glutamatergic innervation of the hypothalamic median eminence and posterior pituitary of the rat. *Neuroscience* **144**, 1383–1392.

187 Fox MA & Sanes JR (2007) Synaptotagmin I and II are present in distinct subsets of central synapses. *J. Comp. Neurol.* **503**, 280–296.

188 Singh U, Kumar S & Singru PS (2012) Interaction between dopamine- and isotocin-containing neurones in the preoptic area of the catfish, *Clarias batrachus*: role in the regulation of luteinising hormone cells. *J. Neuroendocrinol.* **24**, 1398–1411.

189 Bel C, Oguievetskaia K, Pitaval C, Goutebroze L & Faivre-Sarrailh C (2009) Axonal targeting of Caspr2 in hippocampal neurons via selective somatodendritic endocytosis. *J. Cell Sci.* **122**, 3403–3413.

190 Villanueva C, Jacquier S & de Roux N (2012) DLK1 is a somato-dendritic protein expressed in hypothalamic arginine-vasopressin and oxytocin neurons. *PLoS One* **7**, e36134.

191 Blanchart A, De Carlos JA & Lopez-Mascaraque L (2006) Time frame of mitral cell

development in the mice olfactory bulb. *J. Comp. Neurol.* **496**, 529–543.

192 Mueller NK, Di S, Paden CM & Herman JP (2005) Activity-dependent modulation of neurotransmitter innervation to vasopressin neurons of the supraoptic nucleus. *Endocrinology* **146**, 348–354.

193 Salter-Venzon D & Watts AG (2008) The role of hypothalamic ingestive behavior controllers in generating dehydration anorexia: a Fos mapping study. *AJP Regul. Integr. Comp. Physiol.* **295**, R1009–R1019.

194 Ludwig M, Callahan MF, Neumann I, Landgraf R & Morris M (1994) Systemic osmotic stimulation increases vasopressin and oxytocin release within the supraoptic nucleus. *J. Neuroendocrinol.* **6**, 369–373.

195 Sudbury JR, Ciura S, Sharif-Naeini R & Bourque CW (2010) Osmotic and thermal control of magnocellular neurosecretory neurons - role of an N-terminal variant of trpv1. *Eur. J. Neurosci.* **32**, 2022–2030.

196 Zsombok A, Gao H, Miyata K, Issa A & Derbenev AV. (2011) Immunohistochemical localization of transient receptor potential vanilloid type 1 and insulin receptor substrate 2 and their co-localization with liver-related neurons in the hypothalamus and brainstem. *Brain Res.* **1398**, 30–39.

197 De Petrocellis L & Di Marzo V (2005) Lipids as regulators of the activity of transient receptor potential type V1 (TRPV1) channels. *Life Sci.* **77**, 1651–1666.

198 Fischer & Edwardson (2014) V2A2 lidating TRP channel heteromers. *Temperature* **1**, 26–27.

199 Satheesh NJ, Uehara Y, Fedotova J, Pohanka M, Büsselberg D & Kruzliak P (2016) TRPV currents and their role in the nociception and neuroplasticity. *Neuropeptides* **57**, 1–8.

200 Lambert RC, Dayanithi G, Moos FC & Richard P (1994) A rise in the intracellular Ca^{2+} concentration of isolated rat supraoptic cells in response to oxytocin. *J. Physiol.* **478**, 275–87.

201 Leng G, Brown C, Sabatier N & Scott V (2008) Population dynamics in vasopressin cells. *Neuroendocrinology* **88**, 160–172.

202 Gouzènes L, Desarménien MG, Hussy N, Richard P & Moos FC (1998) Vasopressin regularizes the phasic firing pattern of rat hypothalamic magnocellular vasopressin neurons. *J. Neurosci.* **18**, 1879–1885.

203 Wang BC, Share L & Crofton JT (1982) Central infusion of vasopressin decreased plasma vasopressin concentration in dogs. *Am. J. Physiol.* **243**, E365-E369.

204 Ludwig M & Leng G (1997) Autoinhibition of supraoptic nucleus vasopressin neurons in vivo: A combined retrodialysis/electrophysiological study in rats. *Eur. J. Neurosci.* **9**, 2532–2540.

205 Gillard ER, Coburn CG, de Leon A, Snissarenko EP, Bauce LG, Pittman QJ, Hou B & Currás-Collazo MC (2007) Vasopressin autoreceptors and nitric oxide-dependent glutamate release are required for somatodendritic vasopressin release from rat magnocellular neuroendocrine cells responding to osmotic stimuli. *Endocrinology* **148**,

479–489.

206 McKinley MJ & McAllen RM (2007) Neuroendocrine self-control: dendritic release of vasopressin. *Endocrinology* **148**, 477–478.

207 Van Tol, H.H., Voorhuis D.T.& Burbach JP (1987) Oxytocin gene expression in discrete hypothalamic magnocellular cell groups is stimulated by prolonged salt loading. *Endocrinology* **120**, 71–76.

208 Summy-Long JY, Hu S, Pruss A, Chen X & Phillips TM (2006) Response of interleukin-1beta in the magnocellular system to salt-loading. *J. Neuroendocrinol.* **18**, 926–937.

209 Grimm J, Mueller A, Hefti F & Rosenthal A (2004) Molecular basis for catecholaminergic neuron diversity. *Proc. Natl. Acad. Sci. U. S. A.* **101**, 13891–13896.

210 Bonci A, Bernardi G, Grillner P & Mercuri NB (2003) The dopamine-containing neuron: Maestro or simple musician in the orchestra of addiction? *Trends Pharmacol. Sci.* **24**, 172–177.

211 Schultz W (1986) Responses of midbrain dopamine neurons to behavioral trigger stimuli in the monkey. *J. Neurophysiol.* **56**, 1439–1461.

212 Wise RA (2002) Brain reward circuitry: insights from unsensed incentives. *Neuron* **36**, 229–240.

213 Nestler EJ (2005) Is there a common molecular pathway for addiction? *Nat. Neurosci.* **8**, 1445–1449.

214 Kai N, Nishizawa K, Tsutsui Y, Ueda S & Kobayashi K (2015) Differential roles of dopamine D1 and D2 receptor-containing neurons of the nucleus accumbens shell in behavioral sensitization. *J. Neurochem.* **135**, 1232–1241.

215 Singru PS, Fekete C & Lechan RM (2005) Neuroanatomical evidence for participation of the hypothalamic dorsomedial nucleus (DMN) in regulation of the hypothalamic paraventricular nucleus (PVN) by α-melanocyte stimulating hormone. *Brain Res.* **1064**, 42–51.

216 Goswami C, Schmidt H & Hucho F (2007) TRPV1 at nerve endings regulates growth cone morphology and movement through cytoskeleton reorganization. *FEBS J.* **274**, 760–772.

217 Ikegaya Y, Le Bon-Jego M & Yuste R (2005) Large-scale imaging of cortical network activity with calcium indicators. *Neurosci. Res.* **52**, 132–138.

218 Hong JH, Min CH, Jeong B, Kojiya T, Morioka E, Nagai T, Ikeda M & Lee KJ (2010) Intracellular calcium spikes in rat suprachiasmatic nucleus neurons induced by BAPTA-based calcium dyes. *PLoS One* **5**, e9634.

219 Gee KR, Brown KA, Chen WN, Bishop-Stewart J, Gray D & Johnson I (2000) Chemical and physiological characterization of fluo-4 Ca^{2+}-indicator dyes. *Cell Calcium* **27**, 97–106.

220 Zhao-Shea R, Liu L, Soll LG, Improgo MR, Meyers EE, McIntosh JM, Grady SR, Marks MJ, Gardner PD & Tapper AR (2011) Nicotine-mediated activation of dopaminergic neurons in distinct regions of the ventral tegmental area. *Neuropsychopharmacology* **36**, 1021–1032.

221 Shabat-Simon M, Levy D, Amir A, Rehavi M & Zangen A (2008) Dissociation between

rewarding and psychomotor effects of opiates: differential roles for glutamate receptors within anterior and posterior portions of the ventral tegmental area. *J. Neurosci.* **28**, 8406–8416.

222 Upadhya MA, Nakhate KT, Kokare DM, Singh U, Singru PS & Subhedar NK (2012) CART peptide in the nucleus accumbens shell acts downstream to dopamine and mediates the reward and reinforcement actions of morphine. *Neuropharmacology* **62**, 1823–1833.

223 Shelkar GP, Kale AD, Singh U, Singru PS, Subhedar NK & Kokare DM (2015) Alpha-melanocyte stimulating hormone modulates ethanol self-administration in posterior ventral tegmental area through melanocortin-4 receptors. *Addict. Biol.* **20**, 302–315.

224 Kokare DM, Shelkar GP, Borkar CD, Nakhate KT & Subhedar NK (2011) A simple and inexpensive method to fabricate a cannula system for intracranial injections in rats and mice. *J. Pharmacol. Toxicol. Methods* **64**, 246–250.

225 Pires P, Sullivan M, Prichard H, Robinson J & Earley S (2015) Unitary TRPV3 channel Ca2+ influx events elicit endothelium-dependent dilation of cerebral parenchymal arterioles. *Am. J. Physiol. Hear. Circ. Physiol.* **309**, H2031–H2041.

226 Swanson LW (1982) The projections of the ventral tegmental area and adjacent regions: a combined fluorescent retrograde tracer and immunofluorescence study in the rat. *Brain Res. Bull.* **9**, 321–353.

227 Bozarth MA (1987) Ventral tegmental reward system. In *Brain Reward Systems and Abuse* pp. 1–17.

228 Wise RA & Bozarth MA (1984) Brain reward circuitry: four circuit elements "wired" in apparent series. *Brain Res. Bull.* **12**, 203–208.

229 Hyman SE, Malenka RC & Nestler EJ (2006) Neural mechanisms of addiction: the role of reward-related learning and memory. *Annu. Rev. Neurosci.* **29**, 565–598.

230 Lupica CR, Riegel AC & Hoffman AF (2004) Marijuana and cannabinoid regulation of brain reward circuits. *Br. J. Pharmacol.* **143**, 227–234.

231 Koob GF & Volkow ND (2010) Neurocircuitry of addiction. *Neuropsychopharmacology* **35**, 1051.

232 Adinoff B (2004) Neurobiologic processes in drug reward and addiction. *Harvard Rev. Psychiatry* **12**, 305–320.

233 Marinelli S, Di Marzo V, Florenzano F, Fezza F, Viscomi MT, van der Stelt M, Bernardi G, Molinari M, Maccarrone M & Mercuri NB (2007) N-arachidonoyl-dopamine tunes synaptic transmission onto dopaminergic neurons by activating both cannabinoid and vanilloid receptors. *Neuropsychopharmacology* **32**, 298–308.

234 Marinelli S, Di Marzo V, Berretta N, Matias I, Maccarrone M, Bernardi G & Mercuri NB (2003) Presynaptic facilitation of glutamatergic synapses to dopaminergic neurons of the rat substantia nigra by endogenous stimulation of vanilloid receptors. *J. Neurosci.* **23**, 3136–3144.

235 Micale V, Cristino L, Tamburella A, Petrosino S, Leggio GM, Drago F & Di Marzo V (2009) Anxiolytic effects in mice of a dual blocker of fatty acid amide hydrolase and

transient receptor potential vanilloid type-1 channels. *Neuropsychopharmacology* **34**, 593–606.

236 Heng LJ, Huang B, Guo H, Ma LT, Yuan WX, Song J, Wang P, Xu GZ & Gao GD (2014) Blocking TRPV1 in nucleus accumbens inhibits persistent morphine conditioned place preference expression in rats. *PLoS One* **9**, e104546.

237 Beier KT, Steinberg EE, Deloach KE, Xie S, Miyamichi K, Schwarz L, Gao XJ, Kremer EJ, Malenka RC & Luo L (2015) Circuit Architecture of VTA Dopamine Neurons Revealed by Systematic Input-Output Mapping. *Cell* **162**, 622–634.

238 Rodríguez-López C, Clascá F & Prensa L (2017) The Mesoaccumbens Pathway: A Retrograde Labeling and Single-Cell Axon Tracing Analysis in the Mouse. *Front. Neuroanat.* **11**., 25

239 Ikemoto S (2007) Dopamine reward circuitry: Two projection systems from the ventral midbrain to the nucleus accumbens-olfactory tubercle complex. *Brain Res. Rev.* **56**, 27–78.

240 Yamaguchi T, Wang HL, Li X, Ng TH & Morales M (2011) Mesocorticolimbic Glutamatergic Pathway. *J. Neurosci.* **31**, 8476–8490.

241 Koob GF & Le Moal M (2001) Drug addiction, dysregulation of reward, and allostasis. *Neuropsychopharmacology* **24**, 97–129.

242 Skibicka KP, Shirazi RH, Rabasa-Papio C, Alvarez-Crespo M, Neuber C, Vogel H & Dickson SL (2013) Divergent circuitry underlying food reward and intake effects of ghrelin: dopaminergic VTA-accumbens projection mediates ghrelin's effect on food reward but not food intake. *Neuropharmacology* **73**, 274–283.

243 Baik JH (2013) Dopamine signaling in reward-related behaviors. *Front. Neural Circuits* **7**, 152.

244 Ikemoto S, Glazier BS, Murphy JM & McBride WJ (1997) Role of dopamine D1 and D2 receptors in the nucleus accumbens in mediating reward. *J. Neurosci.* **17**, 8580–8587.

245 Kang YS & Kim JM (1999) Permeability of a capsaicin derivative, [14C]DA-5018 to blood-brain barrier corrected with HPLC method. *Arch. Pharm. Res.* **22**, 165–172.

246 Jordt SE & Julius D (2002) Molecular basis for species-specific sensitivity to "hot" chili peppers. *Cell* **108**, 421–430.

247 Bang S, Yoo S, Yang TJ, Cho H & Hwang S (2012) 17(R)-resolvin D1 specifically inhibits transient receptor potential ion channel vanilloid 3 leading to peripheral antinociception. *Br. J. Pharmacol.* **165**, 683–692.

248 Vukelic S, Stojadinovic O, Pastar I, Vouthounis C, Krzyzanowska A, Das S, Samuels HH & Tomic-Canic M (2010) Farnesyl pyrophosphate inhibits epithelialization and wound healing through the glucocorticoid receptor. *J. Biol. Chem.* **285**, 1980–1988.

249 Hensleigh E & Pritchard LM (2013) Glucocorticoid receptor expression and sub-cellular localization in dopamine neurons of the rat midbrain. *Neurosci. Lett.* **556**, 191–195.

250 McKay BE & Turner RW (2005) Physiological and morphological development of the rat cerebellar Purkinje cell. *J. Physiol.* **567**, 829–850.

251 Dale Purves, George J Augustine, David Fitzpatrick, Lawrence C Katz, Anthony-Samuel

LaMantia, James O McNamara and SMW (2001) *Neuroscience*, second ed. Sinauer Associates Inc.

252 Voogd J & Glickstein M (1998) The anatomy of the cerebellum. *Trends Neurosci.* **21**, 370–375.

253 Crepel F, Mariani J & Delhaye-Bouchaud N (1976) Evidence for a multiple innervation of Purkinje cells by climbing fibers in the immature rat cerebellum. *J. Neurobiol.* **7**, 567–578.

254 Dueñas AM, Goold R & Giunti P (2006) Molecular pathogenesis of spinocerebellar ataxias. *Brain* **129**, 1357–1370.

255 Servais L, Hourez R, Bearzatto B, Gall D, Schiffmann SN & Cheron G (2007) Purkinje cell dysfunction and alteration of long-term synaptic plasticity in fetal alcohol syndrome. *Proc. Natl. Acad. Sci. U. S. A.* **104**, 9858–9863.

256 Pietrobon D (2002) Calcium channels and channelopathies of the central nervous system. *Mol. Neurobiol.* **25**, 31–50.

257 Usowicz MM, Sugimori M, Cherksey B & Llinás R (1992) P-type calcium channels in the somata and dendrites of adult cerebellar Purkinje cells. *Neuron* **9**, 1185–1199.

258 Womack MD & Khodakhah K (2004) Dendritic control of spontaneous bursting in cerebellar Purkinje cells. *J Neurosci* **24**, 3511–3521.

259 Hashimoto K, Tsujita M, Miyazaki T, Kitamura K, Yamazaki M, Shin H-S, Watanabe M, Sakimura K & Kano M (2011) Postsynaptic P/Q-type Ca^{2+} channel in Purkinje cell mediates synaptic competition and elimination in developing cerebellum. *Proc. Natl. Acad. Sci. U. S. A.* **108**, 9987–9992.

260 Leitch B, Shevtsova O, Guévremont D & Williams J (2009) Loss of calcium channels in the cerebellum of the ataxic and epileptic stargazer mutant mouse. *Brain Res.* **1279**, 156–167.

261 Iwasaki S, Momiyama A, Uchitel OD & Takahashi T (2000) Developmental changes in calcium channel types mediating central synaptic transmission. *J. Neurosci.* **20**, 59–65.

262 Huguenard JR (1996) Low-threshold calcium currents in central nervous system neurons. *Annu. Rev. Physiol.* **58**, 329–348.

263 Cavelier P & Bossu JL (2003) Dendritic low-threshold Ca^{2+} channels in rat cerebellar Purkinje cells: possible physiological implications. *Cerebellum* **2**, 196–205.

264 Balchen T & Diemer NH (1992) The AMPA antagonist, NBQX, protects against ischemia-induced loss of cerebellar Purkinje cells. *Neuroreport* **3**, 785–788.

265 Piochon C, Levenes C, Ohtsuki G & Hansel C (2010) Purkinje cell NMDA receptors assume a key role in synaptic gain control in the mature cerebellum. *J. Neurosci.* **30**, 15330–15335.

266 Kim SJ, Kim YS, Yuan JP, Petralia RS, Worley PF & Linden DJ (2003) Activation of the TRPC1 cation channel by metabotropic glutamate receptor mGluR1. *Nature* **426**, 285–291.

267 Zamudio-Bulcock PA, Everett J, Harteneck C & Valenzuela CF (2011) Activation of steroid-sensitive TRPM3 channels potentiates glutamatergic transmission at cerebellar Purkinje neurons from developing rats. *J. Neurochem.* **119**, 474–485.

268 Hoffmann A, Grimm C, Kraft R, Goldbaum O, Wrede A, Nolte C, Hanisch UK, Richter-Landsberg C, Brück W, Kettenmann H & Harteneck C (2010) TRPM3 is expressed in

sphingosine-responsive myelinating oligodendrocytes. *J. Neurochem.* **114**, 654–665.

269 Cristino L, Starowicz K, De Petrocellis L, Morishita J, Ueda N, Guglielmotti V & Di Marzo V (2008) Immunohistochemical localization of anabolic and catabolic enzymes for anandamide and other putative endovanilloids in the hippocampus and cerebellar cortex of the mouse brain. *Neuroscience* **151**, 955–968.

270 Friedlander MJ, Kotchabhakdi N & Prosser CL (1976) Effects of cold and heat on behavior and cerebellar function in goldfish. *J. Comp. Physiol.* **112**, 19–45.

271 Gahwiler BH, Mamoon AM & Tobias CA (1973) Spontaneous bioelectric activity of cultured cerebellar Purkinje cells during exposure to agents which prevent synaptic transmission. *Brain Res.* **53**, 71–79.

272 Klapdor K, Dulfer BG, Hammann A & Van Der Staay FJ (1997) A low-cost method to analyse footprint patterns. *J. Neurosci. Methods* **75**, 49–54.

273 Goyal SN, Kokare DM, Chopde CT & Subhedar NK (2006) Alpha-melanocyte stimulating hormone antagonizes antidepressant-like effect of neuropeptide Y in Porsolt's test in rats. *Pharmacol. Biochem. Behav.* **85**, 369–377.

274 Gray JA & Lalljee B (1974) Sex differences in emotional behaviour in the rat: correlation between open-field defecation and active avoidance. *Anim. Behav.* **22**, 856–861.

275 Redmond AM, Kelly JP & Leonard BE (1997) Behavioural and neurochemical effects of dizocilpine in the olfactory bulbectomized rat model of depression. *Pharmacol. Biochem. Behav.* **58**, 355–359.

276 Häusser M & Clark BA (1997) Tonic synaptic inhibition modulates neuronal output pattern and spatiotemporal synaptic integration. *Neuron* **19**, 665–678.

277 Nam SC & Hockberger PE (1997) Analysis of spontaneous electrical activity in cerebellar Purkinje cells acutely isolated from postnatal rats. *J. Neurobiol.* **33**, 18–32.

278 Raman IM & Bean BP (1997) Resurgent sodium current and action potential formation in dissociated cerebellar Purkinje neurons. *J. Neurosci.* **17**, 4517–4526.

279 Jaeger D & Bower JM (1999) Synaptic control of spiking in cerebellar Purkinje cells: dynamic current clamp based on model conductances. *J Neurosci* **19**, 6090–6101.

280 Hall JE & Guyton AC (2011) *Guyton and Hall Textbook of Medical Physiology*.

281 Ludwig M & Stern J (2015) Multiple signalling modalities mediated by dendritic exocytosis of oxytocin and vasopressin. *Philos. Trans. R. Soc. B Biol. Sci.* **370**.

Table 3: Details of the primary antibodies used

S. No.	Antibody	Type	Host	Cat. No.	Dilution	Source
1	Anti-TRPV3 (N-terminal)	Polyclonal	Rabbit	# SAB1300539	1:5000	SIGMA
2	Anti-TRPV3 (C-terminal)	Polyclonal	Goat	# sc-23373	1:500	Santa Cruz Biotechnology Inc., USA
3	Anti-Fluorescent Gold	Polyclonal	Rabbit	# AB153	1:1000	Millipore
4	Anti-c-Fos	Polyclonal	Goat	# sc-253-G	1:500	Santa Cruz Biotechnology Inc., USA
5	Anti-Vasopressin-neurophysin	Monoclonal	Mouse	# PS-41	1:500	Kind gift of Dr. Harold Gainer, NIH
6	Anit Vasopressin	Polyclonal	Rabbit	# ab39363	1:1000	Abcam
7	Anti-Synaptotagmin 1	Monoclonal	Mouse	# mAb 48 (asv 48)	1:500	Developmental Studies Hybridoma Bank
8	Anti-Synaptic vesicle glycoprotein 2A	Monoclonal	Mouse	# SV2	1:500	Developmental Studies Hybridoma Bank
9	Anti-Microtubule-Associated Protein 2 (MAP2)	Polyclonal	Rabbit	# AB5622	1:1000	Millipore
10	Anti-Glutamic Acid Decarboxylase 65	Polyclonal	Rabbit	# G4913	1:1000	SIGMA
11	Anti-Cholera Toxin B Subunit	Polyclonal	Goat	# 703	1:500	List Biological Laboratories Inc.
12	Anti-Tyrosine Hydroxylase	Monoclonal	Mouse	# T2928	1:1000	SIGMA
13	Anti-Tyrosine Hydroxylase	Polyclonal	Rabbit	# T8700	1:5000	SIGMA
14	Anti-Tyrosine Hydroxylase	Polyclonal	Sheep	# AB1542	1:5000	Millipore
15	Anti-Calbindin-D28K	Monoclonal	Mouse	# C9848	1:500	SIGMA